NASA Contractor Report 158994

Formulation of Aerodynamic Prediction Techniques for Hypersonic Configuration Design

ROCKWELL INTERNATIONAL CORPORATION

CONTRACT NAS1-15075
FEBRUARY 1979

National Aeronautics and
Space Administration

Langley Research Center
Hampton, Virginia 23665
AC 804 827-3966

FORMULATION OF AERODYNAMIC PREDICTION TECHNIQUES FOR HYPERSONIC CONFIGURATION DESIGN

PREPARED UNDER CONTRACT NAS1-15075
BY
ROCKWELL INTERNATIONAL
LOS ANGELES, CALIFORNIA

FOR

LANGLEY RESEARCH CENTER
NATIONAL AERONAUTICS AND SPACE ADMINISTRATION

FOREWORD

This final report was prepared by the Aerodynamics Group of the Los Angeles Division and the Fluid Mechanics Section of the Science Center of Rockwell International, Los Angeles, California for the Langley Research Center, National Aeronautics and Space Administration, Hampton, Virginia. The work was performed under Contract No. NAS1-15075, "Formulation of Aerodynamic Prediction Techniques for Hypersonic Configuration Design." Mr. Clyde L. W. Edwards was the Project Monitor of this contract.

Mr. E. Bonner was the Program Manager; Drs. W. C. Clever, N. D. Malmuth and V. Shankar served as Project Engineers. Contributinns have been made by Rockwell Consultants Prof. J. D. Cole of UCLA and Prof. D. Anderson and Mr. C. R. Sukumar of Iowa State.

SUMMARY

An investigation of approximate theoretical techniques for predicting aerodynamic characteristics and surface pressures for relatively slender vehicles at moderate hypersonic speeds was performed. Emphasis was placed on approaches that would be responsive to preliminary configuration design level of effort. Supersonic second order potential theory was examined in detail to meet this objective. Shock layer integral techniques were considered as an alternative means of predicting gross aerodynamic characteristics.

Several numerical pilot codes were developed for simple three dimensional geometries to evaluate the capability of the approximate equations of motion considered. Results from the second order computations indicated good agreement with higher order solutions and experimental results for a variety of wing like shapes and values of the hypersonic similarity parameter $M\delta$ approaching one.

TABLE OF CONTENTS

1. INTRODUCTION

Progress over the past 20 years in hypersonic aerodynamic technology has emphasized space re-entry vehicles. Relatively little advancement has occurred during the same time period in similar applications to hypersonic cruise aircraft. At lower speeds, significant gains in supersonic cruise efficiency have been realized using linear theory optimization techniques. Similar improvements appear feasible for slender hypersonic vehicles. Recent studies have shown that, at a Mach number of 6.0, both passively and actively cooled airframe structures with relatively small leading edge radius can be advantageously employed in hypersonic aircraft optimization. To characterize the aerodynamic implications of such nose shapes and evaluate the consequences of proposed beneficial interference concepts such as those involving propulsive-airframe integration, new analytical tools are required. Although substantial capabilities exist using Euler solution in conjunction with floating shock fitting methods, quicker response analysis tools are required to derive and optimize base point configurations. Less exact non-linear theoretical formulations hold the promise of meeting this objective and providing economic design codes which are responsive to preliminary vehicle definition efforts.

2. LIST OF SYMBOLS*

$\bar{c}$	mean aerodynamic chord
C_D	drag coefficient, $\frac{D}{qS}$
C_L	lift coefficient, $\frac{L}{qS}$
C_m	pitching moment coefficient, $\frac{M}{qS\bar{c}}$
C_p	pressure coefficient, $\frac{P-P_\infty}{q_\infty}$
D	drag
L	lift
M	Mach number or moment
P	static pressure
q	dynamic pressure
S	reference area
α	angle of attack
δ	flow deflection angle

SUBSCRIPTS

L	due to lift
∞	free stream

*Additional specialized nomenclature is defined in the theoretical sections

3.0 METHODOLOGY

Emphasis has been placed on approximate theoretical approaches which are capable of treating relatively general three dimensional problems but still sufficiently simple to be responsive to vehicle preliminary design efforts. The basic intent of the methodology is to produce future improvements in lift-drag ratio of hypersonic cruise vehicles. As a result of the strong impact that favorable interference has had on supersonic design and the use of such concepts in recent advanced hypersonic aircraft studies, candidate analysis should be general enough to systematically treat such problems. Finally, interest in high aerodynamic efficiency usually emphasizes relatively slender configurations at modest angle of attack; that is moderate values of the hypersonic similarity parameter.

Potential theory was selected as a candidate methodology on the basis of its success to markedly improve aircraft efficiency at supersonic speeds, the ability of linear theory to predict the aerodynamic characteristics of slender vehicles at moderate hypersonic speeds (figure 1) and its successful use by Tsien in deriving the hypersonic similarity rule. The systematic extension of first order theory proposed by Van Dyke (1) was specifically chosen for further study on the basis of its ability to approximate exact two dimensional and conical flow results. See figures 2 and 3.

Hypersonic small disturbance theory was selected as a second candidate methodology in recognition of the progressive non-isentropic behavior of the flow as the value of the hypersonic similarity parameter increases. Finite difference analysis of this approximation by Gunness (2) indicated that the solution was essentially as complex as that for the full Euler equations and

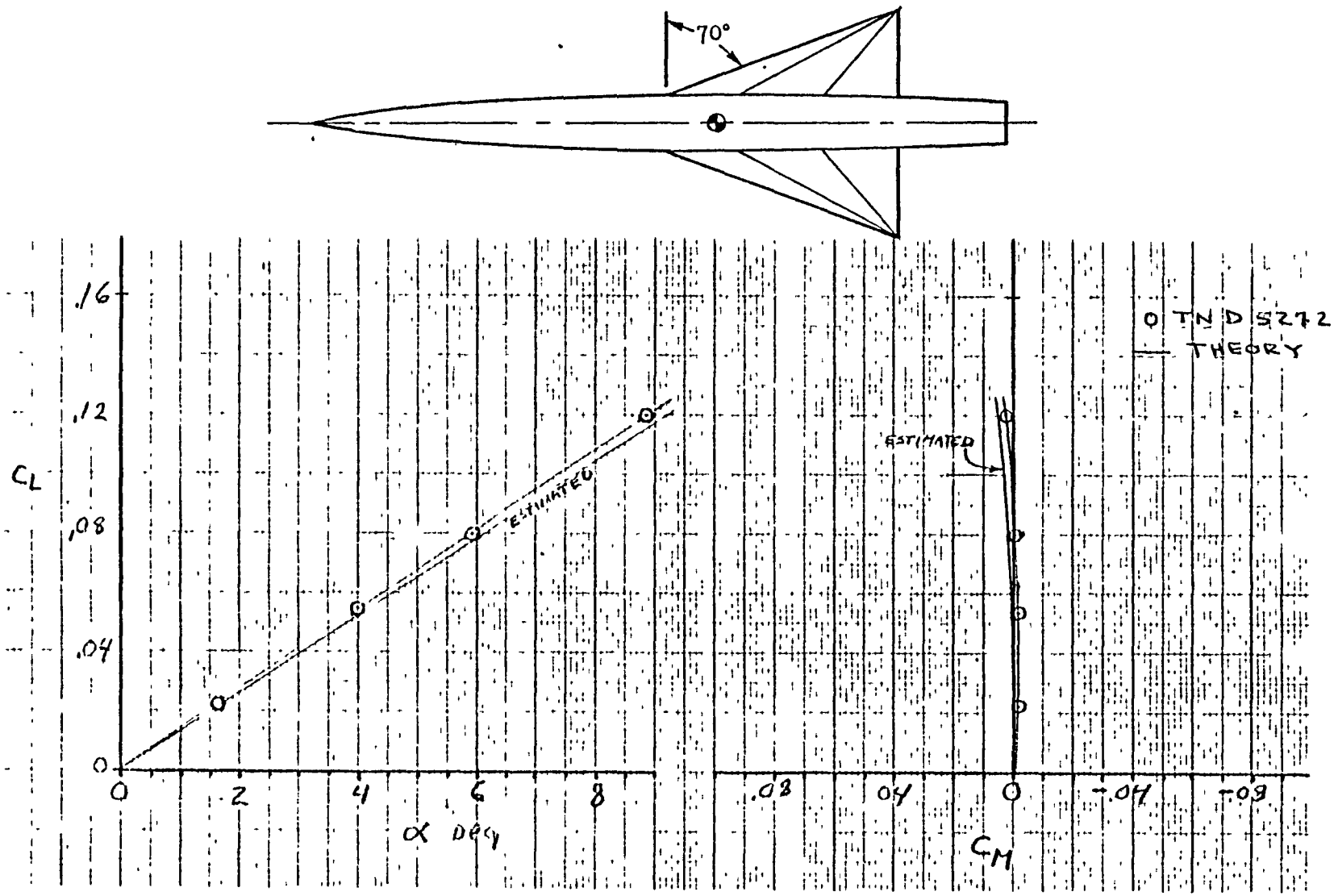

a) Wing-Body

Figure 1. Representative Comparison Between Linear Theory and Measurement at $M_\infty = 5.31$

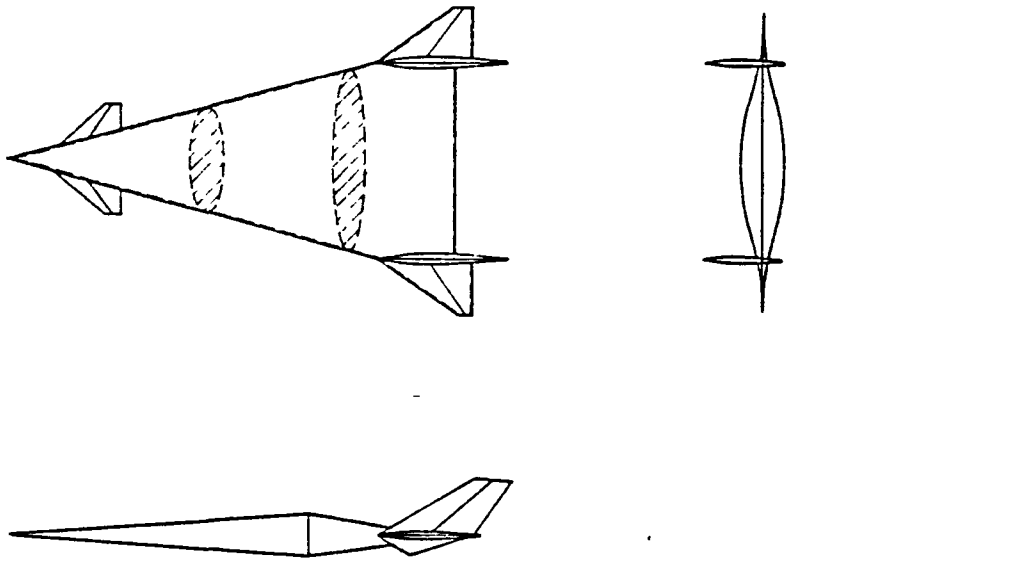

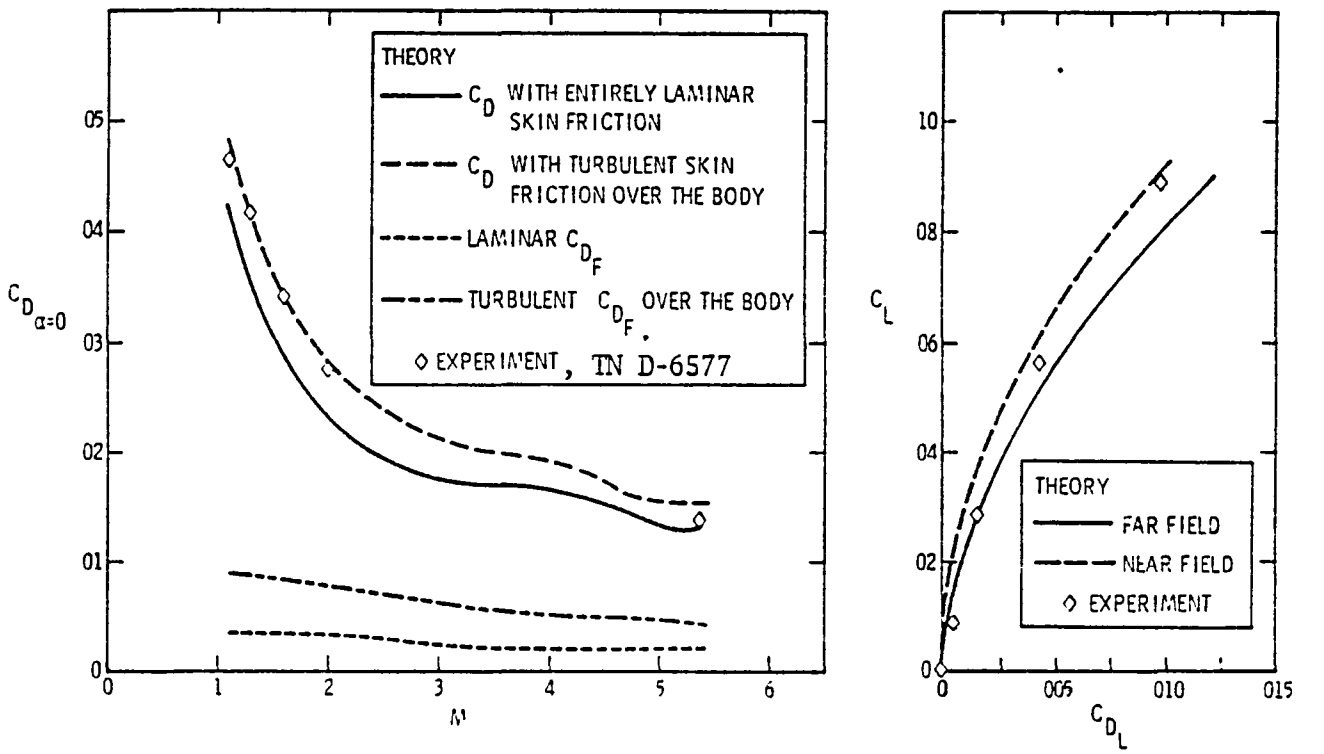

b) All Body Configuration

Figure 1. Concluded

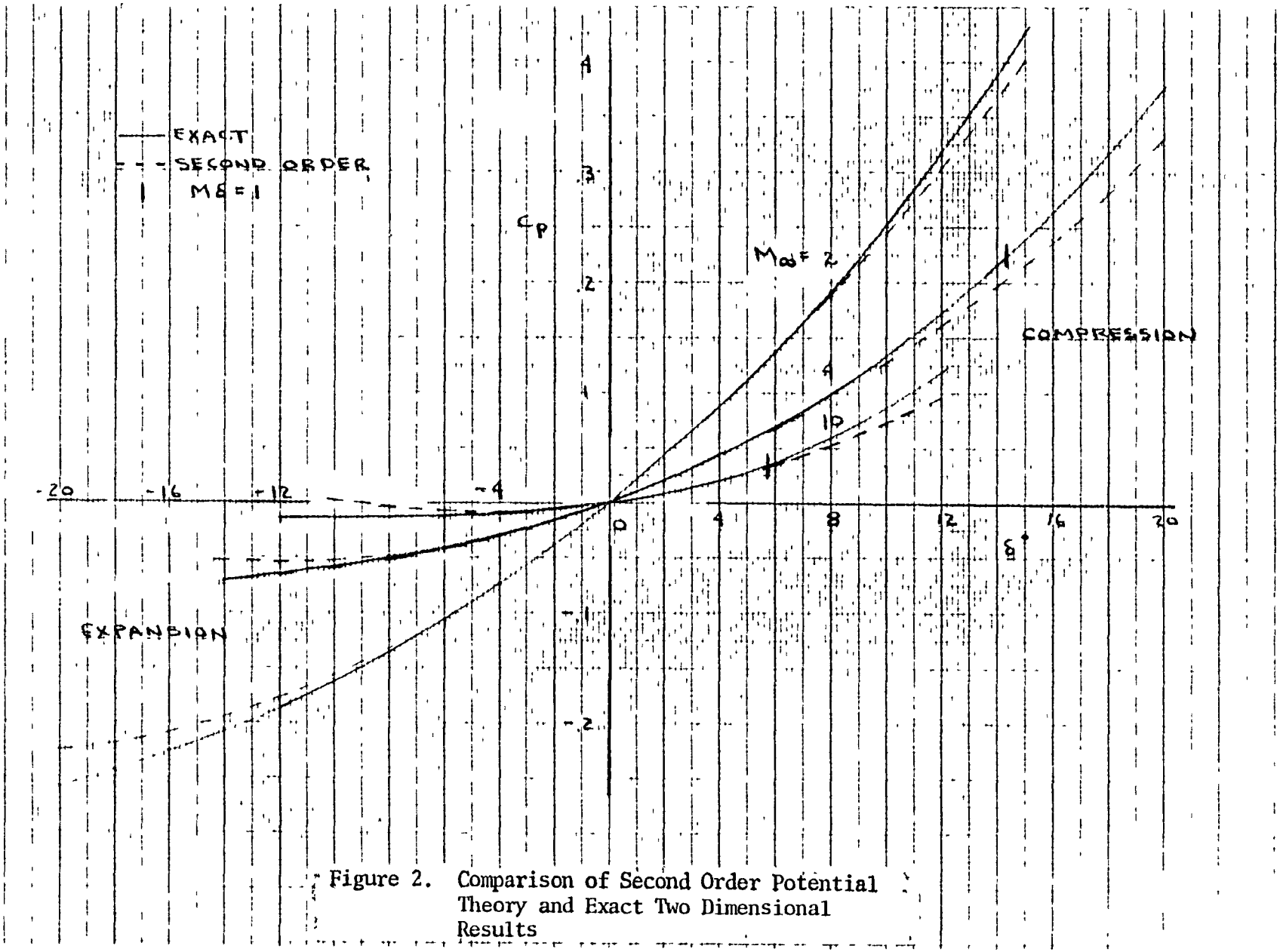

Figure 2. Comparison of Second Order Potential Theory and Exact Two Dimensional Results

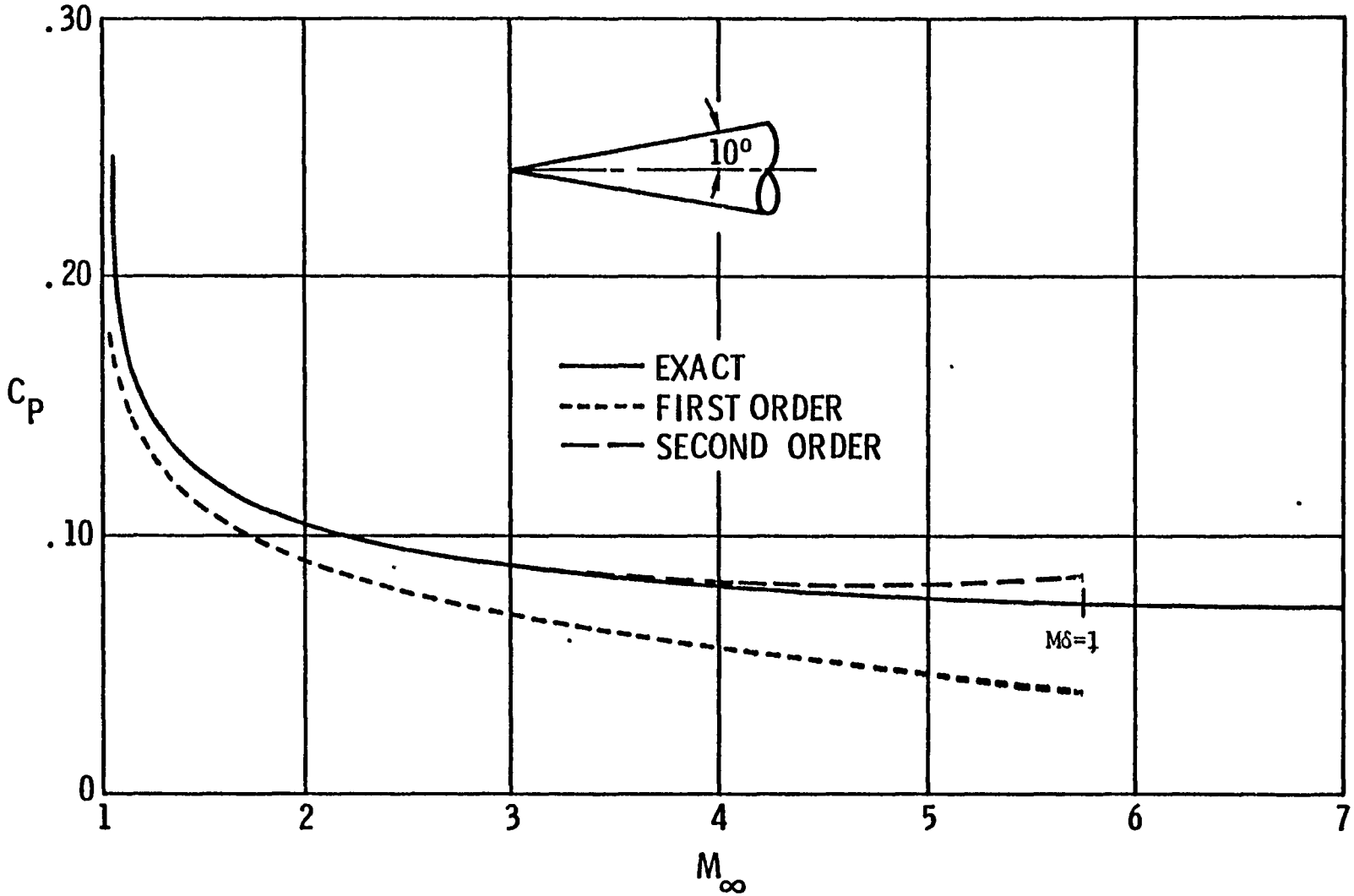

Figure 3. Comparison of First and Second Order Potential Theory with Exact Solution for 10° Cone at Zero Incidence

thus would not be particularly responsive to preliminary design level of effort. Conservation law forms of the equation of motion applied over finite volumes will be examined as an alternative means of developing a solution. Integral theorems for predicting the forces and moments will be derived and evaluated for the rapid evaluation of gross aerodynamic characteristics. Simple variations of the flow properties through the shock layer will be utilized.

4. SECOND ORDER POTENTIAL FORMULATION

The equations for the inviscid flow of a perfect fluid are:

continuity $\quad \nabla\cdot(\rho\vec{u}) = 0$

momentum $\quad \frac{1}{2}\nabla(\vec{u}\cdot\vec{u}) = -\frac{1}{\rho}\nabla p + \vec{u}\times(\nabla\times\vec{u})$

energy $\quad C_p T + \frac{1}{2}\vec{u}\cdot\vec{u} = C_p T_\infty + \frac{1}{2}(U_\infty^2 + W_\infty^2)$

assume that at $\infty \qquad \vec{u} = U_\infty \vec{e}_x + W_\infty \vec{e}_z$

and since $\quad C_p = \frac{\gamma R}{\gamma - 1} \qquad a^2 = \gamma R T$

the energy equation becomes $\quad a^2 = a_\infty^2 + \frac{\gamma-1}{2}\left[(U_\infty^2 + W_\infty^2) - (\vec{u}\cdot\vec{u})\right]$

if $\quad \nabla\times\vec{u} = \nabla s = 0 \qquad$ since $\quad a^2 = \left(\frac{\partial p}{\partial \rho}\right)_s$

the momentum equation becomes $\quad \frac{1}{2}\nabla(\vec{u}\,\vec{u}) = -\frac{1}{\rho}\nabla p = -\frac{a^2}{\rho}\nabla\rho$

The continuity equation can be written in the form

$$a^2\nabla\cdot\vec{u} + \frac{a^2}{\rho}\nabla\rho\cdot\vec{u} = 0$$

or substituting from the momentum and energy equations

$$\left\{a_\infty^2 + \frac{\gamma-1}{2}\left[(U_\infty^2 + W_\infty^2) - (\vec{u}\,\vec{u})\right]\right\}(\nabla\cdot\vec{u}) = \frac{1}{2}\nabla(\vec{u}\,\vec{u})\cdot\vec{u}$$

Since we have assumed $\nabla \times \vec{u} = 0$ we can write (see figure 4)

$$u_1 = U_\infty + \Phi_x$$

$$u_2 = \Phi_y$$

$$u_3 = W_\infty + \Phi_z$$

$$\vec{u} = (u_1, u_2, u_3) \qquad \Phi_x = \frac{\partial \Phi}{\partial x}, \quad \Phi_y = \frac{\partial \Phi}{\partial y}, \quad \Phi_z = \frac{\partial \Phi}{\partial z}$$

then

$$\left\{ a_\infty^2 - \frac{\gamma-1}{2}\left[2(\Phi_x U_\infty + \Phi_z W_\infty) + \Phi_x^2 + \Phi_y^2 + \Phi_z^2 \right] \right\} (\Phi_{xx} + \Phi_{yy} + \Phi_{zz})$$

$$= \left\{ (U_\infty + \Phi_x)\frac{\partial}{\partial x} + \Phi_y \frac{\partial}{\partial y} + (W_\infty + \Phi_z)\frac{\partial}{\partial z} \right\} \left\{ \Phi_x U_\infty + \Phi_z W_\infty + \frac{1}{2}(\Phi_x^2 + \Phi_y^2 + \Phi_z^2) \right\}$$

Now we assume small perturbations and introduce a small parameter ϵ, as well as an angle of attack $\epsilon \alpha_\infty$

let

$$W_\infty = \alpha_\infty \epsilon U_\infty$$

$$\Phi = \sqrt{U_\infty^2 + W_\infty^2}\, \phi = U_\infty \sqrt{1 + \alpha_\infty^2 \epsilon^2}\, \phi$$

$$a_\infty^2 M_\infty^2 = U_\infty^2 + W_\infty^2 = U_\infty^2 (1 + \alpha_\infty^2 \epsilon^2)$$

then

$$\left\{ \sqrt{1+\alpha_\infty^2\epsilon^2} - \frac{\gamma-1}{2} M_\infty^2 \left[2(\phi_x + \alpha_\infty \epsilon \phi_z) + \phi_x^2 + \phi_y^2 + \phi_z^2 \right] \right\} (\phi_{xx} + \phi_{yy} + \phi_{zz})$$

$$= M_\infty^2 \left\{ (1 + \phi_x \sqrt{1+\alpha_\infty^2\epsilon^2}) \frac{\partial}{\partial x} \left[\frac{1}{\sqrt{1+\alpha_\infty^2\epsilon^2}} (\phi_x + \alpha_\infty \epsilon \phi_z) + \frac{1}{2}(\phi_x^2 + \phi_y^2 + \phi_z^2) \right] \right.$$

$$+ \phi_y \sqrt{1+\alpha_\infty^2\epsilon^2}\, \frac{\partial}{\partial y} \left[\frac{1}{\sqrt{1+\alpha_\infty^2\epsilon^2}} (\phi_x + \alpha_\infty \epsilon \phi_z) + \frac{1}{2}(\phi_x^2 + \phi_y^2 + \phi_z^2) \right]$$

$$\left. + (\alpha_\infty \epsilon + \phi_z \sqrt{1+\alpha_\infty^2\epsilon^2}) \frac{\partial}{\partial z} \left[\frac{1}{\sqrt{1+\alpha_\infty^2\epsilon^2}} (\phi_x + \alpha_\infty \epsilon \phi_z) + \frac{1}{2}(\phi_x^2 + \phi_y^2 + \phi_z^2) \right] \right\}$$

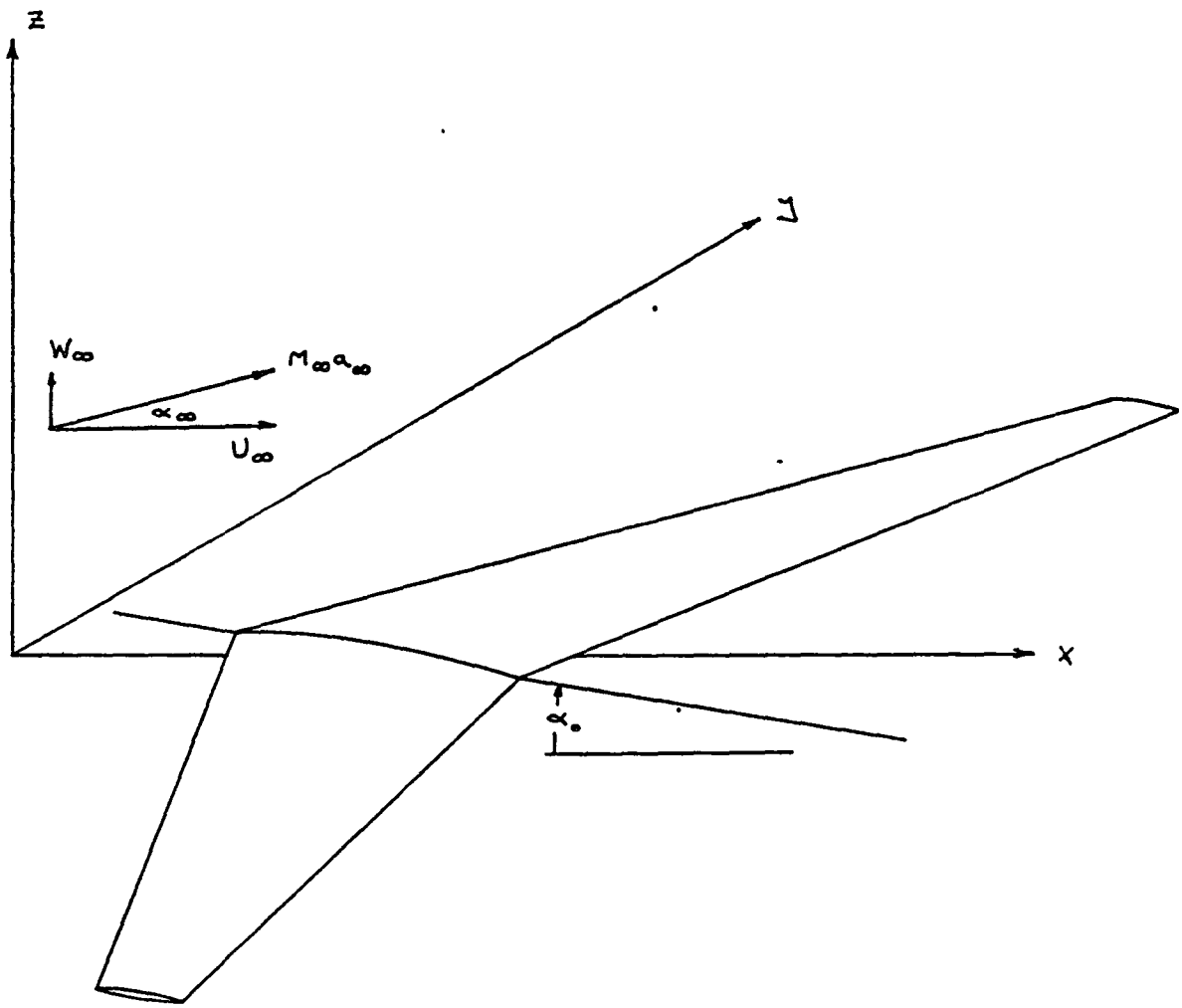

Figure 4. Coordinate System Notation

or

$$\sqrt{1+\alpha_\infty^2\epsilon^2}\left\{\left[1-\frac{M_\infty^2}{(1+\alpha_\infty^2\epsilon^2)}\right]\phi_{xx}+\phi_{yy}+\left[1-\frac{\alpha_\infty^2\epsilon^2 M_\infty^2}{(1+\alpha_\infty^2\epsilon^2)}\right]\phi_{zz}\right\}-2M_\infty^2\frac{\alpha_\infty\epsilon}{\sqrt{1+\alpha_\infty^2\epsilon^2}}\phi_{zx}$$

$$= M_\infty^2\left\{\frac{\gamma-1}{2}\left[2(\phi_x+\alpha_\infty\epsilon\phi_z)+\phi_x^2+\phi_y^2+\phi_z^2\right]\left[(1-M_\infty^2)\phi_{xx}+\phi_{yy}+\phi_{zz}\right]\right.$$

$$+\frac{\gamma-1}{2}\left[2(\phi_x+\alpha_\infty\epsilon\phi_z)+\phi_x^2+\phi_y^2+\phi_z^2\right]M_\infty^2\phi_{xx}$$

$$+\left[\phi_x\frac{\partial}{\partial x}+\phi_y\frac{\partial}{\partial y}+\phi_z\frac{\partial}{\partial z}\right](\phi_x+\alpha_\infty\epsilon\phi_z)+\frac{1}{2}\frac{\partial}{\partial x}(\phi_x^2+\phi_y^2+\phi_z^2)$$

$$\left.+\sqrt{1+\alpha_\infty^2\epsilon^2}\left[\phi_x\frac{\partial}{\partial x}+\phi_y\frac{\partial}{\partial y}+\left(\frac{\alpha_\infty\epsilon}{\sqrt{1+\alpha_\infty^2\epsilon^2}}+\phi_z\right)\frac{\partial}{\partial z}\right](\phi_x^2+\phi_y^2+\phi_z^2)\right\}$$

now let $\phi = \epsilon\phi^{(1)} + \epsilon^2\phi^{(2)} + \cdots$

with the corresponding perturbation velocities

Substituting into the above equation and equating the coefficients of each power of ϵ we obtain the equations for the perturbation potentials.

The first order equation is:

$$(1-M_\infty^2)\phi^{(1)}_{xx}+\phi^{(1)}_{yy}+\phi^{(1)}_{zz}=0$$

The second order equation is:

$$(1-M_\infty^2)\phi^{(2)}_{xx}+\phi^{(2)}_{yy}+\phi^{(2)}_{zz}=M_\infty^2\frac{\partial}{\partial x}\left\{\left[1+\frac{\gamma-1}{2}M_\infty^2\right]\phi_x^{(1)^2}+\phi_y^{(1)^2}+(\phi_z^{(1)}+\alpha_\infty)^2\right\}$$

For a planar problem the solution may be broken into lifting and thickness solutions for each order. Denoting a subscript σ for the thickness and Γ for the lift the equations become:

first order

$$(1-M_\infty^2)\phi^{(1)}_{\Gamma_{xx}}+\phi^{(1)}_{\Gamma_{yy}}+\phi^{(1)}_{\Gamma_{zz}}=0$$

$$(1-M_\infty^2)\phi^{(1)}_{\sigma_{xx}}+\phi^{(1)}_{\sigma_{yy}}+\phi^{(1)}_{\sigma_{zz}}=0$$

second order

$$(1-M_\infty^2)\phi^{(2)}_{\Gamma_{xx}}+\phi^{(2)}_{\Gamma_{yy}}+\phi^{(2)}_{\Gamma_{zz}}=2M_\infty^2\frac{\partial}{\partial x}\left\{\left[1+\frac{\gamma-1}{2}M_\infty^2\right]\phi^{(1)}_{\sigma_x}\phi^{(1)}_{\Gamma_x}+\phi^{(1)}_{\sigma_y}\phi^{(1)}_{\Gamma_y}+\phi^{(1)}_{\sigma_z}(\phi^{(1)}_{\Gamma_z}+\alpha_\infty)\right\}$$

$$(1-M_\infty^2)\phi^{(2)}_{\sigma_{xx}}+\phi^{(2)}_{\sigma_{yy}}+\phi^{(2)}_{\sigma_{zz}}=M_\infty^2\frac{\partial}{\partial x}\left\{\left[1+\frac{\gamma-1}{2}M_\infty^2\right](\phi^{(1)^2}_{\sigma_x}+\phi^{(1)^2}_{\Gamma_x})+(\phi^{(1)^2}_{\sigma_y}+\phi^{(1)^2}_{\Gamma_y})+[\phi^{(1)^2}_{\sigma_z}+(\phi^{(1)}_{\Gamma_z}+\alpha_\infty)^2]\right\}$$

If $\vec{n}$ is the local normal to the surface of an object placed in the flow, then the boundary condition is:

$$\left\{ \frac{1}{\sqrt{1+\alpha_\infty^2\epsilon^2}} (\vec{e}_x + \alpha_\infty \epsilon \vec{e}_z) + \vec{u} \right\} \cdot \vec{n} = 0$$

where $\vec{u}$ is the dimensionless perturbation velocity, $\vec{u} = (\phi_x, \phi_y, \phi_z)$

If the surface is of the form $z = \epsilon Z(x,y)$

then $$\vec{n} \sqrt{1 + \left[\left(\frac{\partial Z}{\partial x}\right)^2 + \left(\frac{\partial Z}{\partial y}\right)^2\right]\epsilon^2} = -\epsilon \frac{\partial Z}{\partial x} \vec{e}_x - \epsilon \frac{\partial Z}{\partial y} \vec{e}_y + \vec{e}_z$$

and therefore

$$\epsilon \frac{\partial}{\partial x} Z(x,y) \left\{ \frac{1}{\sqrt{1+\alpha_\infty^2\epsilon^2}} + \phi_x[x, y, \epsilon Z(x,y)] \right\} + \epsilon \frac{\partial}{\partial y} Z(x,y)\, \phi_y[x, y, \epsilon Z(x,y)]$$

$$= \phi_z[x, y, \epsilon Z(x,y)] + \frac{\alpha_\infty \epsilon}{\sqrt{1+\alpha_\infty^2\epsilon^2}}$$

Now introduce the perturbation velocity expansion

$$\phi = \epsilon \phi^{(1)} + \epsilon^2 \phi^{(2)} + \cdots$$

$$u = \phi_x = \epsilon u^{(1)} + \epsilon^2 u^{(2)} + \cdots$$

$$v = \phi_y = \epsilon v^{(1)} + \epsilon^2 v^{(2)} + \cdots$$

$$\omega = \phi_z = \epsilon \omega^{(1)} + \epsilon^2 \omega^{(2)} + \cdots$$

and expand from the Z = 0 plane

$$u[x, y, \epsilon Z(x,y)] = \epsilon u^{(1)}[x, y, \epsilon Z(x,y)] + \epsilon^2 u^{(2)}[x, y, \epsilon Z(x,y)] + \cdots$$

$$= \epsilon u^{(1)}(x, y, 0) + \epsilon^2 \left[u^{(2)}(x, y, 0) + Z(x,y) \frac{\partial}{\partial z} u^{(1)}(x, y, 0) \right] + \cdots$$

$$= \epsilon u^{(1)}(x, y, 0) + \epsilon^2 \left[u^{(2)}(x, y, 0) + Z(x,y) \frac{\partial}{\partial x} \omega^{(1)}(x, y, 0) \right] + \cdots$$

$$\omega[x, y, \epsilon Z(x,y)] = \epsilon \omega^{(1)}(x, y, 0) + \epsilon^2 \left[\omega^{(2)}(x, y, 0) + Z(x,y) \frac{\partial}{\partial z} \omega^{(1)}(x, y, 0) \right] + \cdots$$

Equating powers of ϵ we obtain the boundary conditions for the various orders of the perturbation velocities at the Z = 0 plane,

$$\omega^{(1)}(x,y,0) = \frac{\partial}{\partial x} Z(x,y) - \alpha_\infty$$

$$\omega^{(2)}(x,y,0) = \frac{\partial}{\partial x} Z(x,y)\, u^{(1)}(x,y,0) + \frac{\partial}{\partial y} Z(x,y)\, v^{(1)}(x,y,0) - Z(x,y) \frac{\partial}{\partial z} \omega^{(1)}(x,y,0)$$

From the first order equation.

$$-\frac{\partial}{\partial z} \omega^{(1)}(x,y,0) = (1-M_\infty^2) \frac{\partial}{\partial x} u^{(1)}(x,y,0) + \frac{\partial}{\partial y} v^{(1)}(x,y,0)$$

Then assuming an upper and lower surface

$$z = 0^+ \qquad Z(x,y) = C(x,y) + T(x,y) - \alpha_0 (x - x_{00})$$

$$z = 0^- \qquad Z(x,y) = C(x,y) - T(x,y) - \alpha_0 (x - x_{00})$$

the following equations result.

$$\frac{1}{2}\left[\omega^{(1)}(x,y,0^+) + \omega^{(1)}(x,y,0^-)\right] = \frac{\partial}{\partial x} C(x,y) - \alpha_0 - \alpha_\infty$$

$$\frac{1}{2}\left[\omega^{(1)}(x,y,0^+) - \omega^{(1)}(x,y,0^-)\right] = \frac{\partial}{\partial x} T(x,y)$$

$$\begin{aligned}\frac{1}{2}\left[\omega^{(2)}(x,y,0^+) \pm \omega^{(2)}(x,y,0^-)\right] &= \left[\frac{\partial}{\partial x} C(x,y) - \alpha_0\right] \frac{1}{2}\left[u^{(1)}(x,y,0^+) \pm u^{(1)}(x,y,0^-)\right] \\ &+ \frac{\partial}{\partial x} T(x,y)\, \frac{1}{2}\left[u^{(1)}(x,y,0^+) \mp u^{(1)}(x,y,0^-)\right] \\ &+ \frac{\partial}{\partial y} C(x,y)\, \frac{1}{2}\left[v^{(1)}(x,y,0^+) \pm v^{(1)}(x,y,0^-)\right] \\ &+ \frac{\partial}{\partial y} T(x,y)\, \frac{1}{2}\left[v^{(1)}(x,y,0^+) \mp v^{(1)}(x,y,0^-)\right] \\ &+ (1-M_\infty^2)\left[C(x,y) - \alpha_0 (x - x_{00})\right] \frac{\partial}{\partial x} \frac{1}{2}\left[u^{(1)}(x,y,0^+) \pm u^{(1)}(x,y,0^-)\right] \\ &+ (1-M_\infty^2)\, T(x,y)\, \frac{\partial}{\partial x} \frac{1}{2}\left[u^{(1)}(x,y,0^+) \mp u^{(1)}(x,y,0^-)\right] \\ &+ \left[C(x,y) - \alpha_0 (x - x_{00})\right] \frac{\partial}{\partial y} \frac{1}{2}\left[v^{(1)}(x,y,0^+) \pm v^{(1)}(x,y,0^-)\right] \\ &+ T(x,y)\, \frac{\partial}{\partial y} \frac{1}{2}\left[v^{(1)}(x,y,0^+) \mp v^{(1)}(x,y,0^-)\right]\end{aligned}$$

and since the problem is planar

$$\frac{1}{2}\left[\omega^{(2)}(x,y,0^+) + \omega^{(2)}(x,y,0^-)\right] = \omega^{(2)}_r(x,y,0)$$

$$\frac{1}{2}\left[\omega^{(2)}(x,y,0^+) - \omega^{(2)}(x,y,0^-)\right] = \omega^{(2)}_\sigma(x,y,0)$$

$$\frac{1}{2}\left[u^{(1)}(x,y,0^+) + u^{(1)}(x,y,0^-)\right] = u^{(1)}_\sigma(x,y,0)$$

$$\frac{1}{2}\left[u^{(1)}(x,y,0^+) - u^{(1)}(x,y,0^-)\right] = u^{(1)}_r(x,y,0)$$

$$\frac{1}{2}\left[v^{(1)}(x,y,0^+) + v^{(1)}(x,y,0^-)\right] = v^{(1)}_\sigma(x,y,0)$$

$$\frac{1}{2}\left[v^{(1)}(x,y,0^+) - v^{(1)}(x,y,0^-)\right] = v^{(1)}_r(x,y,0)$$

where Γ and σ refer to velocities due to lifting and source elements. In this form the boundary conditions become:

$$\omega^{(1)}_r(x,y,0) = \frac{\partial}{\partial x}C(x,y) - \alpha_0 - \alpha_\infty$$

$$\omega^{(1)}_\sigma(x,y,0) = \frac{\partial}{\partial x}T(x,y)$$

$$\begin{aligned}\omega^{(2)}_r(x,y,0) = {} & \left[\frac{\partial}{\partial x}C(x,y)-\alpha_0\right]u_\sigma(x,y,0) \\ & + \frac{\partial}{\partial x}T(x,y)\,u_r(x,y,0) \\ & + \frac{\partial}{\partial y}C(x,y)\,v_\sigma(x,y,0) \\ & + \frac{\partial}{\partial y}T(x,y)\,v_r(x,y,0) \\ & + (1-M_\infty^2)\left[C(x,y)-\alpha_0(x-x_{LE})\right]\frac{\partial}{\partial x}u_\sigma(x,y,0) \\ & + (1-M_\infty^2)\,T(x,y)\frac{\partial}{\partial x}u_r(x,y,0) \\ & + \left[C(x,y)-\alpha_0(x-x_{LE})\right]\frac{\partial}{\partial y}v_\sigma(x,y,0) \\ & + T(x,y)\frac{\partial}{\partial y}v_r(x,y,0)\end{aligned}$$

$$\begin{aligned}\omega^{(2)}_\sigma(x,y,0) = {} & \left[\frac{\partial}{\partial x}C(x,y)-\alpha_0\right]u_r(x,y,0) \\ & + \frac{\partial}{\partial x}T(x,y)\,u_\sigma(x,y,0) \\ & + \frac{\partial}{\partial y}C(x,y)\,v_r(x,y,0) \\ & + \frac{\partial}{\partial y}T(x,y)\,v_\sigma(x,y,0) \\ & + (1-M_\infty^2)\left[C(x,y)-\alpha_0(x-x_{LE})\right]\frac{\partial}{\partial x}u_r(x,y,0) \\ & + (1-M_\infty^2)\,T(x,y)\frac{\partial}{\partial x}u_\sigma(x,y,0) \\ & + \left[C(x,y)-\alpha_0(x-x_{LE})\right]\frac{\partial}{\partial y}v_r(x,y,0) \\ & + T(x,y)\frac{\partial}{\partial y}v_\sigma(x,y,0)\end{aligned}$$

The thickness distribution can be written in the following form.

$$T(x,y) = c(y)\,\tau(y)\,t(\xi,y)$$

where

$$\xi = \frac{x - x_{l.e.}(y)}{c(y)} \quad \text{or fraction of chord}$$

$c(y)$ = local chord

$\tau(y)$ = maximum value of t/c

$$\frac{\partial}{\partial y} c(y) = -(T_{l.e.} - T_{t.e.})$$

$$\frac{\partial}{\partial y}\xi = \frac{1}{c(y)}\left\{-T_{l.e.}(y) + \xi\left[T_{l.e.} - T_{t.e.}\right]\right\} = -\frac{1}{c(y)}T$$

where T is the tangent of the sweep of the local constant percent chord line. Therefore.

$$\frac{\partial}{\partial x}T(x,y) = \frac{1}{c(y)}\,c(y)\,\tau(y)\,\frac{\partial}{\partial \xi}t(\xi,y)$$

$$\frac{\partial}{\partial y}T(x,y) = -T\frac{\partial}{\partial x}T(x,y) + \left\{\frac{c'(y)}{c(y)} + \frac{\tau'(y)}{\tau(y)} + \frac{\frac{\partial}{\partial \xi}t(\xi,y)}{t(\xi,y)}\right\}T(x,y)$$

PRESSURE COEFFICIENT

The pressure coefficient is given by the equation

$$C_p = \frac{p - p_\infty}{\frac{1}{2}\rho_\infty U_\infty^2} = \frac{1}{\frac{1}{2}\gamma M_\infty^2}\left\{\frac{p}{p_\infty} - 1\right\}$$

Since to second order the flow is isentropic

$$C_p = \frac{1}{\frac{1}{2}\gamma M_\infty^2}\left\{\left[\frac{T}{T_\infty}\right]^{\frac{\gamma}{\gamma-1}} - 1\right\}$$

$$\gamma R T_\infty + \frac{\gamma-1}{2} U_\infty^2 = \gamma R T + \frac{\gamma-1}{2} U_\infty^2 \left\{\left[\frac{1}{\sqrt{1+\alpha_\infty^2}} + u\right]^2 + v^2 + \left[\frac{\alpha_\infty}{\sqrt{1+\alpha_\infty^2}} + \omega\right]^2\right\}$$

$$1 + \frac{\gamma-1}{2} M_\infty^2 = \frac{T}{T_\infty} + \frac{\gamma-1}{2} M_\infty^2 \left\{\left[\frac{1}{\sqrt{1+\alpha_\infty^2}} - u\right]^2 + v^2 + \left[\frac{\alpha_\infty}{\sqrt{1+\alpha_\infty^2}} + \omega\right]^2\right\}$$

therefore to second order

$$\left[\frac{T}{T_\infty}\right]^{\frac{\gamma}{\gamma-1}} - 1 = \left\{1 - \frac{\gamma-1}{2} M_\infty^2 \left[2u + u^2 + v^2 + (\omega + \alpha_\infty)^2 - \alpha_\infty^2\right]\right\}^{\frac{\gamma}{\gamma-1}} - 1$$

$$= -\frac{\gamma}{2} M_\infty^2 \left[2u + u^2 + v^2 + (\omega+\alpha_\infty)^2 - \alpha_\infty^2\right] + \frac{\gamma}{(\gamma-1)^2} \frac{(\gamma-1)^2}{2!} M_\infty^4 u^2$$

$$C_p = -\left\{2u + (1 - M_\infty^2) u^2 + v^2 + (\omega + \alpha_\infty)^2 - \alpha_\infty^2\right\}$$

These velocities must be evaluated on the surface

$$z = \epsilon Z(x,y) = C(x,y) \pm T(x,y) - \alpha_0 (x - x_{00})$$

$$\epsilon u[x, y, \epsilon Z(x,y)] = \epsilon u^{(1)}(x,y,0) + \epsilon^2 \left[Z(x,y) \frac{\partial}{\partial z} u^{(1)}(x,y,0) + u^{(2)}(x,y,0) \right]$$

$$= \epsilon u^{(1)}(x,y,0) + \epsilon^2 \left[Z(x,y) \frac{\partial}{\partial x} w^{(1)}(x,y,0) + u^{(2)}(x,y,0) \right]$$

Therefore to second order

$$C_p = -2\epsilon u^{(1)}(x,y,0)$$
$$- \epsilon^2 \left\{ 2u^{(2)}(x,y,0) + (1-M_\infty^2)[u^{(1)}(x,y,0)]^2 + [v^{(1)}(x,y,0)]^2 + [w^{(1)}(x,y,0) + \alpha_\infty]^2 \right.$$
$$\left. + 2Z(x,y) \frac{\partial}{\partial x} w^{(1)}(x,y,0) \right\}$$

on the upper and lower surfaces

$$\epsilon^2 Z^{\pm}(x,y) \frac{\partial}{\partial x} w^{(1)}(x,y,0)^{\pm} = [C(x,y) - \alpha_0 (x - x_{00}) \pm T(x,y)] \frac{\partial^2}{\partial x^2} [C(x,y) \pm T(x,y)]$$

$$C_{p_n}(x,y) = \frac{1}{2} [C_p(x,y,0^+) - C_p(x,y,0^-)]$$
$$-2 \left\{ u_n^{(1)}(x,y,0) + u_n^{(2)}(x,y,0) + T(x,y) \frac{\partial^2}{\partial x^2} C(x,y) + [C(x,y) - \alpha_0 (x - x_{00})] \frac{\partial^2}{\partial x^2} T(x,y) \right.$$
$$\left. + (1-M_\infty^2) u_\sigma^{(1)}(x,y,0) u_n^{(1)}(x,y,0) + v_\sigma^{(1)}(x,y,0) v_n^{(1)}(x,y,0) + w_\sigma^{(1)}(x,y,0) [w_n^{(1)}(x,y,0) + \alpha_\infty] \right\}$$

$$C_{p_\sigma}(x,y) = \frac{1}{2} [C_p(x,y,0^+) + C_p(x,y,0^-)]$$
$$= -2 \left\{ u_\sigma^{(1)}(x,y,0) + u_\sigma^{(2)}(x,y,0) + [C(x,y) - \alpha_0 (x - x_{00})] \frac{\partial^2}{\partial x^2} C(x,y) + T(x,y) \frac{\partial^2}{\partial x^2} T(x,y) \right\}$$
$$- (1-M_\infty^2)[u_\sigma^{(1)}(x,y,0)]^2 - [v_\sigma^{(1)}(x,y,0)]^2 - [w_\sigma^{(1)}(x,y,0)]^2$$
$$- (1-M_\infty^2)[u_n^{(1)}(x,y,0)]^2 - [v_n^{(1)}(x,y,0)]^2 - [w_n^{(1)}(x,y,0) + \alpha_\infty]^2 + \alpha_\infty^2$$

Three different approaches were examined for solving the supersonic second order potential equation of motion. They were

a) Discovery of a particular integral for three dimensional flow

b) Source volume analysis

c) Finite difference analysis

4.1. Particular Integral Existence

Second order theory expands the exact potential Φ in terms of thickness (δ) or angle of attack α

$$\Phi = U\left\{ x + \delta\phi^{(1)} + \delta^2\phi^{(2)} + \cdots \right\}$$

$\phi^{(1)}$, satisfies the usual linearized theory, $\phi^{(2)}$ is the second order correction and satisfies a forced equation

$$\Box^2\phi^{(1)} = \phi^{(1)}_{yy} + \phi^{(1)}_{zz} - \beta^2\phi^{(1)}_{xx} = 0 \qquad \beta^2 = M_\infty^2 - 1$$

$$\Box^2\phi^{(2)} = \phi^{(2)}_{yy} + \phi^{(2)}_{zz} - \beta^2\phi^{(2)}_{xx} = M_\infty^2 \frac{\partial}{\partial x}\left\{\left[1 + \frac{\gamma-1}{2}M_\infty^2\right]\phi_x^{(1)2} + \phi_y^{(1)2} + \phi_z^{(1)2}\right\} = f$$

An algebraic integral would have the form

$$\phi^{(2)} = F\left(x, y, z, \phi^{(1)}, \phi^{(1)}_x, \phi^{(1)}_y, \phi^{(1)}_z\right) \qquad \Box^2\phi^{(2)} = \Box^2 F = f \qquad (1)$$

Van Dyke has found such integrals for 2-D and axisymmetry. However, a straightforward study of conditions on F in the general case shows that no such algebraic integral can exist. To do this consider $\phi^{(1)} = \psi$ given; then for example

$$\phi^{(2)}_x = F_x + F_\psi\psi_x + F_{\psi_x}\psi_{xx} + F_{\psi_y}\psi_{yx} + F_{\psi_z}\psi_{zx}$$

Comparing like terms on the RHS and LHS of (1) gives a set of relations with no solution F.

4.2. Source Volume Analysis

For a thick lifting wing system, the first order solution may be obtained using a Woodward type finite element. Using this scheme the entire planform is divided into quadrilateral panels having two streamwise edges and placed in the mean chord plane. Each panel has a distribution of source and vorticity strength to account for the effects of thickness and lift. The source and vorticity singularity strengths are determined by satisfying the boundary conditions at a set of control points. When these strengths are known the first order velocities may be computed anywhere in the field. In particular the value of

$$\rho(x,y,z) = M_\infty^2 \frac{\partial}{\partial x}\left\{ \left[1 + \frac{\gamma-1}{2} M_\infty^2\right] \phi_x^{(1)^2} + \phi_y^{(1)^2} + \left(\phi_z^{(1)} + \kappa_\infty\right)^2 \right\}$$

used in the solution of the second order velocity potential can be calculated anywhere. This function is computed at the centroid of a set of source volumes distributed throughout space, giving the strengths of these source volumes.

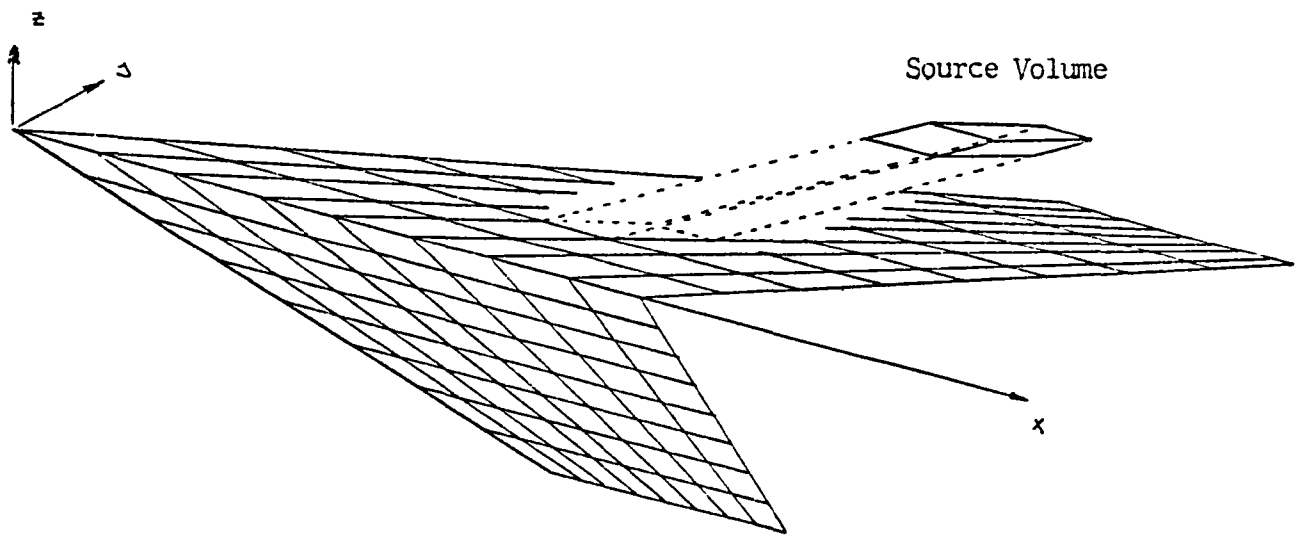

Using the influence equations for these source volumes, the velocities induced back on the planform from the spatial source distribution may be calculated. The source volumes have the property that:

$$\Box^2 \Phi = \begin{cases} \rho \text{ within volume} \\ 0 \text{ outside volume} \end{cases} \qquad \rho \text{ is a constant}$$

The source volumes to be considered have top and bottom faces composed of two identical quadrilateral panels separated by a distance Δz. The panels have two streamwise edges and swept leading and trailing edges. The corresponding corners of the panels lie along lines $x - \tau z = \text{const}$. Therefore the two side faces have two streamwise edges and leading and trailing edge sweeps of magnitude τ.

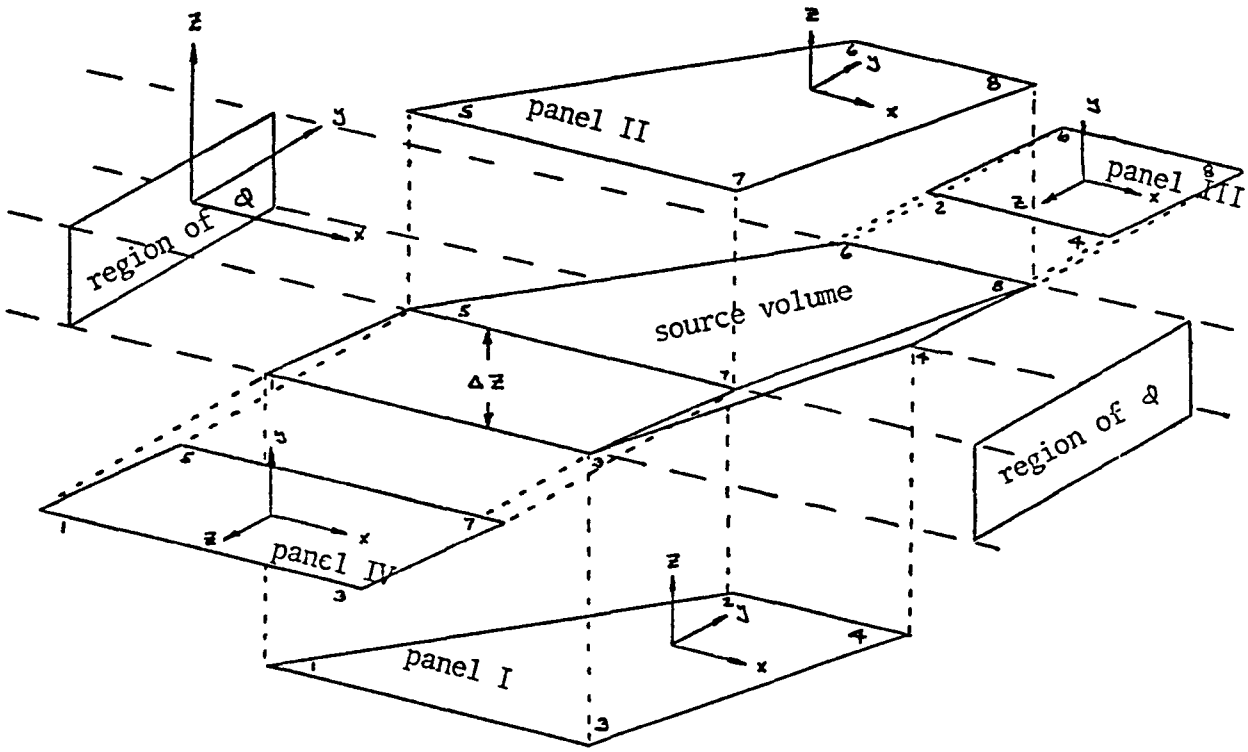

The velocity potential Φ induced by this volume is such that

$$(1-M_\infty^2)\,\Phi_{xx} + \Phi_{yy} + \Phi_{zz} = \begin{cases} \sigma & \text{inside the volume} \\ 0 & \text{outside the volume} \end{cases}$$

where $$\Phi = \phi_I - \phi_{II} + \phi_{III} - \phi_{IV} + \varphi$$

The ϕ_i refer to the velocity potential contributions from each of the four panels which form the top, bottom and sides of the volume, and φ is an additional term which is nonzero only within the volume formed by the four planes of the top, bottom and side faces.

The ϕ for each of the four panel faces is composed of a contribution from each corner, each corresponding to an integration limit.

$$\phi = \phi_1 - \phi_2 - \phi_3 + \phi_4$$

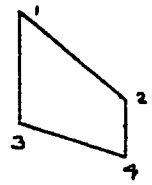

On any given panel or face, at a corner with an edge having a sweep T and where τ is the sweep of the edge at the corresponding corner on the adjacent panel

$$\phi = \frac{\sigma}{[T^2+\tau^2+\beta^2]}[\phi_v + \tau\phi_s] \qquad \beta^2 = 1 - M_\infty^2 \qquad k = \begin{cases} 1 & M_\infty^2 < 1 \\ 2 & M_\infty^2 > 1 \end{cases}$$

$$R^2 = x^2 + \beta^2(y^2+z^2)$$

where

$$u_v = \frac{\partial\phi_v}{\partial x} = \frac{k}{2\pi}\left\{ Tzf_1 - (T^2+\beta^2)zf_2 + (x-Ty)f_3 \right\}$$

$$v_v = \frac{\partial\phi_v}{\partial y} = \frac{k}{2\pi}\left\{ -z(T^2+\tfrac{1}{2}\beta^2)f_1 + Tz(T^2+\beta^2)f_2 - T(x-Ty)f_3 - \frac{1}{2}\frac{zxR}{y^2+z^2} \right\}$$

$$w_v = \frac{\partial\phi_v}{\partial z} = \frac{k}{2\pi}\left\{ [T(x-Ty)-\tfrac{1}{2}\beta^2 y]f_1 - (T^2+\beta^2)(x-Ty)f_2 - (T^2+\beta^2)zf_3 + \left[\frac{1}{2}\frac{xy}{(y^2+z^2)} - T\right]R \right\}$$

$$u_s = \frac{\partial\phi_s}{\partial x} = -\frac{k}{2\pi}\left\{ yf_1 + (x-Ty)f_2 + zf_3 \right\}$$

$$v_s = \frac{\partial\phi_s}{\partial y} = -\frac{k}{2\pi}\left\{ (x-Ty)f_1 - T(x-Ty)f_2 - Tzf_3 - R \right\}$$

$$w_s = \frac{\partial\phi_s}{\partial z} = -\frac{k}{2\pi}\left\{ Tzf_1 - (T^2+\beta^2)zf_2 + (x-Ty)f_3 \right\}$$

$$f_1 = \frac{1}{2}\log\frac{R+x}{R-x} \qquad f_2 = \frac{1}{\sqrt{T^2+\beta^2}}\frac{1}{2}\log\frac{\sqrt{T^2+\beta^2}\,R + (Tx+\beta^2 y)}{\sqrt{T^2+\beta^2}\,R - (Tx+\beta^2 y)} \qquad f_3 = \tan^{-1}\frac{zR}{xy - T(y^2+z^2)}$$

The velocity potentials ϕ_v and ϕ_s have the property that

$$\frac{\partial\phi_v}{\partial x} = \phi_{v_o} \qquad \frac{\partial\phi_s}{\partial x} = \phi_{s_o}$$

where ϕ_{v_o} and ϕ_{s_o} are the velocity potentials induced by panel corners on panels having constant vorticity, and constant source strength respectively.

The additional term φ is such that

outside V_x $\qquad \varphi = 0$

inside V_x

$$\frac{\partial \varphi}{\partial x} = \frac{\sigma}{[\tau^2+\tau^2+\beta^2]} \frac{k}{2} \left\{ |\xi_1| - |\xi_2| \right\}$$

$$\frac{\partial \varphi}{\partial y} = \frac{-\sigma}{[\tau^2+\tau^2+\beta^2]} \frac{k}{2} \left\{ \tau_1 |\xi_1| - \tau_2 |\xi_2| \right\}$$

$$\frac{\partial \varphi}{\partial z} = \frac{-\sigma}{[\tau^2+\tau^2+\beta^2]} \frac{k}{2} \left\{ \tau_1 |\xi_1| - \tau_2 |\xi_2| \right\}$$

where V_x is the volume determined by the planes comprising the four panels.

and $\qquad m = \tau$

$$\xi_1 = \left[x - \tfrac{1}{4}(x_1+x_2+x_5+x_6)\right] - \tau_1 \left[y - \tfrac{1}{2}(y_1+y_2)\right] - \tau \left[z - \tfrac{1}{2}(z_1+z_2)\right]$$

$$\xi_2 = \left[x - \tfrac{1}{4}(x_3+x_4+x_7+x_8)\right] - \tau_2 \left[y - \tfrac{1}{2}(y_1+y_2)\right] - \tau \left[z - \tfrac{1}{2}(z_1+z_2)\right]$$

where T_1 and T_2 are the leading and trailing edge sweeps of panel I. Therefore ξ_1 and ξ_2 are the x distance behind a point on the front and rear faces of the source volume which has the same y and z values as the point being influenced. For supersonic flow ξ_1 and ξ_2 are zero upstream of their respective faces.

Each corner yields a contribution to the volume influence coefficient from each of two adjacent faces. This fact may be used to write the influence equations for a given corner in a different form. On a panel whose normal is in the z direction the influence coefficients yield.

$$\begin{Bmatrix} u \\ v \\ w \end{Bmatrix} = \vec{F}(x, y, z, T, \tau)$$

On the adjacent face, with normal in the y direction, the corresponding influence is

$$\begin{Bmatrix} u \\ w \\ -v \end{Bmatrix} = -\vec{F}(x, z, -y, \tau, -T)$$

where (x,y,z,T,τ) and (u,v,w) are both expressed in the coordinate system of the face with the normal in the z direction. Therefore, the equivalent set of influence coefficients for a corner of a given face are:

$$u = \frac{\sigma k}{2\pi\epsilon}\left\{ - z\epsilon f_2 - \xi(\tau f_2 - f_3) \right\}$$

$$v = \frac{\sigma k}{2\pi\epsilon}\left\{ - \epsilon z f_1 + T z \epsilon f_2 + T\xi(\tau f_2 - f_3) \right\}$$

$$w = \frac{\sigma k}{2\pi\epsilon}\left\{ - \epsilon\xi f_2 + \tau\xi(\tau f_2 - f_3) - z\epsilon f_3 \right\}$$

$$\epsilon = T^2 + \tau^2 + \beta^2 \qquad \xi = x - Ty - \tau z$$

The (x,y,z,t,τ) and (u,v,w) are now expressed in a coordinate system whose origin is at the corner and whose z axis is in the direction of the normal to the face.

As $\epsilon = \tau^2 + \tau' + \beta^2 \to 0$ the quantity $(\tau f_2 - f_3)$ will cancel with a corresponding term on the adjacent face and the velocities become indeterminate. By expanding about $\epsilon = 0$ the following form for the velocity influence coefficients results.

$$u = \frac{\sigma k}{2\pi}\left\{ \quad - z f_2 - \frac{1}{2}\left[T\xi f_2 - \frac{1}{2}R \right]\frac{1}{\tau T} \right\}$$

$$V = \frac{\sigma k}{2\pi}\left\{ - z f_1 + T z f_2 + \frac{1}{2}\left[T\xi f_2 - R \right]\frac{1}{\tau} \right\}$$

$$\omega = \frac{\sigma k}{2\pi}\left\{ \quad - \frac{1}{2}\xi f_2 - z f_3 \right\}$$

This form is indeterminate when T = 0 and must be rewritten in the following form.

$T = 0 \qquad \epsilon = 0$

$$u = \frac{\sigma k}{2\pi}\left\{ \quad - z f_2 - \frac{1}{2}\,\xi F_2\,\frac{1}{\tau} \right\}$$

$$V = \frac{\sigma k}{2\pi}\left\{ - z f_1 + T z f_2 + \frac{1}{2}\left[T\xi f_2 - R \right]\frac{1}{\tau} \right\}$$

$$\omega = \frac{\sigma k}{2\pi}\left\{ \quad - \frac{1}{2}\xi f_2 - z f_3 \right\}$$

$\tau = 0 \qquad \epsilon = 0$

$$u = \frac{\sigma k}{2\pi}\left\{ \quad - z f_2 + \frac{1}{2}\,z R\,\frac{1}{3T} \right\}$$

$$V = \frac{\sigma k}{2\pi}\left\{ - z f_1 + T z f_2 - \frac{1}{2}\,z R\,\frac{1}{\xi} \right\}$$

$$\omega = \frac{\sigma k}{2\pi}\left\{ \quad - \frac{1}{2}\xi f_2 - z f_3 \right\}$$

This spatial source distribution can then be used to solve for $\phi^{(2)}$.

$$\Box^2 \phi^{(2)} = (1-M_\infty^2)\phi^{(2)}_{xx} + \phi^{(2)}_{yy} + \phi^{(2)}_{zz} = \rho(x,y,z)$$

A solution for $\phi^{(2)}$ can be obtained by using a solution to the equation

$$\Box^2 \phi^{(2)} = 0$$

with the boundary conditions adjusted to cancel the normal velocities induced on the planform by the spatial source distribution, $\rho(x,y,z)$. Therefore $\phi^{(2)}$ on the planform may be obtained by using the same Woodward panel scheme with boundary conditions determined by the normal velocities induced by $\rho(x,y,z)$ and the second order boundary conditions.

A pilot code based on this approach was developed. Computations and comparison with higher order solutions and experiments is presented in section 6.1.

4.3 Finite Difference Analysis

The first and second order theory equations and boundary conditions derived in the previous sections are rewritten here for completeness with a slightly different notation.

First Order

$$\Box\phi_1 = \phi_{1_{yy}} + \phi_{1_{zz}} - \beta^2\phi_{1_{xx}} = 0 \tag{1}$$

with boundary conditions on the body given by

$$\phi_{1_y}(x,0,z) = \frac{\partial F}{\partial(1)}(x,z/b) - a \tag{2}$$

Second Order

$$\Box\phi_2 = \phi_{2_{yy}} + \phi_{2_{zz}} - \beta^2\phi_{2_{xx}} = M_\infty^2 \frac{\partial}{\partial x}\left\{\left(1 + \frac{\gamma-1}{2}M_\infty^2\right)\phi_{1_x}^2 + \phi_{1_y}^2 + \phi_{1_z}^2\right\} \tag{3}$$

with boundary conditions

$$\begin{aligned}\phi_{2_y}(x,0,z) = &\left(\frac{\partial F}{\partial(1)}(x,z/b) - a\right)\phi_{1_x}(x,0,z) \\ &- \left(F(x,z/b) - ax\right)\phi_{1_{yy}}(x,0,z) \\ &+ b^{-1}\,\phi_{1_z}(x,0,z)\,\frac{\partial F}{\partial(2)}(x,z/b)\end{aligned} \tag{4}$$

where $y = \delta F(x,z/b) + \alpha x$ defines the body geometry, and $a \equiv \alpha/\delta$. For a flat plate delta wing, $a = -1$ on the compression side, and $a = 1$ on the expansion side. The angle of attack is α.

The pressure coefficient is computed from

$$C_p \equiv \frac{p-p_\infty}{q_\infty} = -2\delta\phi_{1_x} - \delta^2\left(2\phi_{2_x} - \beta^2\phi_{1_x}^2 + \phi_{1_y}^2 + \phi_{1_z}^2\right). \tag{5}$$

Finite Difference Procedure

In this section two different finite difference procedures are discussed. In one, the velocity potential is determined from a single equation and in the other, the velocities $u = \phi_x$, $v = \phi_y$ and $w = \phi_z$ are computed by treating a system of partial differential equations for these quantities, denoted hereinafter as the systems approach.

Scalar Approach

Equations (1) and (2) are hyperbolic in the x-direction provided $\beta^2 = M_\infty^2 - 1$ is positive. Considering a grid molecule as shown in figure 5, for an explicit finite difference procedure the information at point (i+1,j,k) can be computed based on past information. A simple explicit procedure for Equations (1) and (3) are obtained by central differencing all the terms in the equation about point (i,j,k). Thus, for equal mesh spacing (Δx, Δy and Δz are constants), the appropriate discretizations are:

$$\phi_{xx} = \frac{\phi_{i+1,j,k} - 2\phi_{i,j,k} + \phi_{i-1,j,k}}{(\Delta x)^2}$$

$$\phi_{yy} = \frac{\phi_{i,j+1,k} - 2\phi_{i,j,k} + \phi_{i,j-1,k}}{(\Delta y)^2}$$

$$\phi_{zz} = \frac{\phi_{i,j,k+1} - 2\phi_{i,j,k} + \phi_{i,j,k-1}}{(\Delta z)^2}$$

$$\left[\frac{\partial}{\partial x}\left(\phi_i^2{}_x\right)\right]_{i,j,k} = \frac{1}{\Delta x}\left[\left(\phi_i^2{}_x\right)_{i+1/2} - \left(\phi_i^2{}_x\right)_{i-1/2}\right]_{j,k}$$

$$= \frac{1}{\Delta x^3}\left[\left(\phi_{i_{i+1}} - \phi_{i_{i-1}}\right)\left(\phi_{i_{i+1}} - 2\phi_{i_i} + \phi_{i_{i-1}}\right)\right]_{j,k}$$

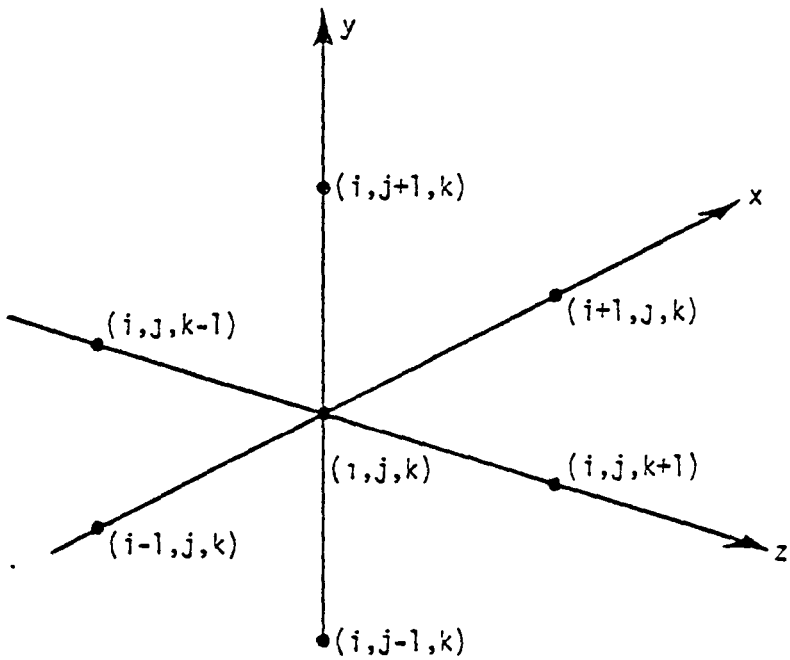

Figure 5. Computational Star

$$\left[\frac{\partial}{\partial x}\left(\phi_{1_y}^2\right)\right]_{i,j,k} = \frac{1}{\Delta x}\left[\left(\phi_{1_y}^2\right)_{i+1/2} - \left(\phi_{1_y}^2\right)_{i-1/2}\right]_{j,k}$$

$$= \frac{2}{\Delta x}\left[\left(\phi_{1_y}\right)_i \left\{\left(\phi_{1_y}\right)_{i+1/2} - \left(\phi_{1_y}\right)_{i-1/2}\right\}\right]_{j,k}$$

$$= \frac{1}{4\Delta y^2 \Delta x}\left[\left(\phi_{1_{i,j+1}} - \phi_{1_{i,j-1}}\right)\left\{\left(\phi_{1_{i+1,j+1}} - \phi_{1_{i+1,j-1}}\right)\right.\right.$$

$$\left.\left. - \left(\phi_{1_{i-1,j+1}} - \phi_{1_{i-1,j-1}}\right)\right\}\right]_k .$$

The term $\left[\frac{\partial}{\partial x}\left(\phi_{1_z}^2\right)\right]_i$ is differenced similarly. All these finite differenced quantities are substituted into Equations (1) and (3) and the first order velocity potential $\phi_{1_{i+1,j,k}}$ and the second order velocity potential $\phi_{2_{i+1,j,k}}$ are solved for. The boundary conditions are imposed using a boundary point operator.

Boundary Point Operator

The boundary conditions can be applied in two different ways. Figure 6 shows the two arrangements. In one (refer to figure 6a), grid points are placed right on the body and dummy points below the body are used. For this arrangement, the term ϕ_{yy} at the body point (point 1) is differenced in the following way.

$$\left(\phi_{yy}\right)_{\text{at } 1} = \frac{\phi_2 - 2\phi_1 + \phi_0}{\Delta y^2} .$$

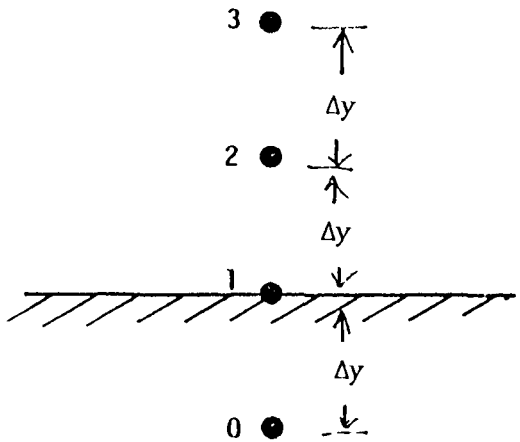

Figure 6a. Dummy Point Arrangement

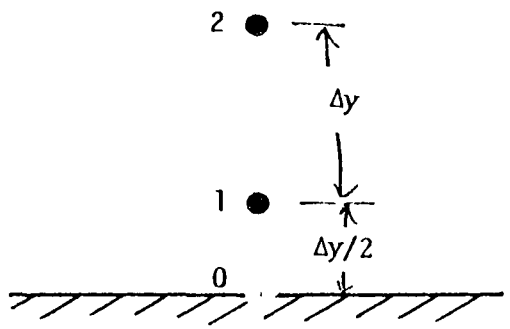

Figure 6b. No Body Point Arrangement

The dummy point value ϕ_0 is replaced in terms of the body boundary condition (ϕ_y) as

$$\phi_0 = \phi_2 - 2\Delta y \, (\phi_y)_{\text{at } 1}$$

Substituting for ϕ_0 we get

$$(\phi_{yy})_{\text{at } 1} = \frac{2\phi_2 - 2\phi_1 - 2\Delta y \, (\phi_y)_{\text{at } 1}}{(\Delta y)^2} .$$

In the other arrangement (refer to figure 6b), grid points are not used on the body. While differencing for ϕ_{yy} at the first point above the body, the body boundary condition ϕ_y will come in to play.

$$(\phi_{yy})_{\text{at } 1} = \frac{\phi_2 - \phi_1 - (\phi_y)_0 \, \Delta y}{(\Delta y)^2} .$$

Stability

In general, all hyperbolic explicit schemes are subjected to stability conditions to achieve convergence. This stability condition is usually in terms of the mesh spacing Δx, Δy and Δz. Basically, stability is achieved if the discretized domain of dependence completely includes the continuum domain of dependence. This is illustrated in figure 7. The continuum domain of dependence for the point P(i+1,j,k) is shown by the dotted line Mach cone whose projection on the i^{th} plane is represented by points B',C',D' and E'. To ensure stability, the grid points B(i,j,k+1), C(i,j-1,k), D(i,j,k-1) and E(i,j+1,k) should fall outside of Mach cone projection B'C'D'E'. This means that the discretized

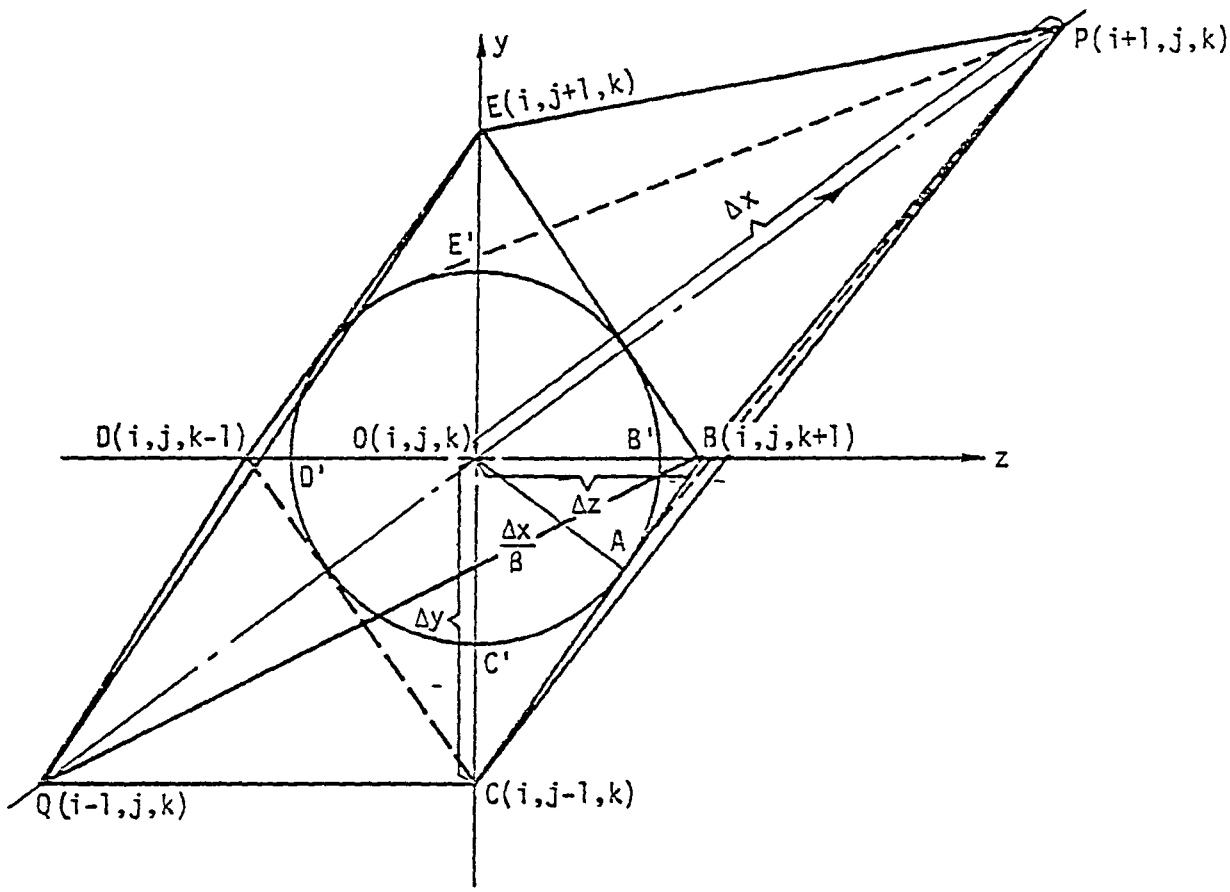

Figure 7. Continuum and Discrete Cones of Dependence

Mach rhombus BCDEBP must enclose the continuum Mach cone B'C'D'E'B'P. This is achieved if the following condition is met.

$$\frac{1}{\beta^2}\left(\frac{\Delta x^2}{\Delta y^2} + \frac{\Delta x^2}{\Delta z^2}\right) \leq 1 \ .$$

For a special case $\Delta y = \Delta z$, the stability condition is

$$\frac{\Delta x}{\Delta y} \leq \frac{\beta}{\sqrt{2}} \ . \tag{6}$$

Usually, best results are obtained when the equality sign in Eq. (6) is satisfied.

Artificial Damping

The explicit scheme that is used to solve Eq. (1) is completely neutral. If one solves for the spectral radius of the amplification term in the frequency domain we get

$$\lambda_{1,2} = 1 - 2\left[\nu_y^2 \sin^2 \frac{\beta_y}{2} + \nu_z^2 \sin^2 \frac{\beta_z}{2}\right] \pm i\left[1 - \left\{1 - 2\left[\nu_y^2 \sin^2 \frac{\beta_y}{2} + \nu_z^2 \sin^2 \frac{\beta_z}{2}\right]\right\}^2\right]^2 \ . \tag{7}$$

For a wave solution, we require that the spectrum be complex, which means the quantity in the radical must always be positive. This term is positive only if

$$\nu_y^2 + \nu_z^2 \leq 1 \quad , \quad \nu_y = \frac{1}{\beta}\frac{\Delta x}{\Delta y} \quad , \ \nu_z = \frac{1}{\beta}\frac{\Delta x}{\Delta z} \tag{8}$$

which is the stability requirement on Courant number. However, the real requirement is that

$$|\lambda_{1,2}| \leq 1 \ . \tag{9}$$

We can see that the restriction (8) provides us with roots which always lie on the unit circle for all stable Courant numbers. Any discretization errors which are introduced can never damp out. They will simply be trapped in the mesh as the solution proceeds. Another interesting property of this scheme is that the usual damping terms which are appended to the right side of the difference equation are of no value. They are either destabilizing or fail to alter the modulus of the eigenvalues.

To damp out any errors that creep into the solution, a smoothing operator to the final result has been introduced. Let L_C be the difference operator such that

$$\phi_{i+1,j,k} = L_C \, \phi_{i,j,k} \, .$$

Now let a purely dissipative operator L_D be applied to the result and let this result be $\phi^{final}_{i+1,j,k}$ such that

$$\phi^{final}_{i+1,j,k} = L_D \, \phi_{i+1,j,k} \, . \tag{10}$$

Then

$$\phi^{final}_{i+1,j,k} = L_D \, L_C \, \phi_{i,j,k} \, . \tag{11}$$

For stability, we require

$$\| L_C \, L_D \| \leq 1 \tag{12}$$

or

$$\| L_D \| \| L_C \| \leq 1 \, .$$

Since $\| L_C \| \equiv 1$ we simply require that $\| L_D \| \leq 1$. Any operator which is dissipative will not disturb the stability of the system. It is suggested that the difference operator be of the form

$$(1 - \frac{\omega}{8} \delta_z^4) \, \phi_{i+1,j,k} \tag{13}$$

where the z-direction is indicated. The symbol δ_z^4 represents a fourth order differencing operator. A similar damping term in the y-direction is added with no problems. For this type of operator, the difference equation becomes

$$\phi^{final}_{i+1,j,k} = \phi_{i+1,j,k} - \frac{\omega}{8} \left[\phi_{i+1,j,k+2} - 4\phi_{i-1,j,k+1} + 6\phi_{i+1,j,k} - 4\phi_{i+1,j,k-1} + \phi_{i+1,j,k-2} \right] . \tag{14}$$

Stability is assured since

$$\| L_D \| = \left| 1 - 2\omega \sin^4 \frac{\gamma}{2} \right| \leq 1$$

if

$$0 \leq \omega \leq \frac{1}{2} \, . \tag{15}$$

This form of dissipation should leave the low frequency components of the solution relatively unaltered while the high frequency waves are attenuated. The formal accuracy of the solution should not be altered

using this procedure. The damping really appears as a fourth-order term and the second-order result obtained should still be intact. Solutions obtained with and without using this damping operator are discussed in Section 6.1.

Systems Approach

Although the potential formulation is fairly straightforward to solve with only one dependent variable, it has a few drawbacks which are described below. To alleviate some of these deficiencies, a different approach has been studied. Here, instead of solving the single velocity potential equation a system of equations in u, v, and w (perturbation velocities) are treated.

Comments on Velocity Potential and Systems Approach

1. The ϕ equation in a Cartesian coordinate system involves second derivatives. This poses a problem if we have to make any coordinate transformation because the transformed equation may get so complicated that even a simple explicit scheme would require time and storage consuming matrix inversion procedures just as in the case of implicit schemes.
2. To solve the problem in Cartesian coordinates requires too many field points. This can be avoided by means of a simple coordinate transformation (preferably body fitted system). On the other hand, a velocity potential formulation is not very accessible to transformations of any kind for the above reason.
3. The u,v,w systems approach involves only first derivatives, and can be put in conservative form for any arbitrary general coordinate transformation (described in the later section of this report).

4. The existing three-dimensional Euler solvers use continuity, and the three momentum equations in vector form along with the integrated energy equation. The u,v,w systems approach has the strong advantage over the velocity potential formulation in the sense it can be easily incorporated into any one of the existing Euler codes. Within such a framework, the perturbation velocity formulation is linear and simple looking compared to Euler equations and hence can save computational time. This simplified formulation will now be described.

First Order Equations

$$\left.\begin{aligned} u_{1_x} - \frac{1}{\beta^2} v_{1_y} - \frac{1}{\beta^2} w_{1_z} &= 0 \\ v_{1_x} - u_{1_y} &= 0 \\ w_{1_x} - u_{1_z} &= 0 \end{aligned}\right\} \qquad (16)$$

The second and third equations in (16) are the vorticity equations. Here $u_1 = \phi_{1_x}$, $v_1 = \phi_{1_y}$ and $w_1 = \phi_{1_z}$ where ϕ_1 is the first order perturbation velocity potential. Eq. (16) can be written as

$$E_{1_x} + F_{1_y} + G_{1_z} = 0 \ . \qquad (17)$$

The first order boundary condition is

$$v_1(x,0,z) = F_x - \frac{\alpha}{\delta} \qquad (18)$$

where $y = \delta F(x,z) + \alpha x$ prescribes the body shape. The angle of attack is denoted by α.

Second Order Equations

$$\left.\begin{aligned} u_{2_x} - \frac{1}{\beta^2} v_{2_y} - \frac{1}{\beta^2} w_{2_z} &= - \frac{M_\infty^2}{\beta^2} \frac{\partial}{\partial x} \left[\left(1 + \frac{\gamma-1}{2} M_\infty^2 \right) u_1^2 + v_1^2 + w_1^2 \right] \\ v_{2_x} - u_{2_y} &= 0 \\ w_{2_x} - u_{2_z} &= 0 \end{aligned}\right\} \qquad (19)$$

where $u_2 = \phi_{2_x}$, $v_2 = \phi_{2_y}$ and $w_2 = \phi_{2_z}$, and ϕ_2 is the second order perturbation velocity potential.

Equation (19) can be rewritten in the following way:

$$E_{2_x} + F_{2_y} + G_{2_z} = 0 \qquad (20)$$

where

$$E_2 = \begin{pmatrix} u_2 + \frac{M_\infty^2}{\beta^2} \left[\left(1 + \frac{\gamma-1}{2} M_\infty^2 \right) u_1^2 + v_1^2 + w_1^2 \right] \\ v_2 \\ w_2 \end{pmatrix}$$

$$F_2 = \begin{pmatrix} - \frac{v_2}{\beta^2} \\ - u_2 \\ 0 \end{pmatrix} \qquad G_2 = \begin{pmatrix} - \frac{w_2}{\beta^2} \\ 0 \\ - u_2 \end{pmatrix} .$$

The second order boundary condition is

$$v_2(x,0,z) = (F_x - \frac{\alpha}{\delta})\, u_1 - (F - \frac{\alpha}{\delta} x)\, v_{1_y} + w_1 F_z \,. \tag{21}$$

The first order equations (17) and (18) and the second order equations (20) and (21) are in Cartesian system. Any general transformation of the form

$$\left.\begin{aligned} \zeta &= x \\ \eta &= \eta(x,y,z) \\ \xi &= \xi(x,y,z) \end{aligned}\right\} \tag{22}$$

does not change the form of these equations. After the transformation Eqs. (17) and (20) result in

$$\hat{E}_{1_\zeta} + \hat{F}_{1_\eta} + \hat{G}_{1_\xi} = 0 \tag{23}$$

$$\hat{E}_{2_\zeta} + \hat{F}_{2_\eta} + \hat{G}_{2_\xi} = 0 \tag{24}$$

where

$$\hat{E}_1 = \frac{E_1}{J} \qquad \hat{E}_2 = \frac{E_2}{J}$$

$$\hat{F}_1 = \frac{E_1 \eta_x + F_1 \eta_y + G_1 \eta_z}{J} \qquad \hat{F}_2 = \frac{E_2 \eta_x + F_2 \eta_y + G_2 \eta_z}{J}$$

$$\hat{G}_1 = \frac{E_1 \xi_x + F_1 \xi_y + G_1 \xi_z}{J} \qquad \hat{G}_2 = \frac{E_2 \xi_x + F_2 \xi_y + G_2 \xi_z}{J}$$

and J is the Jacobian of the transformation given by $J = \eta_x \xi_y - \eta_y \xi_x$.

At this point, we note the identical form of the first order Eqs. (17) and (23) and second order equations (20) and (24). By contrast, in the velocity potential scalar formulation any transformation completely alters the Cartesian form of the equation.

Conical Wing-Body Problem

To study the usefulness of the systems approach, conical delta wings and wing-body combinations with supersonic leading edges are studied first. To take advantage of the conical nature of the flow field and to map the leading edge planar shock into a constant coordinate surface the following conical transformation is incorporated. Referring to the coordinate system of figure 8, we let

$$\left.\begin{aligned} \zeta &= x \\ \eta &= \frac{y}{x - z \tan \chi} \\ \xi &= \frac{z}{x} \end{aligned}\right\} \tag{25}$$

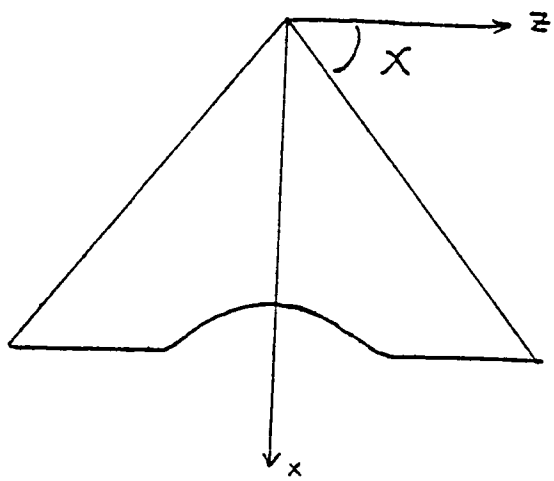

Figure 8. Conical Wing-Body Geometry

Corresponding to the transformation (10) we have

$$\eta_x = \frac{-\eta}{\zeta(1 - \xi \tan \chi)} \qquad \eta_y = \frac{1}{\zeta(1 - \xi \tan \chi)} \qquad \eta_z = \frac{\eta \tan \chi}{\zeta(1 - \xi \tan \chi)}$$

$$\xi_x = \frac{-\xi}{\zeta} \qquad \xi_y = 0 \qquad \xi_z = \frac{1}{\zeta}$$

and

$$J = \frac{1}{\zeta^2(1 - \xi \tan \chi)}$$

The computational domain (η,ξ) is a rectangle as shown in figure 9b. Various other transformations besides (25) are also possible. For example, $\zeta = x$, $\eta = y/x$, and $\xi = z/x$ is another such conical transformation.

Computational Boundaries

M=1, L=1, L_{max} is the plane of symmetry of the delta wing.

$M=M_{max}$, L=1, L_{max} is the right boundary of the computational domain. Physically, points on this boundary lie in the region where the solution is two dimensional.

L=1, M=1, M_{max} is the body boundary or it is the boundary to which the boundary conditions are transferred and where the boundary conditions are applied.

$L=L_{max}$, M=1, M_{max} is the top boundary lying in the physical region undisturbed by the presence of the wing (zone of silence).

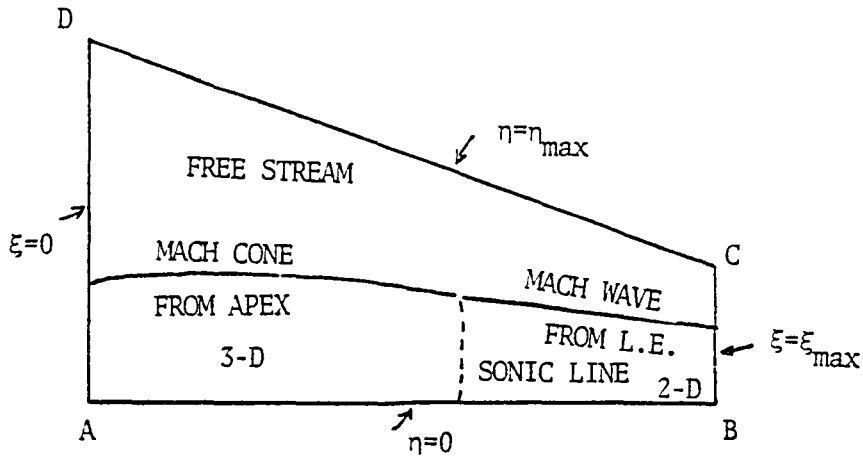

Figure 9a. Physical Plane for Delta Wing

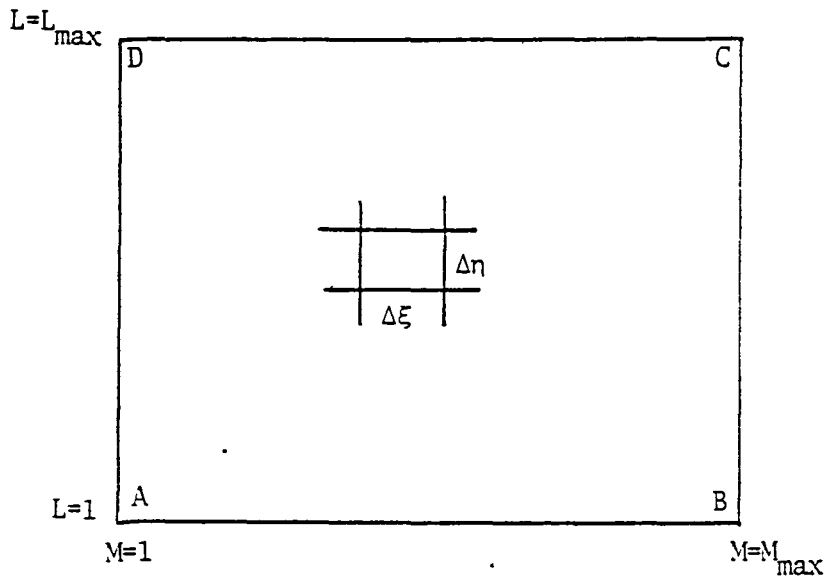

Figure 9b. Computational Rectangular Plane

MacCormack's Difference Scheme

Applied to equation of the form

$$\hat{E}_{\zeta} + \hat{F}_{\eta} + \hat{G}_{\xi} = 0$$

$$\hat{E}^{\overline{n+1}}_{L,M} = \hat{E}^{n}_{L,M} - \frac{\Delta\zeta}{\Delta\eta}\left(\hat{F}^{n}_{L+1,M} - \hat{F}^{n}_{L,M}\right) - \frac{\Delta\zeta}{\Delta\xi}\left(\hat{G}^{n}_{L,M} - \hat{G}^{n}_{L,M-1}\right)$$

$$\hat{E}^{n+1}_{L,M} = \frac{1}{2}\left[\hat{E}^{n}_{L,M} + \hat{E}^{\overline{n+1}}_{L,M} - \frac{\Delta\zeta}{\Delta\eta}\left(\hat{F}^{\overline{n+1}}_{L,M} - \hat{F}^{\overline{n+1}}_{L-1,M}\right) - \frac{\Delta\zeta}{\Delta\xi}\left(\hat{G}^{\overline{n+1}}_{L,M+1} - \hat{G}^{\overline{n+1}}_{L,M}\right)\right] .$$

Once $\hat{E}^{n+1}_{L,M}$ is computed $(u,v,w)^{n+1}_{L,M}$ is known. For a conical problem as n gets large, the solution approaches a radially asymptotic value. The marching step size $\Delta\zeta$ is chosen to satisfy the stability conditions.

Boundary Differencing of Boundary Conditions

At the top boundary the values of u,v,w are kept fixed at zero (undisturbed flow region).

At the symmetry boundary the equations are integrated using a forward predictor and corrector for the differencing along varying M index and the boundary condition w=0 is applied.

At the body boundary the equations are integrated using a forward predictor and corrector for the differencing along varying L index and the boundary condition v=prescribed is applied.

At the right boundary which is in the region of two dimensional solution, it is assumed that

$$u_{1_{\xi}} = u_{2_{\xi}} = v_{1_{\xi}} = v_{2_{\xi}} = w_{1_{\xi}} = w_{2_{\xi}} = 0 .$$

Computationally this is implemented by setting

$$(u_1, v_1, w_1, u_2, v_2, w_2)_{M_{max}} = (u_1, v_1, w_1, u_2, v_2, w_2)_{M_{max}-1} .$$

Symmetric Subsonic Leading Edge

In general, if the leading edge is subsonic, then the bottom and the top surface communicate which means the computational domain must include both the top and bottom right hand side quarter plane. The special case of zero angle of attack symmetric wedge delta wing case shown in figure 10a can be handled by considering only the right hand side upper quarter plane as shown in figure 10b. The boundary condition on the wing is just v=1 and off the wing v=0. Calculations for such a case using a transformation $\zeta = x$, $\eta = y/x$, and $\xi = z/x$ are shown in Section 6.1.

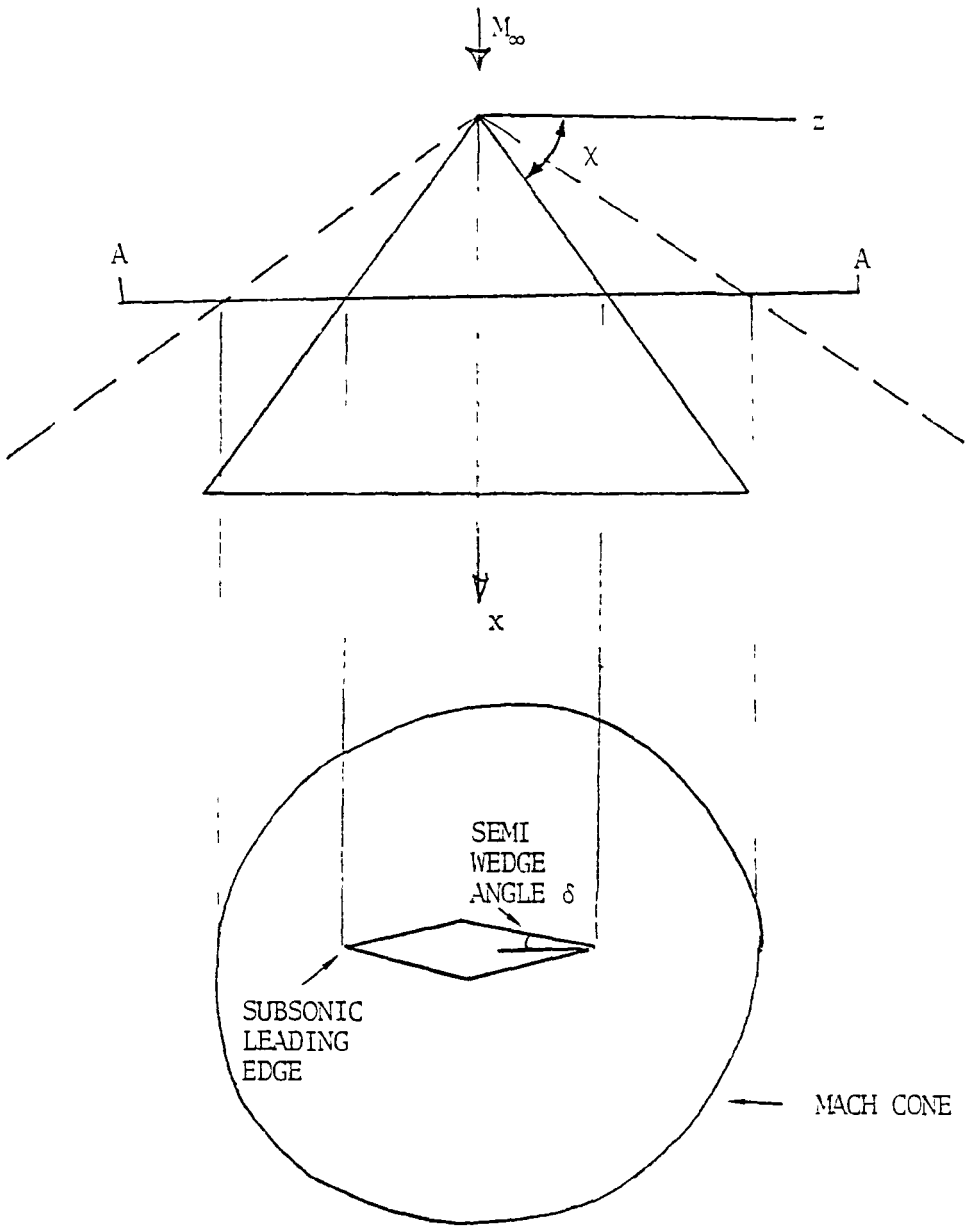

a) Physical Domain

Figure 10. Symmetric Delta Wing Subsonic Leading Edge Case

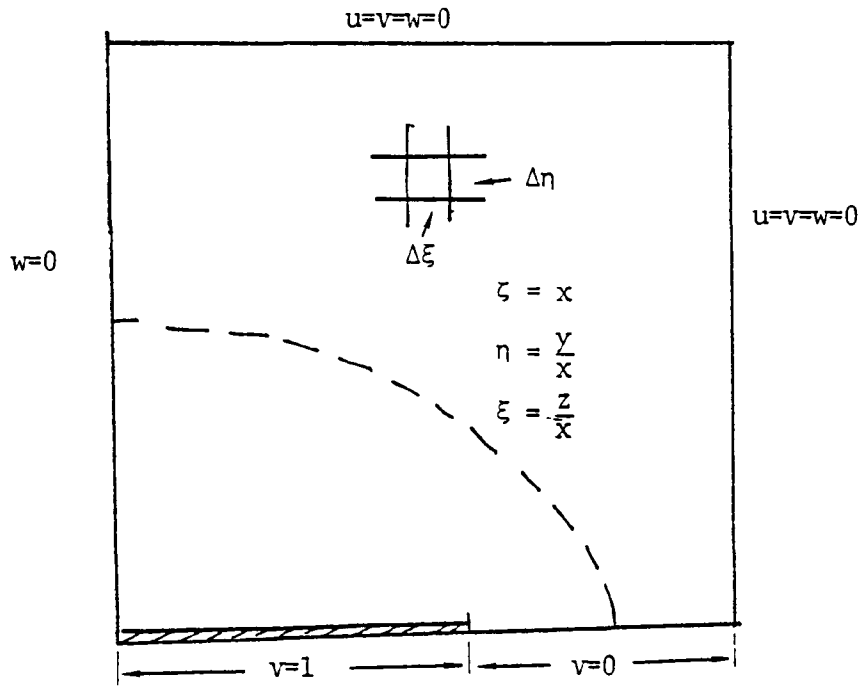

b) Computational Domain

Figure 10. Completed

5. INTEGRAL FORMULATIONS

In addition to the previous approach, conservation law forms of the equation of motion applied over finite volumes also appear promising for rapid turnaround aerodynamic analysis and design methods. Referring to figure 11, a control volume denoted as ABCD in the plan view will be considered. Without loss of generality, we will illustrate the method to be studied within the framework of hypersonic small disturbance theory (HSDT). Generalization of these developments to the Euler equations is straightforward. The HSDT model should be adequate to describe flows for freestream Mach numbers, M_∞ greater than 5 and characteristic flow deflections, Δ, generated by incidence angles α, and thickness or fineness ratios δ of the order of 0.2 radian, or more generally, flows with the hypersonic similarity parameter $1/M_\infty^2\Delta^2$ of order unity. For higher values of H, or lower incidence combinations, a different type of integral method based on Prandtl Glauert and second order theory will be formulated and evaluated herein.

5.1 Hypersonic Small Disturbance Theory

The HSDT problem is obtained by substituting into the exact equations asymptotic expansions which are approximate representations of the velocity $\vec{q}$, pressure P, and density ρ in a limit involving a characteristic flow deflection parameter δ, and M_∞. In this limit, strained coordinates are required as in boundary layer theory to keep the flow field between the shock and body in view. The asymptotic expansions are

$$\frac{\vec{q}}{U}(\bar{x},\bar{y},\bar{z},M_\infty,\delta) = \vec{i}\,(1 + \delta^2 u(x,y,z,H) + \ldots) + \delta v(x,y,z)\vec{j} - \delta w\vec{k} + \ldots \quad (1a)$$

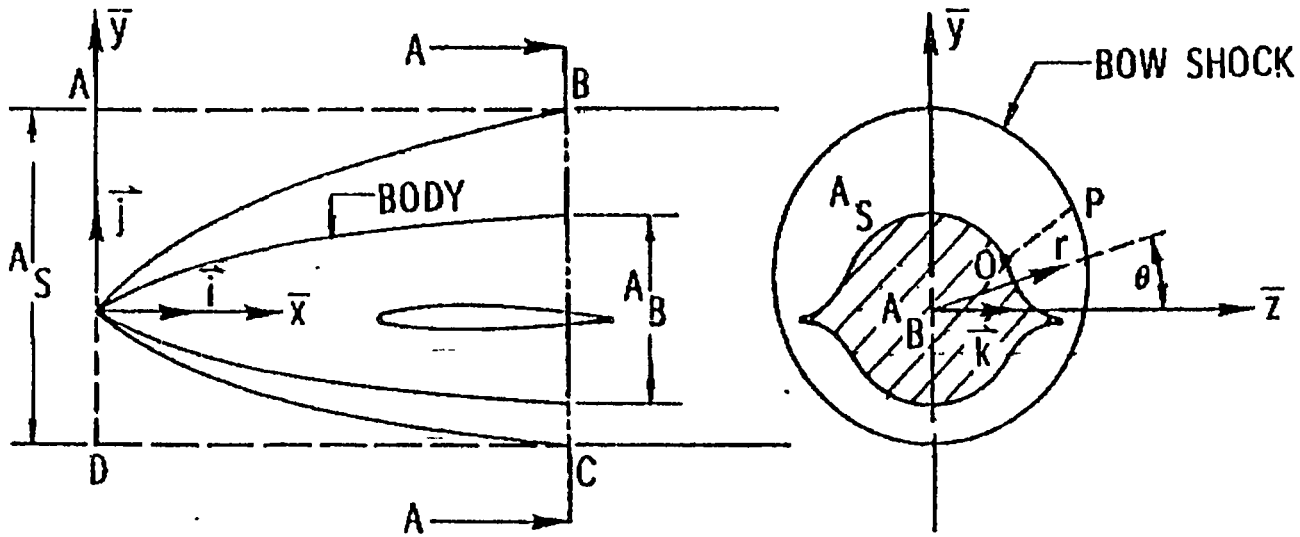

Figure 11. Control Volume for Typical Vehicle Geometry

$$\frac{P - P_\infty}{\rho_\infty U^2_\infty} = \delta^2 p + \ldots \tag{1b}$$

$$\frac{\rho}{\rho_\infty} = \sigma + \ldots \tag{1c}$$

for $H = 1/M^2_\infty \delta^2$, $x \equiv \bar{x}$, $y \equiv \bar{y}/\delta$, $z \equiv \bar{z}/\delta$, $B \equiv b/\delta$, $A \equiv \alpha/\delta$ fixed as $\delta \to 0$ where b is the maximum lateral dimension of the configuration, δ is the fineness ratio, U_∞ is the freestream velocity, ∞ subscripts refer to freestream conditions, $\vec{i}$, $\vec{j}$, and $\vec{k}$ are unit vectors in the $\bar{x}$, $\bar{y}$, and $\bar{z}$ directions, respectively. In what follows, attachment of the shock only at the nose will be assumed for convenience. Generalization of the analysis to more complicated situations will be considered in the future.

Substituting Eqs. (1) into the exact equations of motion and retaining like order terms gives the HSDT equations

$$\sigma_x + \nabla_T \cdot \vec{V}_T = 0 \tag{2a}$$

$$D\vec{V}_T + \nabla_T p = 0 \tag{2b}$$

$$D\mathscr{P} = 0 \tag{2c}$$

where

$$D \equiv \partial/\partial x + \vec{V}_T \cdot \nabla_T$$

$$\nabla_T = \frac{\partial}{\partial y}\vec{j} + \frac{\partial}{\partial z}\vec{k}$$

$$\vec{V}_T = v\vec{j} + w\vec{k} \tag{2d}$$

$$\mathscr{P} \equiv (p + H/\gamma)/\sigma^\gamma$$

$\gamma \equiv$ specific heat ratio .

On substitution of (1) into the shock conditions, the following approximate relations are obtained on the shock $S(x,y,z) = 0$

$$\vec{V}_T \times \nabla S = 0 \tag{3a}$$

$$|\vec{V}_T| \equiv \frac{2}{\gamma+1} [T - H/T] \tag{3b}$$

where

$$T \equiv S_x/|\nabla_T S| \tag{3c}$$

$$p_s \equiv p|_{S=0} = \frac{2}{\gamma+1} [T^2 - H] \tag{3d}$$

$$\sigma_s^{-1} = \frac{\gamma-1}{\gamma+1} + T^{-2} \ . \tag{3e}$$

The body boundary conditions are obtained in a similar manner for flow tangency on the body $B(x,y,z) = 0$, giving

$$B_x + \vec{V}_T \cdot \nabla_T B = 0 \ . \tag{4}$$

Note that if S is known, (3a) and (3b) uniquely determine $\vec{V}_T/S$.

One approach which has been considered utilizes conservation theorems and the HSDT formulation embodied in Eqs. (1)-(4). This method is the full nonlinear analogue of the integral theorems and area rules developed by Rockwell for hypersonic lifting wing body combinations in Refs. 3-5. There, a linear perturbation problem was obtained for configurations with "very supersonic" leading edges. Applying these theorems to the previously indicated control volume, we obtain

$$A_s = \iint_{\Delta A} \sigma dA \qquad \text{, continuity} \tag{5a}$$

$$\tilde{C}_L \equiv \frac{2L}{\rho_\infty U^2 \delta} = -\int\int_{\Delta A} \sigma v \, dy dz \quad , \text{ y momentum} \tag{5b}$$

$$\tilde{C}_Z = \frac{2Z}{\rho_\infty U^2 \delta} = -\int\int_{\Delta A} \sigma w \, dy dz \quad , \text{ z momentum} \tag{5c}$$

$$\tilde{C}_D = \frac{2D}{\rho_\infty U^2 \delta} = -\int\int_{\Delta A} \left(\frac{p + H/\gamma}{\gamma - 1} + \frac{\sigma}{2}(v^2 + w^2) \right) dy dz + HA_B/\gamma \quad , \text{ x momentum} \tag{5d}$$

where $\Delta A \equiv A_S - A_B$, L, Z, D, are, respectively, the lift, side force, and drag and $\tilde{C}_L$, $\tilde{C}_Z$, and $\tilde{C}_D$ are their normalized counterparts, and the area integrals are taken over the projection of the shock layer in the section A-A. Analogous expressions for the moments will be obtained using the moment of momentum theorem.

To evaluate the integrals in Eqs. (5) various methods have been considered. One approach that could lead to a fairly rapid procedure is to make an "averaging" hypothesis that neglects variations in the flow quantities along lines such as OP in the cross flow plane in figure 11. Thus, the values of the integrands in (5) are taken along the shock. For example, if a polar coordinate system is used with the lines OP assumed as θ = const., as shown in figure 11, then Eqs. (5) simplify to

$$\tilde{C}_L = -\int_0^{2\pi} K \sigma_S v_S \, d\theta \tag{6a}$$

$$\tilde{C}_Z = -\int_0^{2\pi} K \sigma_S w_S \, d\theta \tag{6b}$$

$$\tilde{C}_D = -\int_0^{2\pi} K \left[\frac{p_S + H/\gamma}{\gamma - 1} + \frac{\sigma_S (v_S^2 + w_S^2)}{2} + \frac{HA_B}{\gamma} \right] d\theta \tag{6c}$$

where $K \equiv G^2(x,\theta) - F^2(x,\theta)$ with the explicit representation of the shock and body taken respectively as

$$S = r - G(\theta,x) = 0 \quad , \quad \text{shock} \tag{7a}$$

$$B = r - F(\theta,x) = 0 \quad , \quad \text{body} \tag{7b}$$

where $r^2 = y^2 + z^2$ and $\theta = \tan^{-1} y/z$.

The integrands in (6) can be calculated from the shock relations (3) providing the shock shape S is known. In line with the previous assumption, S can be determined by equating the value of the transverse velocity on the body to its corresponding shock value and using the shock relation (3b) to obtain the following nonlinear first order partial differential equation for G:

$$T - H/T = \frac{\gamma+1}{2} FF_x/\sqrt{F^2 + F_\theta^2} \tag{8a}$$

where

$$|\vec{V}_T|_S \doteq FF_x/\sqrt{F^2 + F_\theta^2} \tag{8b}$$

$$T = |\vec{V}_T|_S = GG_x/\sqrt{G^2 + G_\theta^2} \tag{8c}$$

and

$$|\vec{V}_T|_S \times \nabla B = 0 \tag{8d}$$

has been assumed.

Equation (8) can be solved as an initial value problem using the characteristic construction described in Ref. 6, or other numerical methods. This procedure should be fast since there are only two independent variables involved. In

particular, Eq. (8) simplifies to an ordinary differential equation for axial symmetric or conical bodies such as delta wing.

Note however, that Eqs. (8) and (3d) uniquely determine p_s without the need to solve (8) as a differential equation for the shock shape G. If the additional approximation over and above those used is made that

$$p_s = p_B \tag{9}$$

(consistent with thin shock layers at high Mach numbers), then a surface pressure integration rather than the momentum theorems of Eqs. (6) can be used to determine the inviscid overall forces and moments. In analogy to Eqs. (5), these are given by

$$C_L = \frac{L}{\frac{\rho_\infty U^2 S}{2}} = 2 \iint_S p_S \, \vec{n}\cdot\vec{j} \, dS \tag{10a}$$

$$C_Z = \frac{Z}{\frac{\rho_\infty U^2 S}{2}} = 2 \iint_S p_S \, \vec{n}\cdot\vec{k} \, dS \tag{10b}$$

$$C_D = \frac{D}{\frac{\rho_\infty U^2 S}{2}} = 2 \iint_S p_S \, \vec{n}\cdot\vec{i} \, dS \tag{10c}$$

where S refers to the surface area of the configuration.

For lower hypersonic Mach numbers of the order of 4 to 6, the assumption (9) is questionable, and the formulae (10) must be modified by replacing p_s by p_B, the true surface pressure. The relative accuracies associated with application of (5) as contrasted with (10) when certain simplifying assumptions are made concerning the structure of the shock layer or disturbance field are under

examination. If the conservation laws associated with (5) are to be used, then the factor K in the integrands must be determined and the differential equation (8) for the shock shape must be solved.

Assumptions (8) and (9) appear to be reasonable approximations at high supersonic Mach numbers as shown in figure 12 taken from Ref. 7. Calculations for $M_\infty = \infty$ are indicated for a right circular cone at zero incidence where for lower Mach numbers these assumptions correspond to the wedge curve in the figure. A partial evaluation of the method was presented in Ref. 8 for axisymmetric cones at incidence and zero angle of attack. In that assessment, the ambient pressure was neglected compared to the static pressure on the shock layer. This provided agreement of the order 16-20% with the numerical solution of the Euler equations from Babenko et al. given in Ref. 9. A somewhat more consistent procedure which has been recently investigated and accounts for the ambient pressure increases the discrepancies to approximately 36% as indicated in Section 6.2. Similar inaccuracies will be discussed there in connection with studies on elliptic cones performed in this aspect of the contract. To reduce these errors, additional effort is proposed to construct some sort of nonlinear feedback model involving the equations of motion. This concept will be discussed again in Section 6.2.

5.2 Prandtl Glauert and Second Order Theory – Transverse Integral Method

To simplify the calculation of overall loads and moments and bypass some of the difficulties associated with pressure calculations according to second order theory, an integral method has been developed. Although similar in the objective of reducing the dimensionality of the problem, the thrust of this technique differs from that embodied in the integral methods described in Section 5.1. Rather

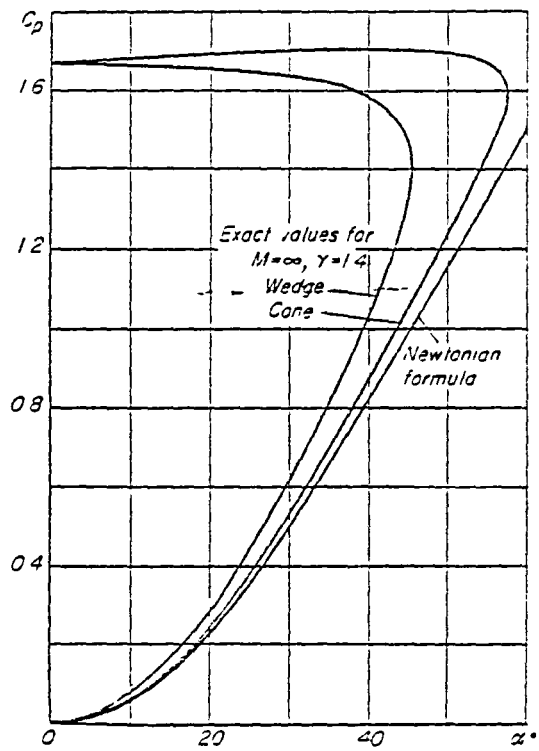

Figure 12. Surface Pressure for a Wedge and Cone According to the Exact Theory for $M = \infty$ and $\gamma = 1.4$, and According to the Newtonian Model.

than dealing with volume fluxes of conserved quantities such as mass, momentum, and energy as Eqs. (5), we consider integrals of the pressure that specialize to loading along strips on the body approximately normal to the freestream direction. This "transverse integral" technique, originally developed by Lagerstrom and Miles, has been used by Malmuth in Refs. 3-5 to estimate L/D performance of conical wing-bodies at hypersonic speeds. In this section, we formulate similar rules for Prandtl Glauert theory and outline the procedure to be further developed to treat the second order linear problem.

With the notation associated with the winglike ogive shown in figure 13, we consider initially the transverse integral technique appropriate to Prandtl Glauert theory. Denoting u as the perturbation velocity in the freestream direction the appropriate equation of motion for the perturbation velocity potential ϕ and boundary conditions when differentiated with respect to x the streamwise coordinates are

$$\Box u = 0 \tag{11a}$$

$$u_y(x,0,z) = f_{xx}$$

where $\Box \equiv \partial^2/\partial y^2 + \partial^2/\partial z^2 - \beta^2\, \partial^2/\partial x^2$, $\beta^2 = M_\infty^2 - 1$, and the body is given by the equation $B = y - \delta f(x,z) = 0$, with δ a characteristic flow deflection angle on thickness. Assuming for initial simplicity that the ogive has supersonic leading edges here and in what follows, a characteristic surface emanates from the leading edges. This surface is shown schematically in phantom in figure 13. We remark here that if the edges are subsonic, certain additional relations over those to be discussed must be introduced to treat the initially unknown velocity components off the wing.

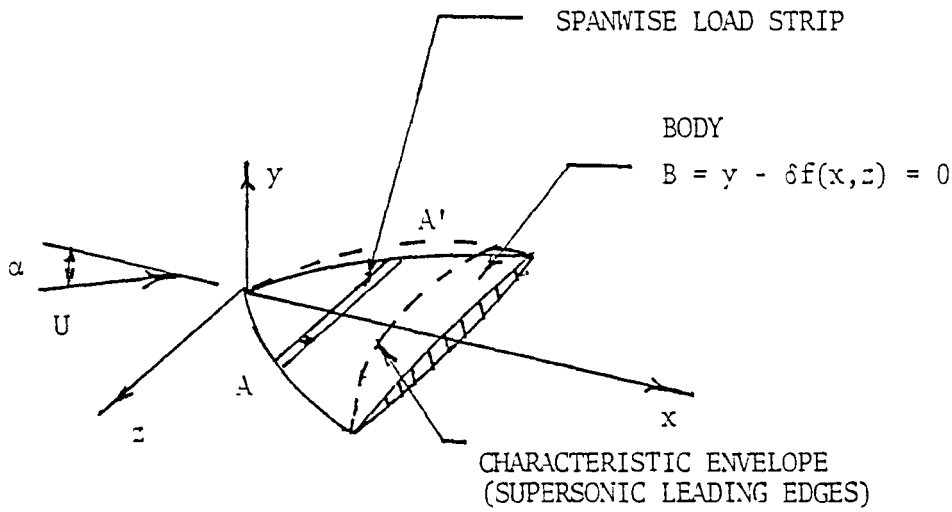

Figure 13. Notation for Transverse Integral Method in Prandtl Glauert and Second Order Van Dyke Theories

Returning to the supersonic leading edge case, we define a spanwise "pressure" integral of the form

$$Q(x,y) = \int_0^{z_c(x,y)} u(x,y,z)\, dz \tag{12}$$

where $z = z_c(x,y)$ is the equation of the characteristic envelope. On integration of Eqs. (11) with respect to z and introduction of symmetry for convenience for which $u_z(x,y,0) = 0$, we obtain a two-dimensional "reduced" version of (11), i.e.,

$$Q_{yy} - \beta^2 Q_{xx} = S(x,y) \tag{13a}$$

where

$$S(x,y) \equiv \frac{\partial}{\partial y}\left(u_c \frac{\partial z_c}{\partial y}\right) + \left.\frac{\partial u}{\partial y}\right|_c \frac{\partial z_c}{\partial y} - \beta^2 \left[\frac{\partial}{\partial x}\left(u_c \frac{\partial z_c}{\partial x}\right) + \left.\frac{\partial u}{\partial x}\right|_c \frac{\partial z_c}{\partial x}\right] \tag{13b}$$

and the subscript c denotes conditions on the characteristic envelope. Turning to the appropriate boundary conditions for (13), we use (11b) and (12) to obtain

$$Q_y(x,0) = F(x) + u_c \left.\frac{\partial z_c}{\partial y}\right|_{y=0} \equiv -\beta G'(x) \tag{14a}$$

where

$$F(x) = \int_0^{z_{LE}} f_{xx}(x,z)\, dz \tag{14b}$$

with subscript LE denoting the leading edge value.

To complete the formulation of an initial boundary value problem for Q in the x,y plane, we introduce the condition

$$Q(x,\tfrac{x}{\beta}) = 0 \tag{14c}$$

which is appropriate if the parabolic Mach cone intersects the plane of symmetry such as for a supersonic leading edge delta wing. Equation (14c) is derived on the basis that the cone carries zero lateral load.

Heuristically, we assert that S=0 in (13b). It is anticipated that a rigorous justification of this assertion can be made using the characteristic compatibility relations and the fact that the characteristic surface is an equipotential. A similar argument was used to derive the hypersonic integral theorems presented in Ref. 5.

The solution of the initial boundary value problem embodied in (13) and (14) is the "simple wave"

$$Q = G(x - \beta y) \tag{15}$$

where G is obtained from (14).

SPECIALIZATION TO DELTA WING

Referring to figure 14, (15) will be specialized to treat the case in which $f_{xx} = 0$ in (14b) to illustrate the concepts. Thus,

$$Q_y = u_c \frac{\partial z_c}{\partial x} \qquad \text{on } y = 0 \tag{16}$$

and hence

$$Q = a(y - x/\beta)$$

where a is to be determined by (16).

In particular,

$$Q(x,0) = - ax/\beta \ .$$

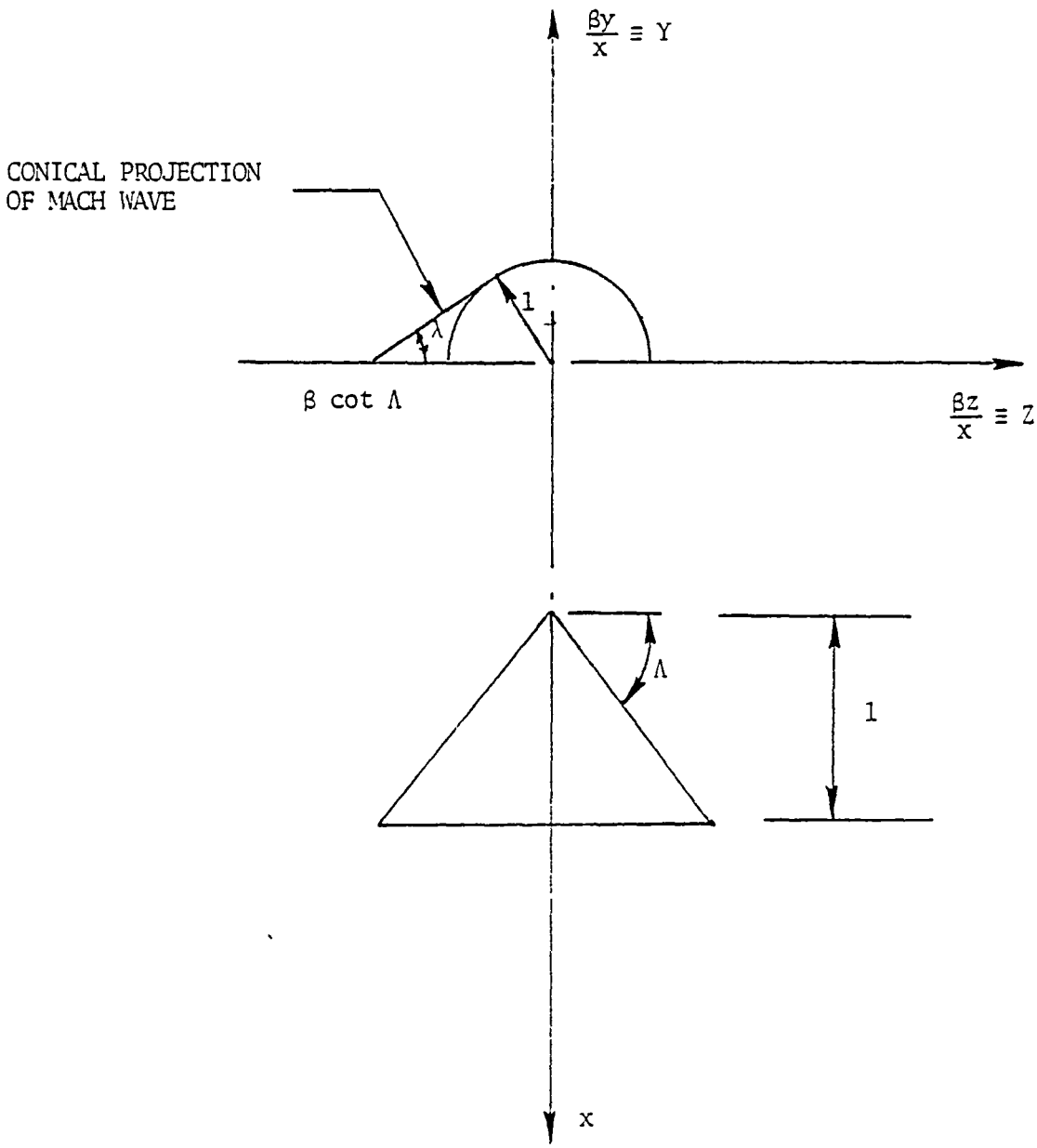

Figure 14. Notation for Delta Wing Solution by Integral Method

Hence,

$$C_L = \frac{-4\alpha}{S_{w/2}} \int_0^1 Q(x,0)\, dx = \frac{a\alpha}{\beta \cot \Lambda}$$

where C_L is the lift coefficient representing an integral of loads along strips such as AA' in figure 13, $S_{w/2}$ is the half planform area and Λ is the sweepback angle. Now from figure 14, the Mach wave plane is given by

$$z_c = x \cot \Lambda - y \cot \lambda$$

and,

$$\partial z_c / \partial y = - \cot \lambda$$

where λ is the ray angle to the point of tangency of the wave to the Mach circle. Since u_c is the two-dimensional value of the "pressure" obtained from sweepback theory, evaluation of (16) gives

$$\frac{a}{U} = \sec \lambda \cot \lambda = \csc \lambda = 2 \operatorname{ctn} \Lambda$$

so that we obtain finally from (17) that

$$C_L = 4\alpha/\beta \ . \qquad (18)$$

This result checks the appropriate value obtained from the full three-dimensional theory. This example illustrates the relative ease that this procedure can be applied to obtain an overall force coefficient which avoids entirely function theory methods or surface singularity procedures. Extensions to curved leading edges and more general geometries appear feasible.

SECOND ORDER TRANSVERSE INTEGRAL METHOD

In this section, we outline the extension of the procedure to treat the second order theory problem, which can be written in abbreviated form as

$$\Box u_2 = g(x,y,z)$$

$$u_{2_y}(x,0,z) = h(x,z)$$

where g and h are functions of the first order Prandtl Glauert solution. Denoting second order quantities corresponding to those previously introduced by a subscript 2, and using procedures applied in the previous section, we obtain

$$\Box' Q_2 = \int_0^{z_c} g \, dz + S_2(x,y) \tag{19a}$$

$$Q_{2_y}(x,0) = - \beta G_2'(x) \tag{19b}$$

$$Q_2(x,x/\beta) = 0 \tag{19c}$$

where G_2' is a known function, and

$$\Box' = \frac{\partial^2}{\partial y^2} - \beta^2 \frac{\partial^2}{\partial x^2} .$$

Introducing the characteristic coordinates

$$\xi = x - \beta y$$

$$\eta = x + \beta y ,$$

Eq. (19a) can be written as

$$\frac{\partial^2 Q_2}{\partial \xi \partial \eta} = H(\xi,\eta) \tag{20}$$

and can be solved with simple quadratures using the boundary conditions (19b) and (19c). Thus, the complete second order problem for the normal force has been reduced to a problem similar to that for the first quantities embodied in (13) and (14), with a slight complication involving inhomogeneities in the strip loading equation. In future work, it is intended to solve (19) for a delta wing and compare the results for the lift and other forces obtained in this fashion with those obtained using the source volume and finite difference analyses described previously in Section 4. The obvious advantage of this method is that it reduces the three dimensional problem to one in two dimensions and has the potential of being generalized to more complicated geometries. On the other hand, it has the disadvantage of yielding only gross loadings and not detailed pressures.

6. RESULTS

6.1 Second Order Theory

The initial test cases for the source volume formulation of second order potential theory were selected to verify the correctness of the theoretical development and coding. Available analytic and higher order two dimensional results were used for this purpose. Comparisons were subsequently made with measurements for delta wings covering the range of leading edge sweep from 50 to 70 degrees, Mach numbers of 2.3 to 6.0, and a range of angle of attack such that $M\alpha \to 1$.

Comparisons for a NACA 0012 airfoil at zero angle of attack are presented on figures 15 and 16. The incompressible result of figure 15 established the correctness of the second order boundary condition by comparison to the conformal mapping solution of Theodorsen. The well known inadequacy of the first order chord plane boundary condition transfer in the leading edge region is clearly illustrated. The second order result essentially eliminates this deficiency. The compressible subcritical comparison of figure 16 was used to establish the correctness of the spatial source volume terms by comparison to the higher order Euler equation solution of Sells. The results indicate that the source contribution generally improves the comparison although the boundary condition correction is the more dominant of the two at this Mach number. Higher order contributions are apparently required to entirely resolve the leading edge region.

Numerical second order calculations at M = 4 were performed for a swept taper ratio one lifting wing with a 10% circular arc section (figure 17). The results for an essentially two dimensional region of the flow were compared with Busemann's or Van Dyke's analytic second order expression for yawed wings.

$$C_p = \frac{2}{\sqrt{M_\infty^2 - 1 - TAN^2\theta}}\alpha(x) + \frac{(\gamma+1)M_\infty^4 \cos^2\theta - 4\left[M_\infty^2 - 1 - TAN^2\theta\right]}{2\cos^2\theta\left[M_\infty^2 - 1 - TAN^2\theta\right]^2}\alpha^2(x)$$

The only difference between the analytic and numerical result is in the second order net pressure and is due to the chordwise variation of camber induced by the source volumes. The camber is measured at the control point, which is at 0.95 chord of each vortex panel, while the ΔCp is assumed to occur at the centroid. For a supersonic two-dimensional region the net pressure depends only on the local angle of attack.

The chordwise variation of the three terms which contribute to the second order ΔCp are shown in figure 17c. The magnitude of the three terms is different depending upon whether the free stream is placed at angle of attack or the planform is place at angle of attack. For either choice in the essentially two dimensional region, the exact second order results and the program results reduce to the same value. Both show there is no change in lift due to thickness which is in agreement with analytic results for an uncambered two dimensional section which begins and ends with zero thickness.

Numerical second order calculations for a clipped fifty-five degree leading edge sweep delta wing with a 4% circular arc airfoil at M = 2.3 to 4.6 are compared to wind tunnel measurements on figures 18 through 20. Predictions of lift surve slope by

the first and second order analysis are essentially the same, and both are in satisfactory agreement (figure 18) with experiment. The prediction for aerodynamic center exhibits a marked improvement for the second order result and is in good agreement with test results. A comparison between prediction and measurement as a function of angle of attack is presented on figure 19 at a M = 4.6. Figure 20 presents representative chordwise pressure distribution comparisons. The general expression for the upper and lower surface pressures, as predicted by second order theory, for a planar wing with zero camber is of the form:

$$C_{P_u} = b_1\left(\frac{t}{c}\right) + b_2\left(\frac{t}{c}\right)^2 + a_1\alpha + a_2\alpha\left(\frac{t}{c}\right) + c_2\alpha^2$$

$$C_{P_L} = b_1\left(\frac{t}{c}\right) + b_2\left(\frac{t}{c}\right)^2 - a_1\alpha - a_2\alpha\left(\frac{t}{c}\right) + c_2\alpha^2$$

where a_1, b_1, a_2, b_2, and c_2 depend on planform geometry and thickness distribution. The chordwise pressure distributions from the wind tunnel data where curve fit by an equation of the form

$$C_p = f_0 + f_1\alpha + f_2\alpha^2 + f_3\alpha^3$$

The data used for the curve fit was limited to ±11° to avoid problems assoicated with flow separation. Since there was data available at more than twice as many angles of attack as there were unknown coefficients, the curve fit was performed in a least square sense. This helped to eliminate the scatter in the wind tunnel data. The f_0 term represents the Cp due to thickness while the f_2 term represents the second order contribution to Cp due to lift. The f_1 term can be used to represent the ΔCp while the f_3 term was found to be negligible.

Calculated second order results for the compression side of a 50 degree swept delta wing at a Mach number of 4 and an angle of attack of 5 degrees are compared to the higher order method of lines on figure 21A. Good agreement is indicated and a substantial improvement over first order analysis realized.

Finally, second order results for the compression side of a 70 degree swept delta wing at a Mach number of 6 and an angle of attack of 8 degrees are compared to measurements on figure 21B. The agreement is satisfactory and again provides a substantial improvement over first order predictions. The non-smoothness of the second order predictions is attributed to the coarseness of the source volume density which for the case under consideration is 10 chordwise by 8 spanwise by 8 vertical.

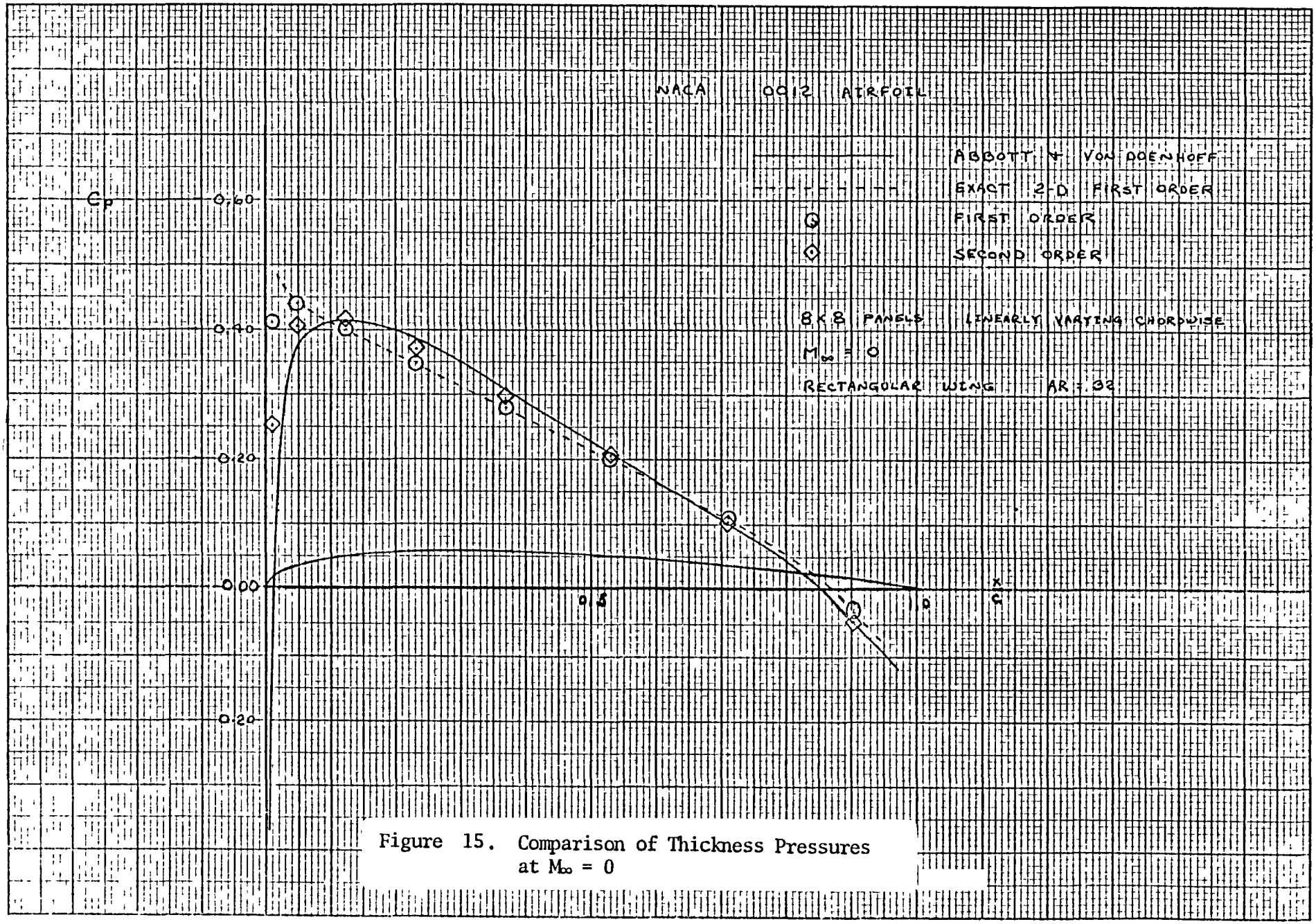

Figure 15. Comparison of Thickness Pressures at $M_\infty = 0$

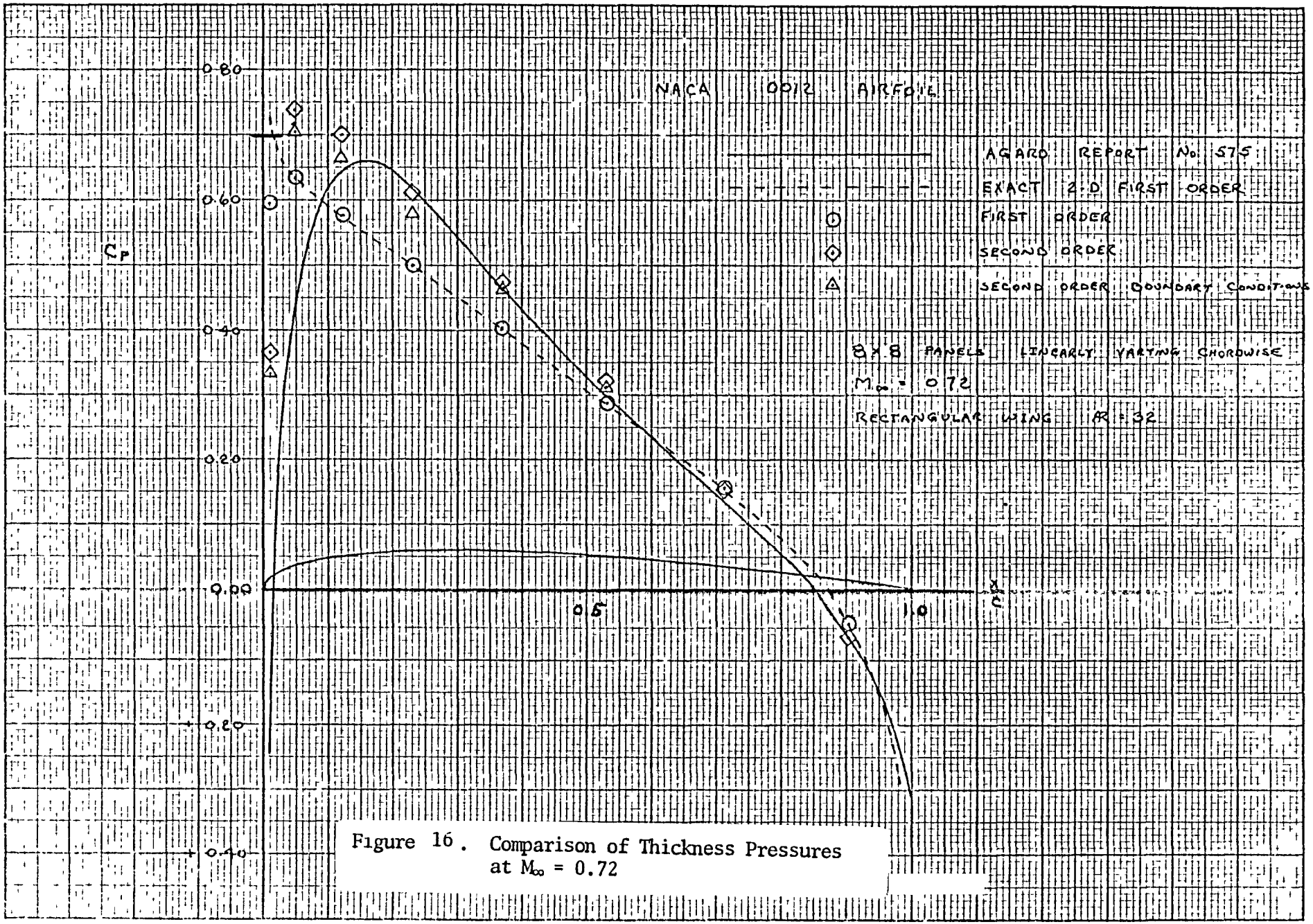

Figure 16. Comparison of Thickness Pressures at $M_\infty = 0.72$

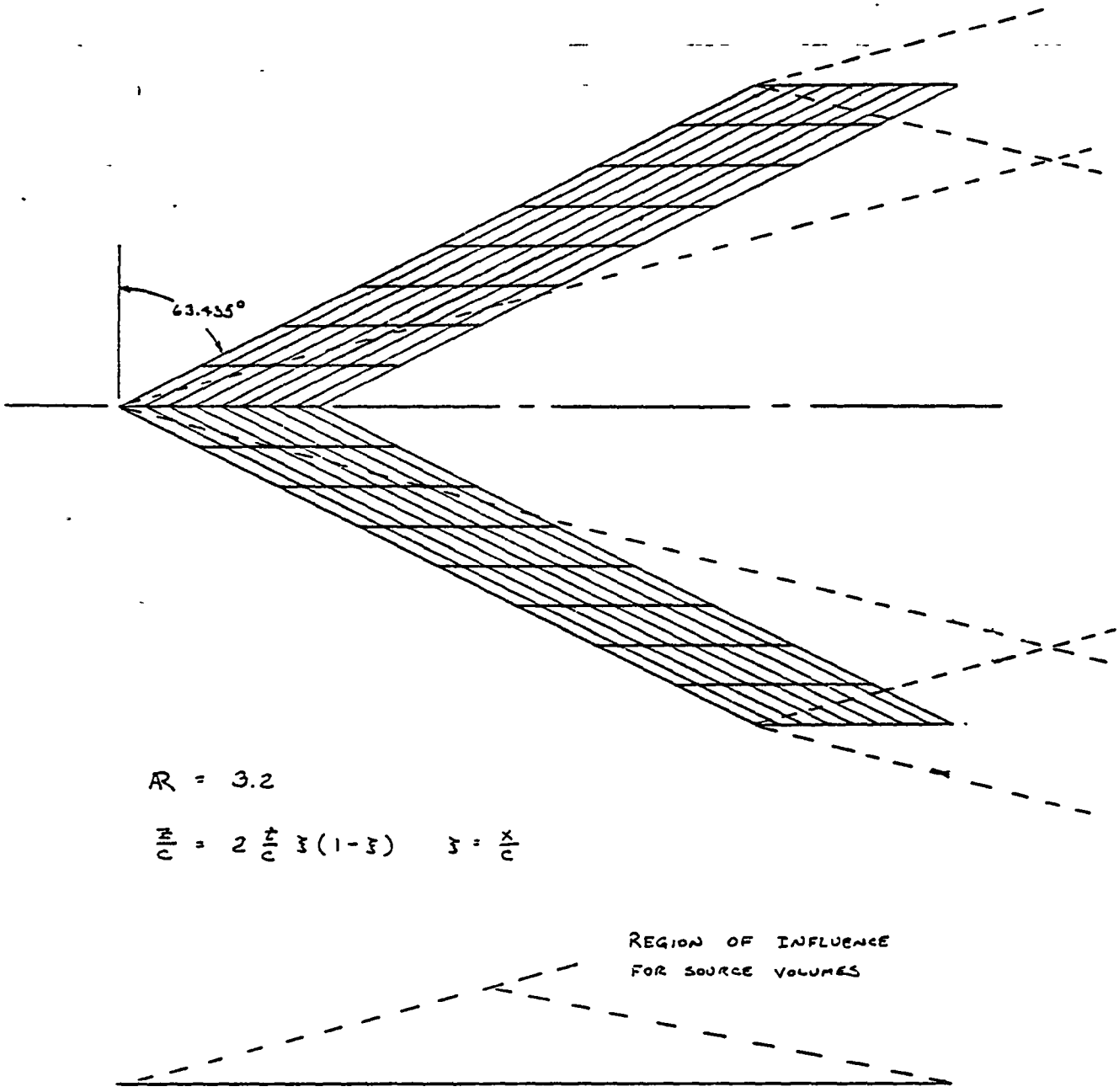

a) Planform and Paneling

Figure 17. Second Order Results for a Swept Untapered Wing at $M_\infty = 4.0$

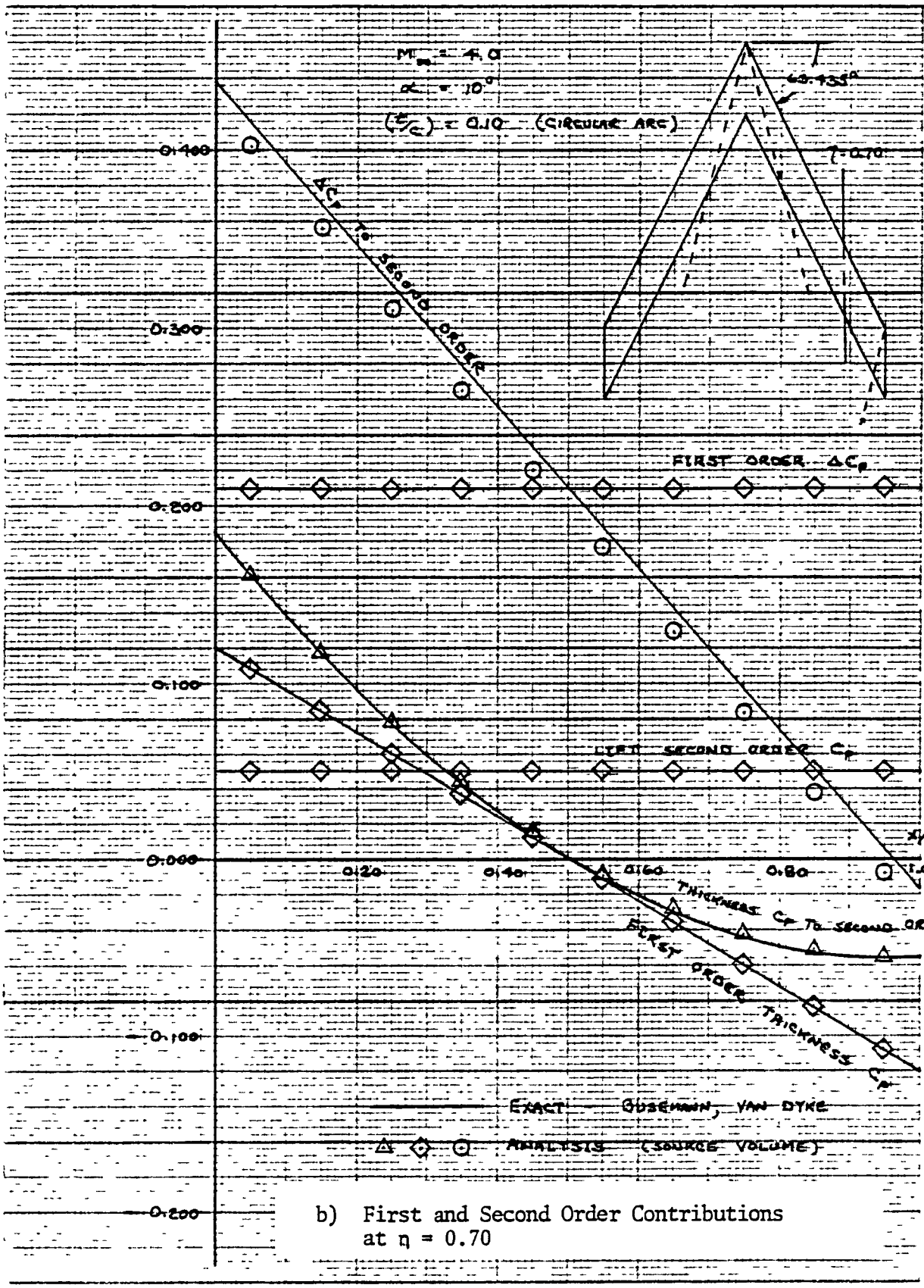

b) First and Second Order Contributions at $\eta = 0.70$

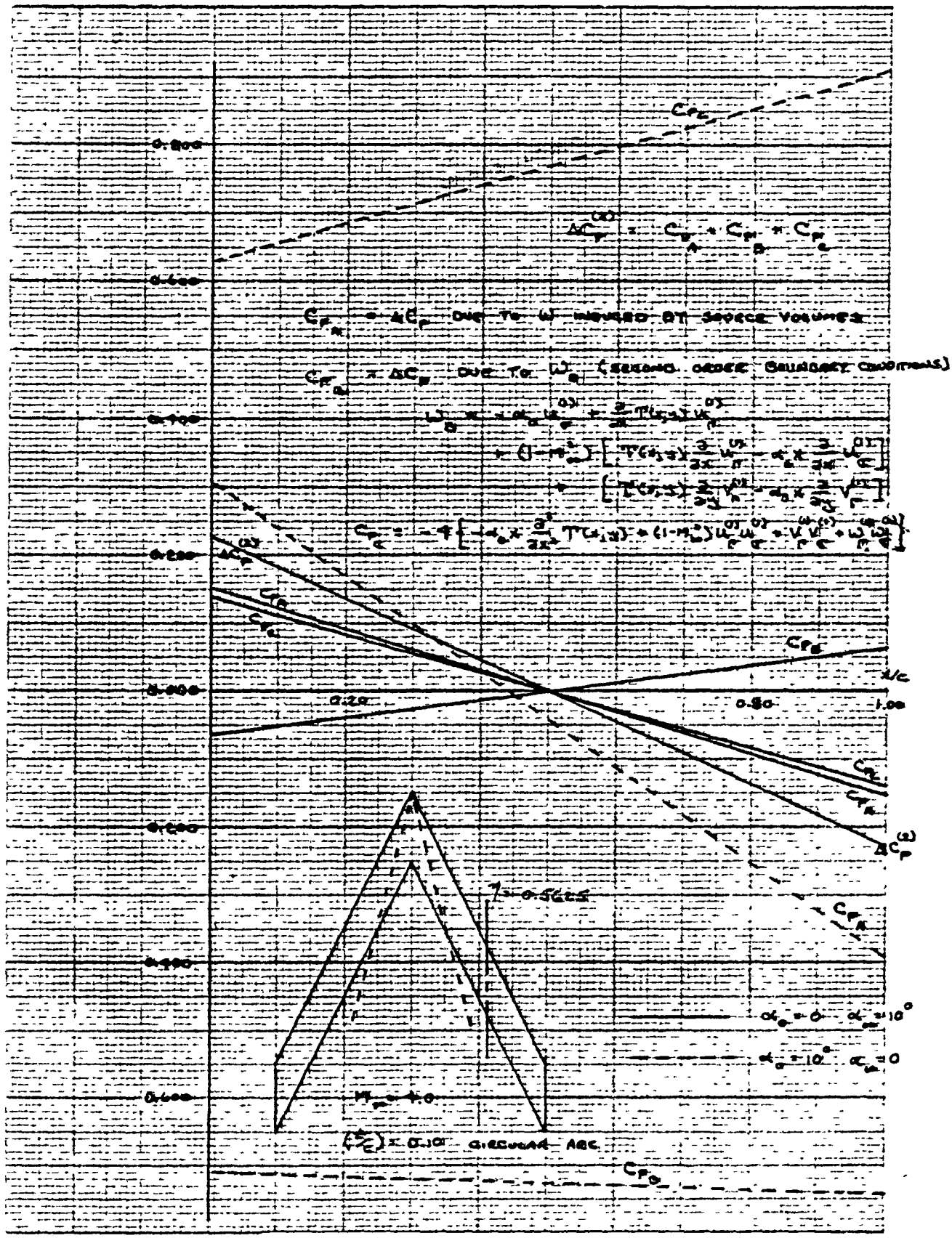

c) Wind and Body Axis Second Order Contributions

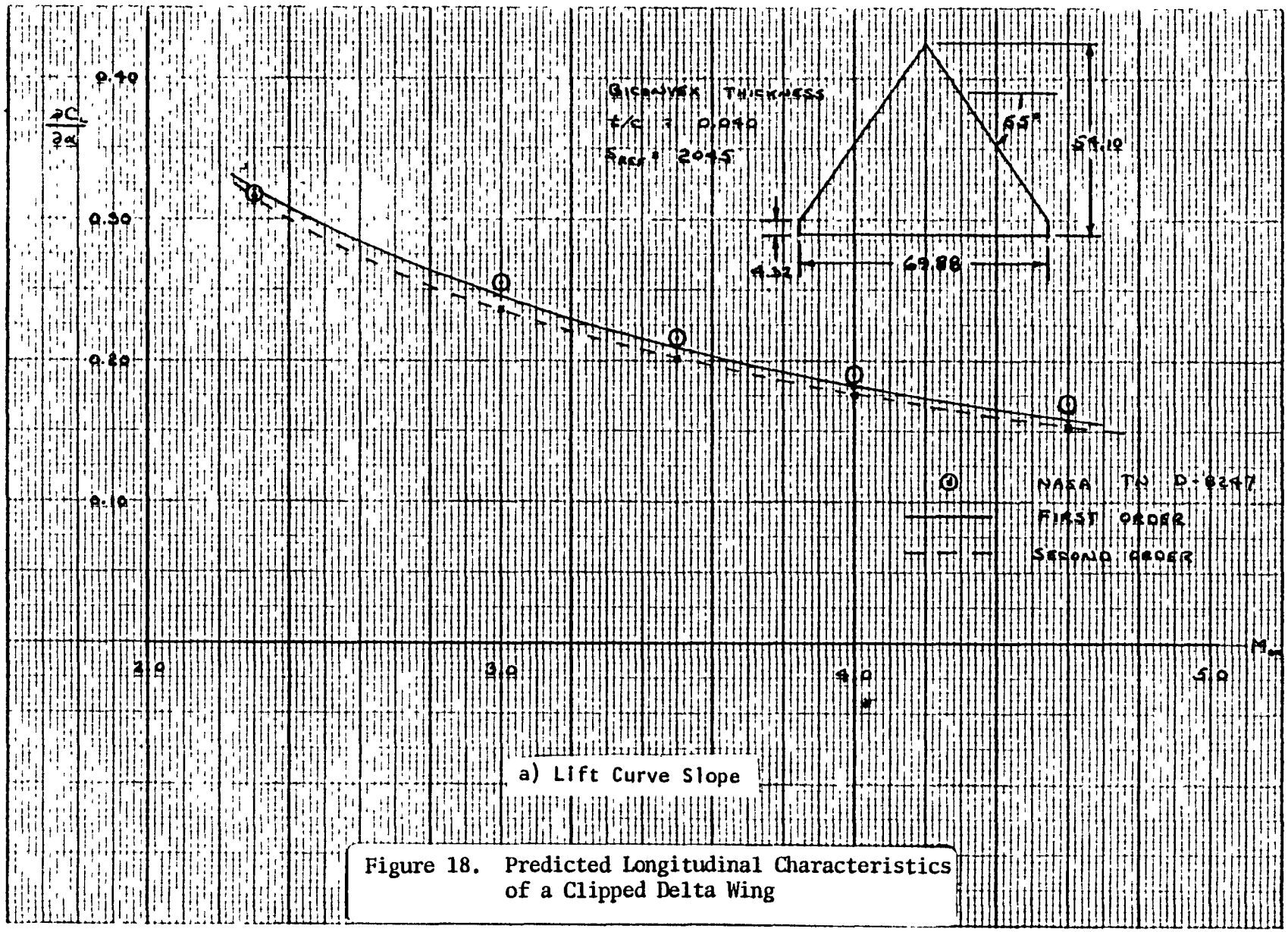

a) Lift Curve Slope

Figure 18. Predicted Longitudinal Characteristics of a Clipped Delta Wing

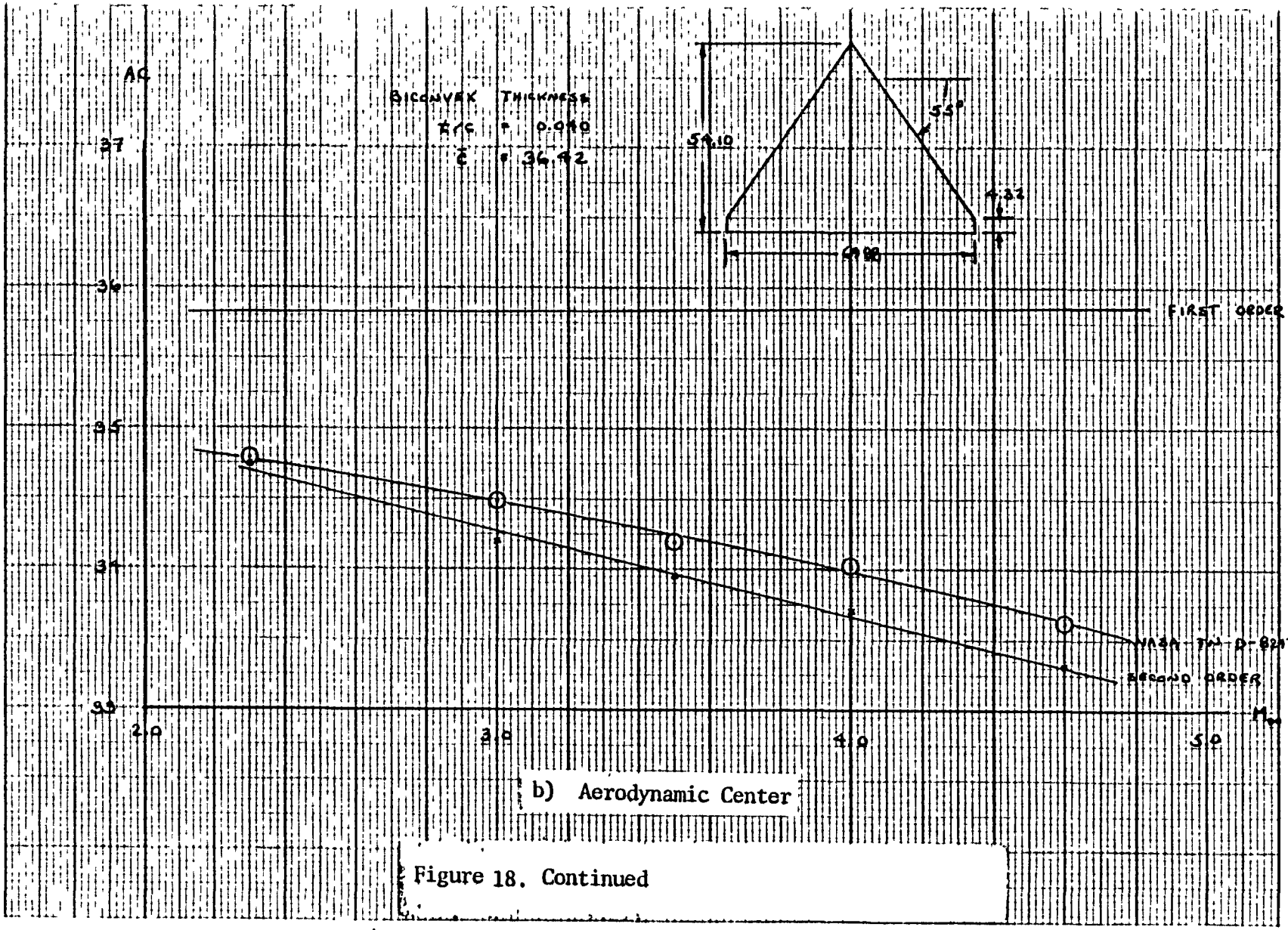

b) Aerodynamic Center

Figure 18. Continued

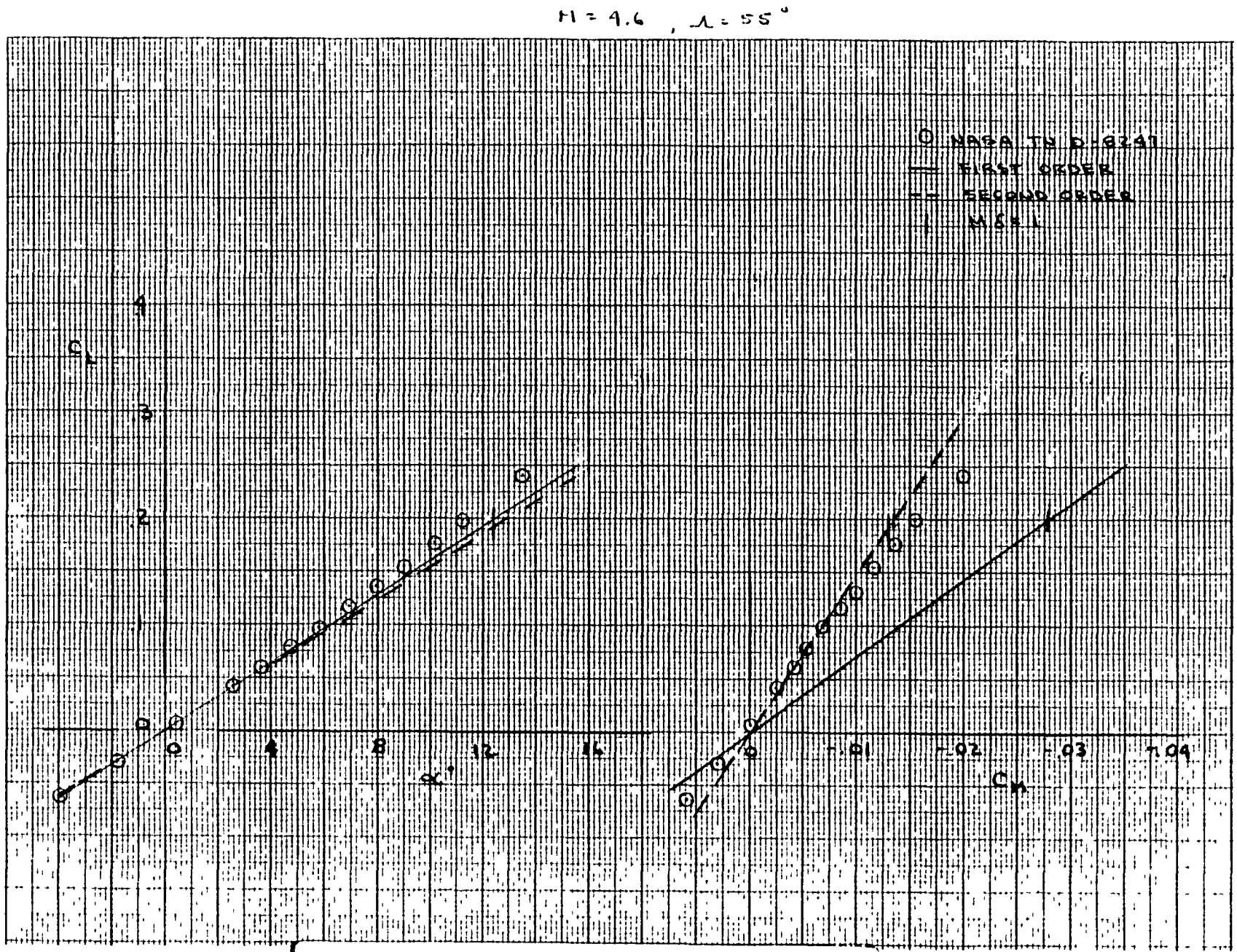

Figure 19. Predicted Longitudinal Characteristics of a Clipped Delta Wing at M = 4.6

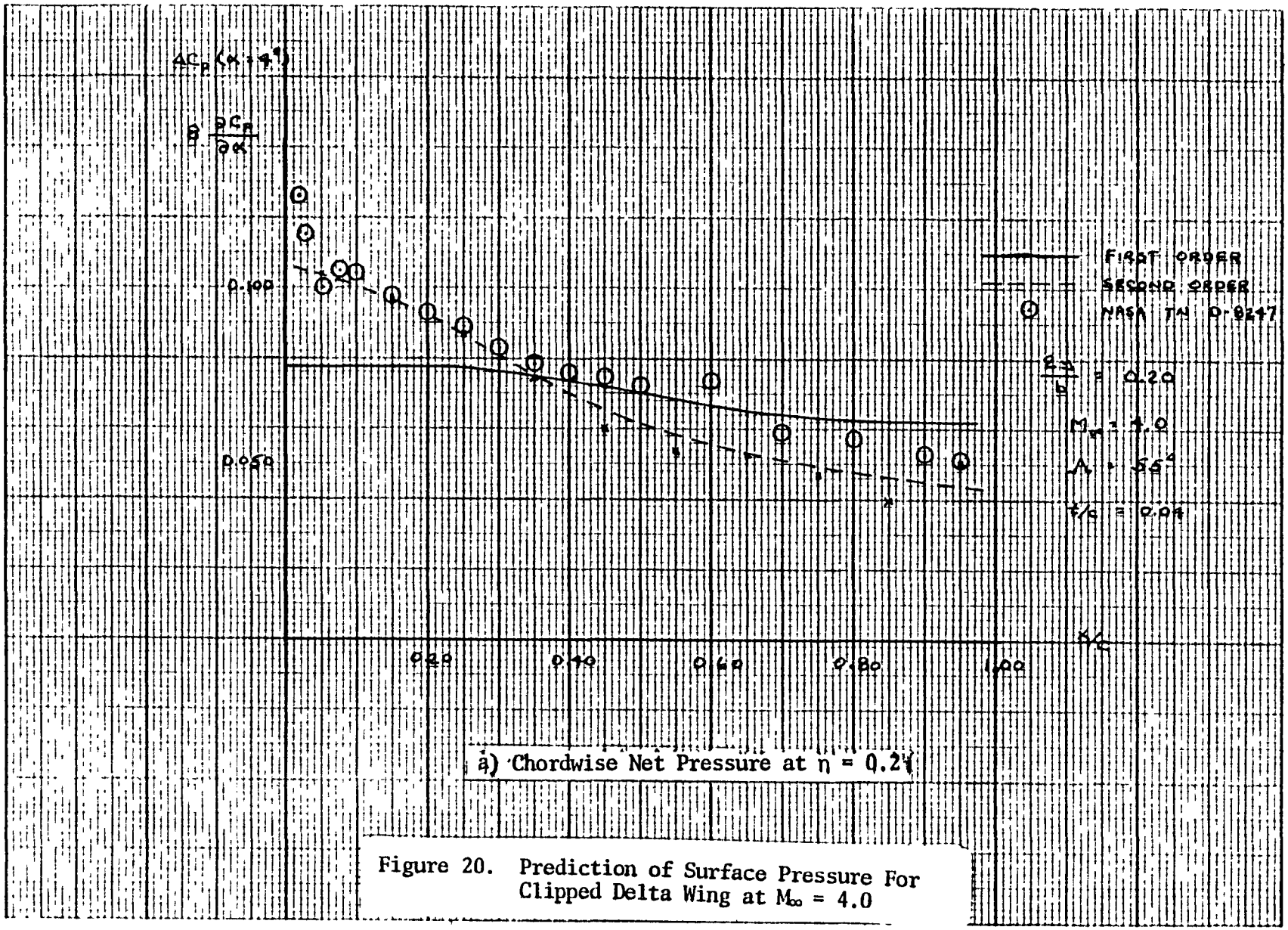

a) Chordwise Net Pressure at $\eta = 0.2$

Figure 20. Prediction of Surface Pressure For Clipped Delta Wing at $M_\infty = 4.0$

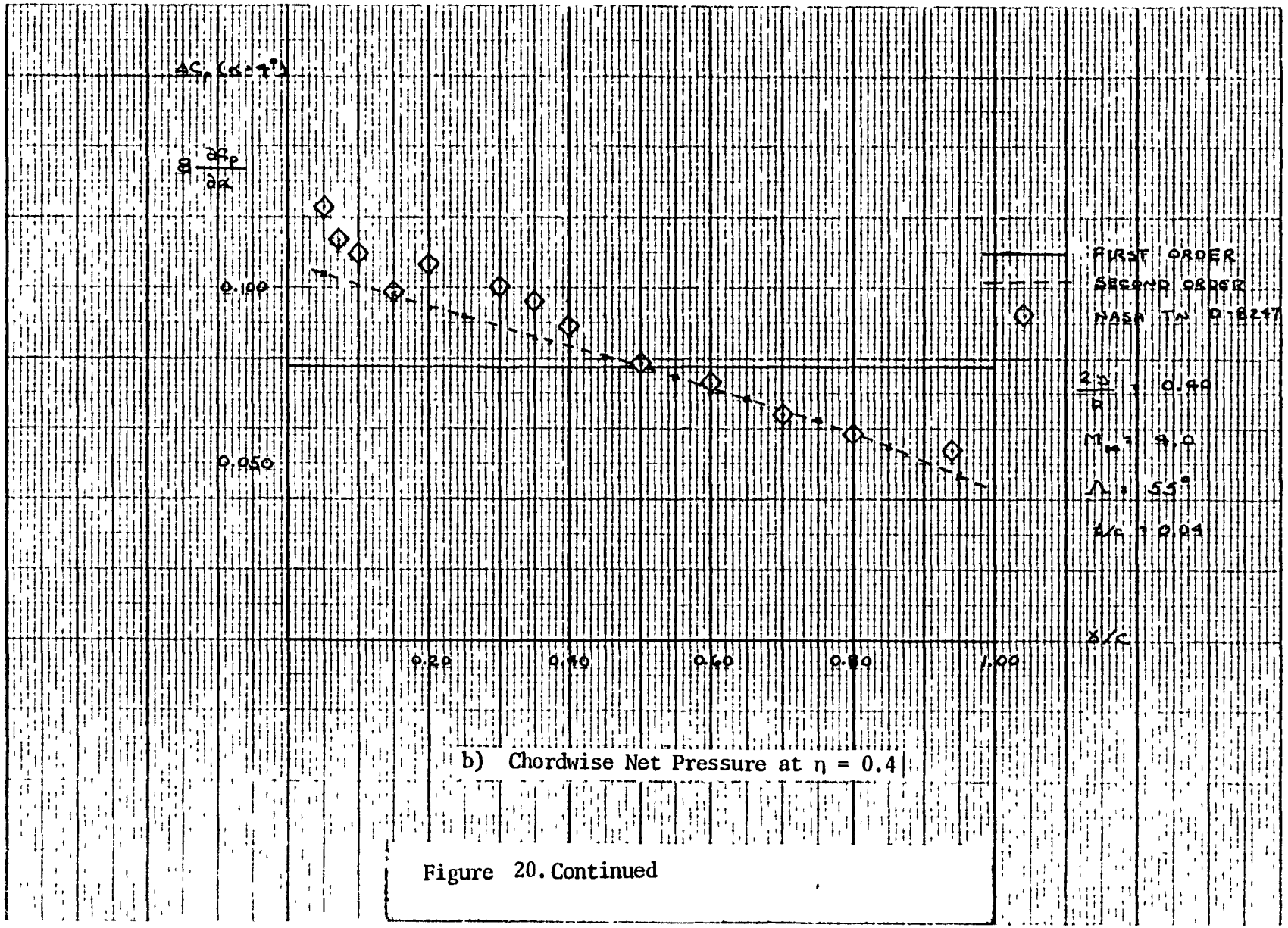

b) Chordwise Net Pressure at $\eta = 0.4$

Figure 20. Continued

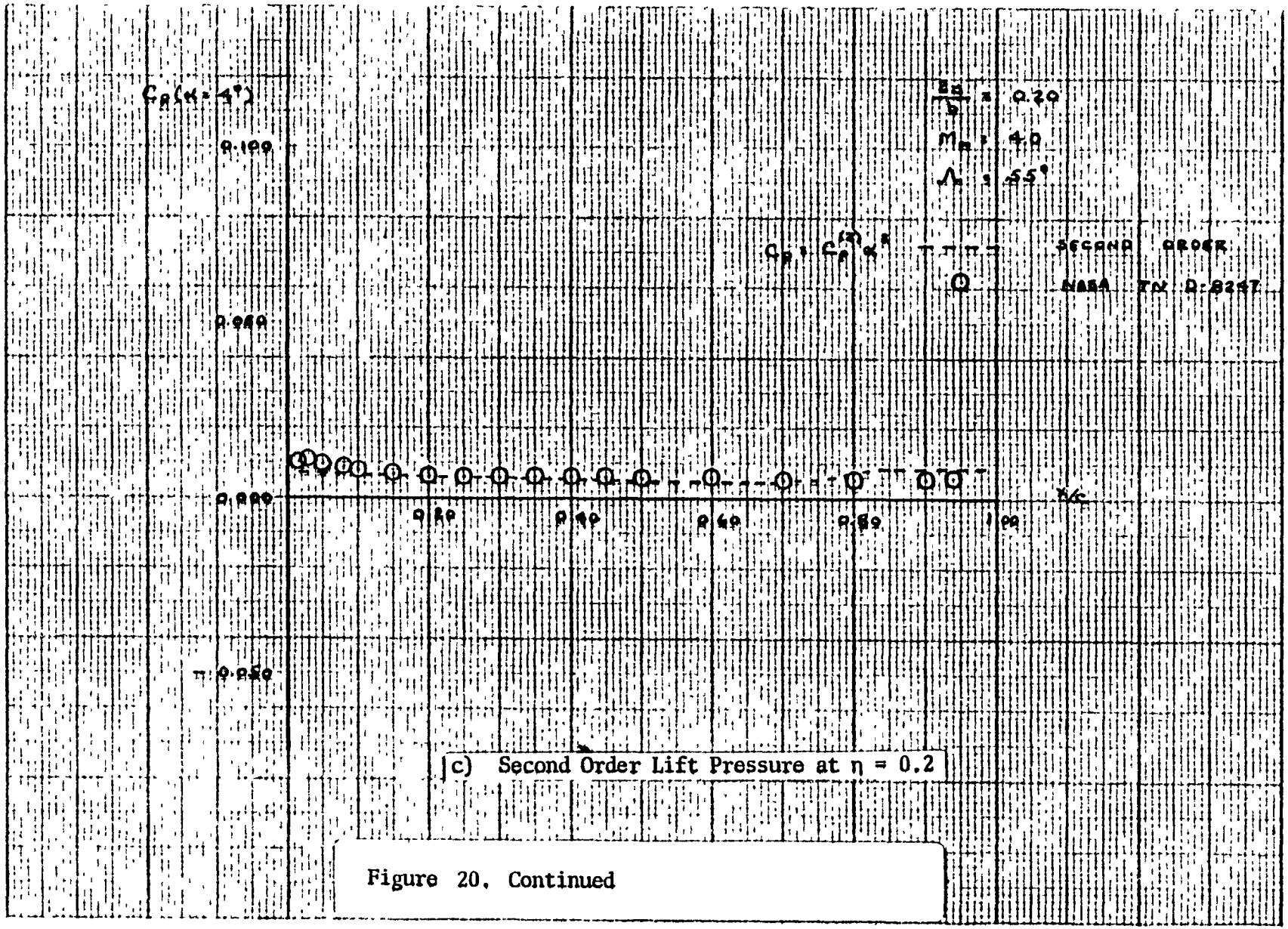

(c) Second Order Lift Pressure at $\eta = 0.2$

Figure 20. Continued

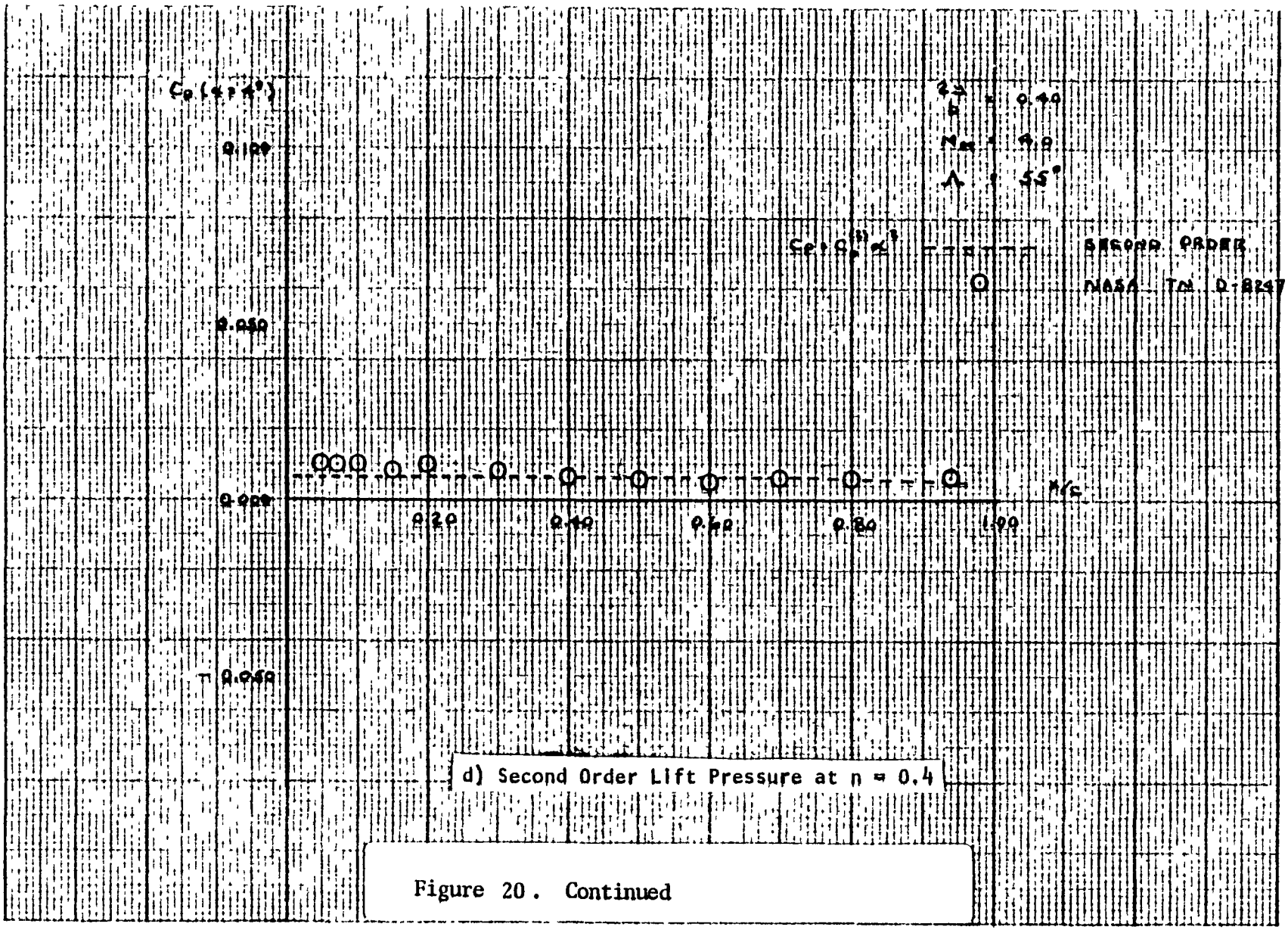

d) Second Order Lift Pressure at $\eta = 0.4$

Figure 20. Continued

Figure 20. Continued

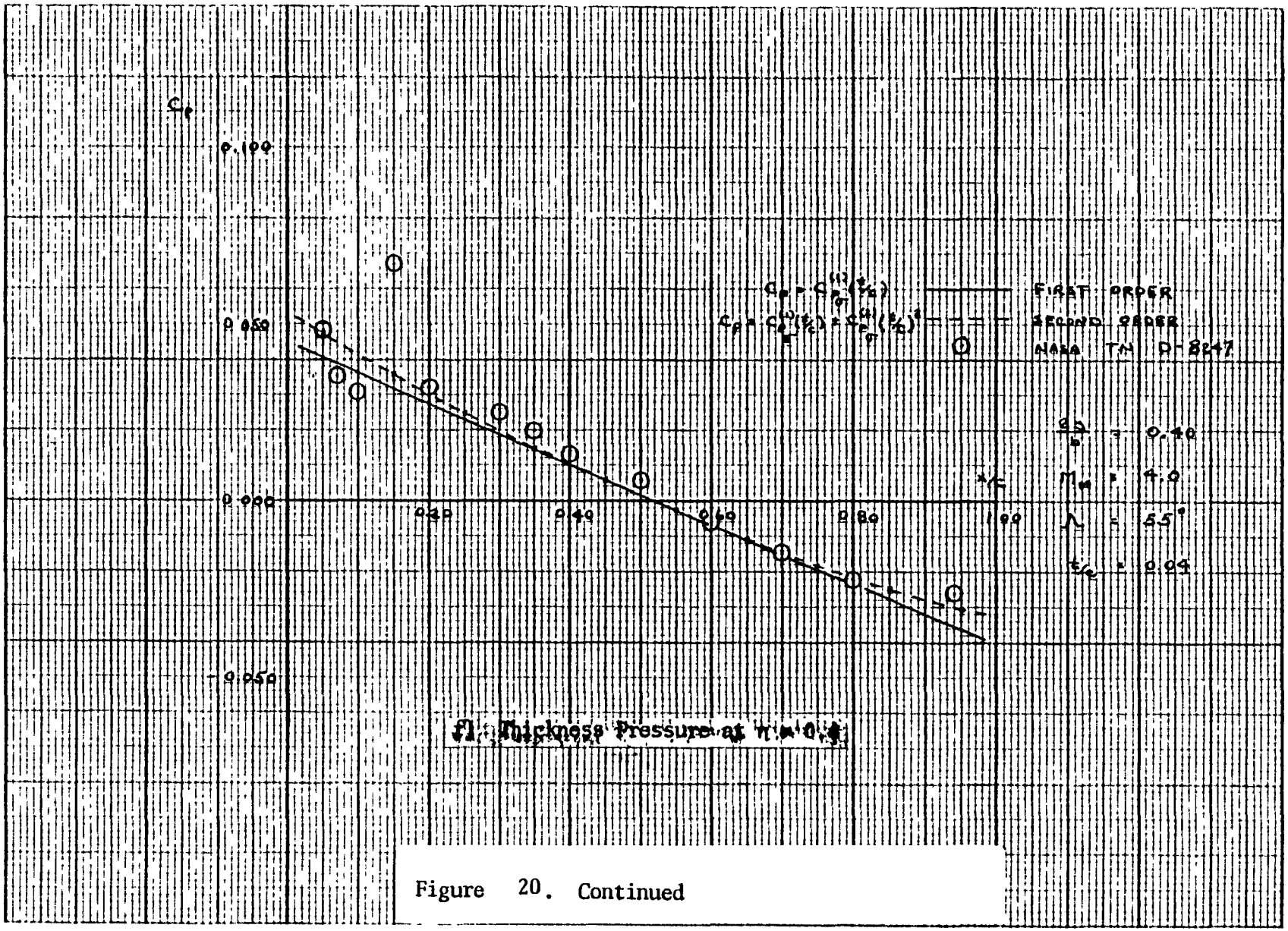

Figure 20. Continued

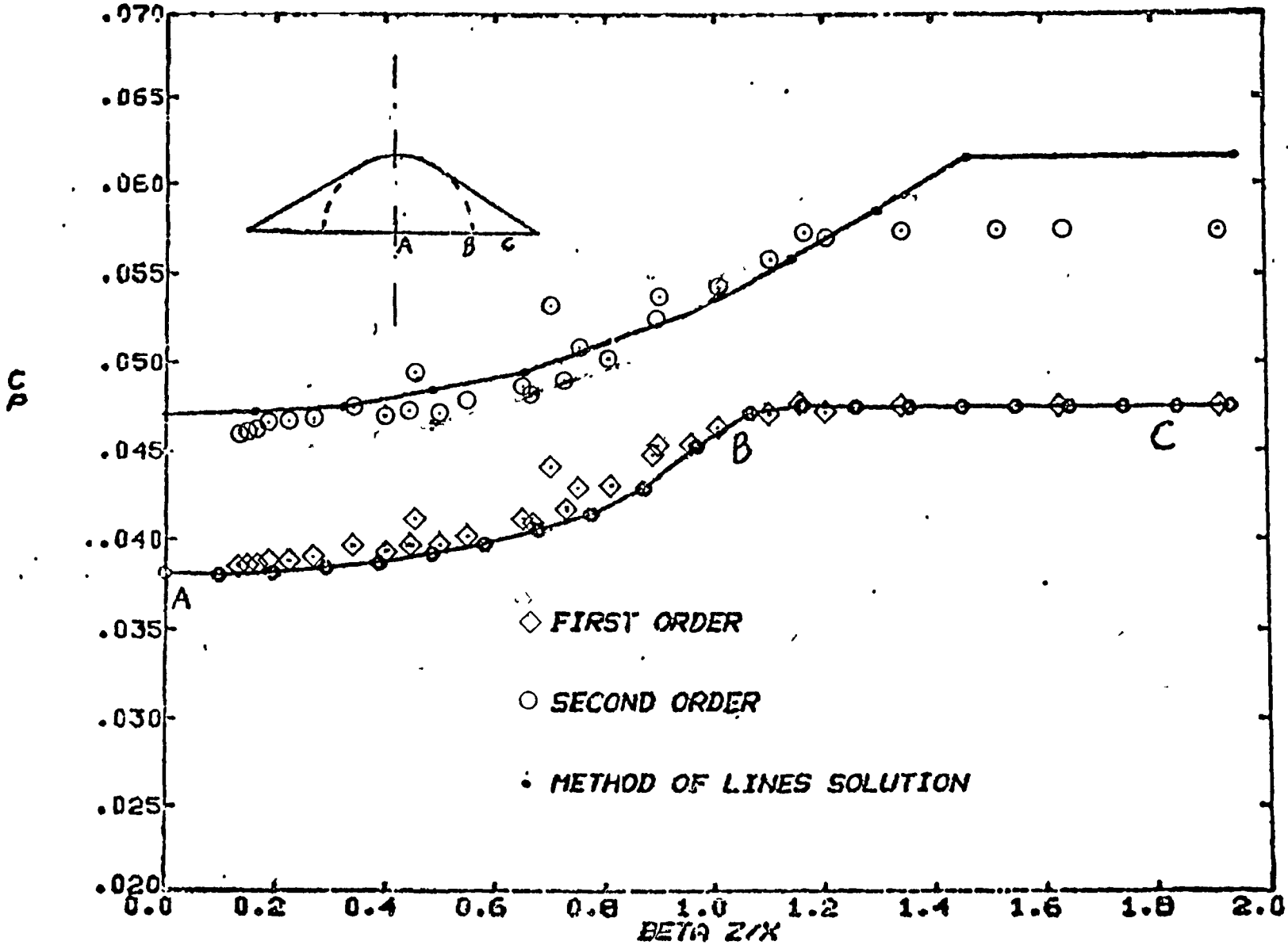

Figure 21A. Compression Side - Delta Wing
$M_\infty = 4$, $\chi = 50°$, $\alpha = 5°$

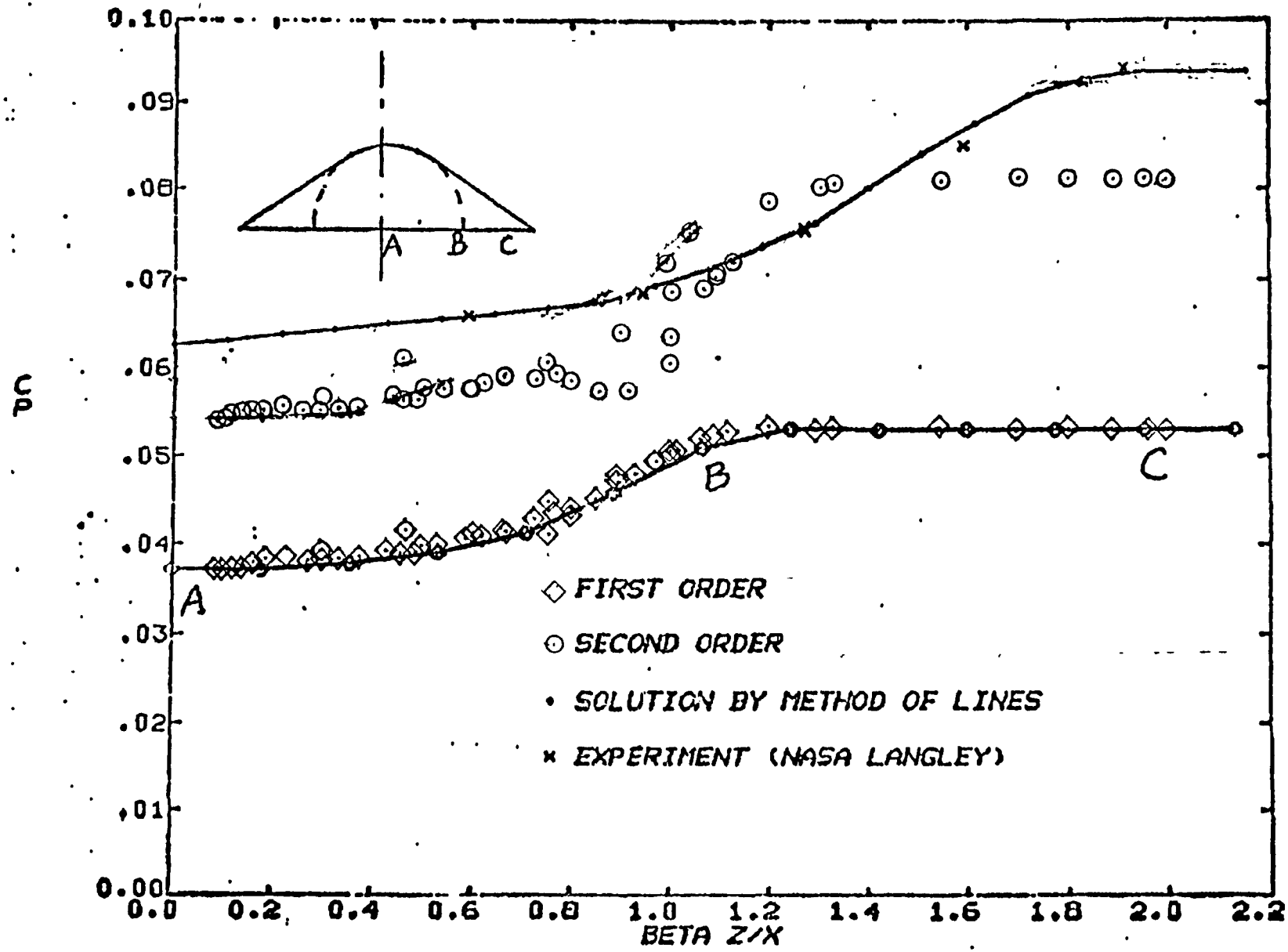

Figure 21B. Compression Side - Delta Wing

$M_\infty = 6$, $\chi = 70°$, $\alpha = 8°$

Finite Difference Second Order Theory - Velocity Potential Scalar Approach

Calculations were performed for flat delta wings at $M_\infty = \sqrt{2}$ and sweep angle χ = arctan (0.7071) with and without fourth-order damping. The results for the first order equation are shown in figure 22. Even when points are placed at the leading edge, some oscillations are seen inside the Mach cone when no damping is used. The addition of damping seems to remove these high frequency oscillations as shown in figure 22. Considerable improvements were also noticed when damping terms are added for cases with points not on the leading edge of the delta wing.

Second-order calculations were also performed for flat plate delta wing geometry with grid points on the leading edge. Two typical results are shown in figures 23 and 24. Considerable improvements over the linear theory

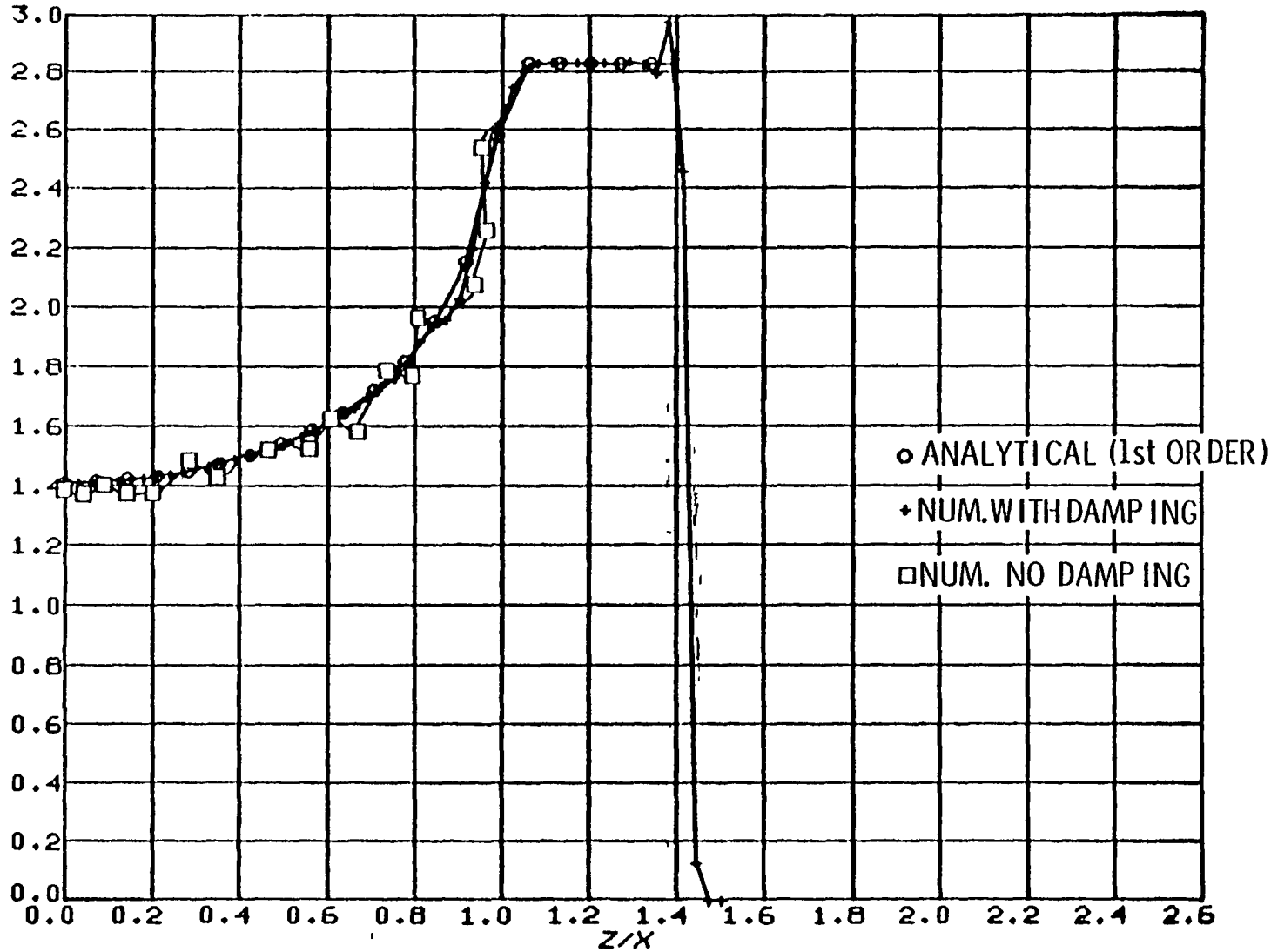

Figure 22. Comparison of analytical and numerical solutions with and without fourth-order damping. $M_\infty = \sqrt{2}$, $\chi = \arctan 0.707$

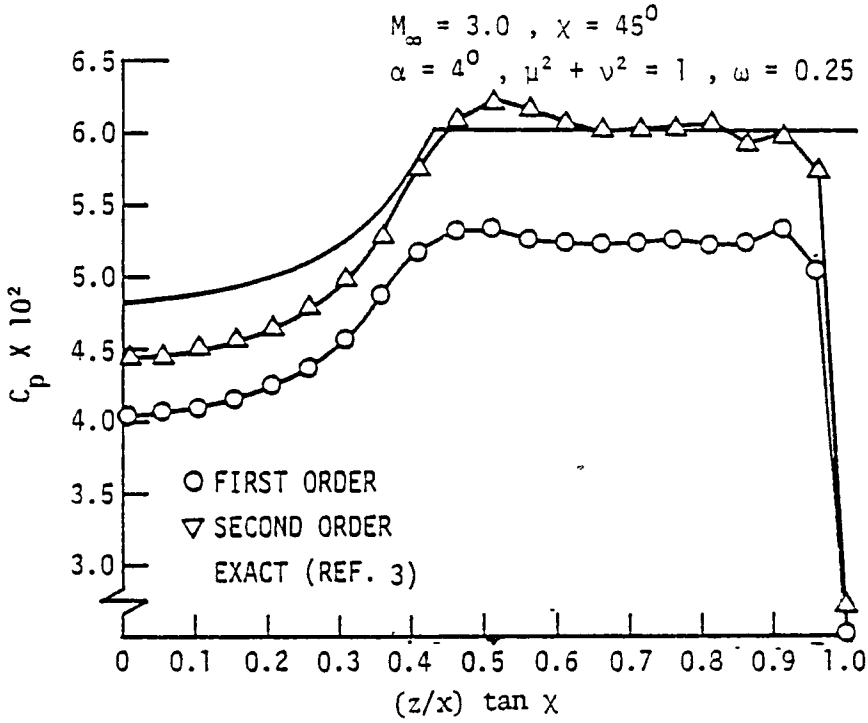

Figure 23. Compression side — delta wing Murman boundary point operator with damping

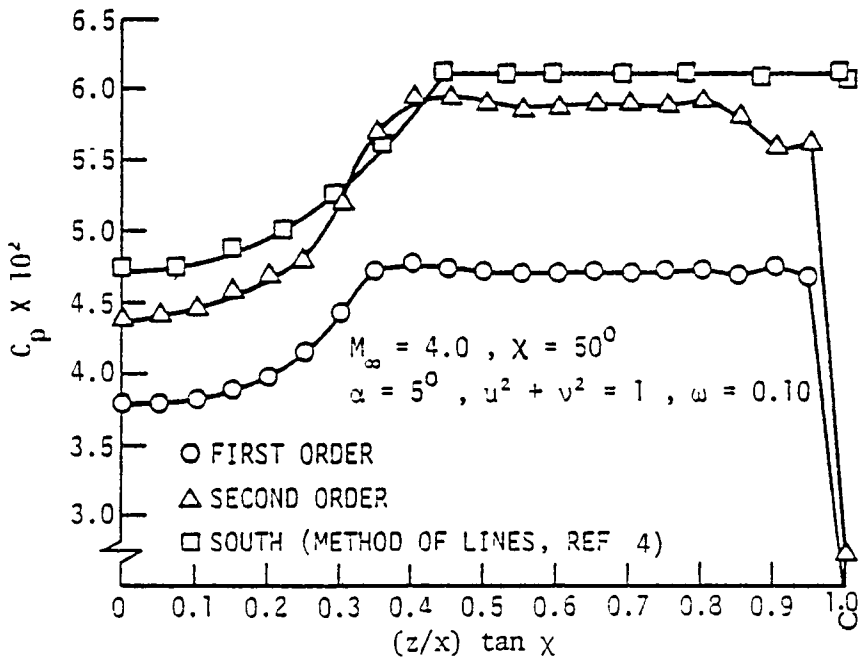

Figure 24. Compression side — delta wing Murman boundary point operator with damping

are obtained when the second-order theory is used. In figure 23, the linear and the second-order theory results for $M_\infty = 3$, $\chi = 45°$ are compared with Fowell's (Ref. 10) exact solution. At 4° angle of attack, the two-dimensional region computed by the second-order theory compares well with the exact solution with some deviation inside the Mach cone. In figure 24, the exact solution using method of lines (Ref. 11) is shown for comparison with the second-order results. For a preliminary design code concept, the improvements obtained with the second-order theory over the first-order solution is very encouraging at this point.

One other check was performed to validate the results obtained from the computer using second-order calculations. The pressure coefficient for a flow turning angle of $\Delta\theta$ and Mach number M_∞ is given by Busemann theory (two-dimensional unswept value)

$$C_p = \frac{p - p_\infty}{\frac{1}{2}\gamma p_\infty M_\infty^2} = \pm C_1 \Delta\theta + C_2 (\Delta\theta)^2 \pm C_3 (\Delta\theta)^3 + \cdots \tag{26}$$

where $\Delta\theta$ is positive when counterclockwise. The upper and lower signs refer respectively to left-running and right-running Mach waves, and the coefficients are as follows:

$$C_1 = 2/\sqrt{M_\infty^2 - 1}$$

$$C_2 = [(M_\infty^2 - 2)^2 + \gamma M_\infty^4]/2(M_\infty^2 - 1)^2$$

$$C_3 = \frac{M_\infty^4}{(M_\infty^2 - 1)^{7/2}} \left[\frac{\gamma+1}{6} \left(M_\infty^2 - \frac{5 + 7\gamma - 2\gamma^2}{2(\gamma+1)} \right)^2 \right.$$

$$\left. + \frac{-4\gamma^4 + 28\gamma^3 + 11\gamma^2 - 8\gamma - 3}{24(\gamma+1)} \right] + \frac{3(M_\infty^2 - 4/3)^2}{4(M_\infty^2 - 1)^{7/2}} .$$

It will be noted that the first term of Eq. (26) represents the linearized solution, and the first two terms the second-order solution.

Equation (26) does not have the sweep effects taken into account. By replacing M_∞ by $M_\infty \cos\chi$ and $\Delta\theta$ by arctan $(\tan\Delta\theta/\cos\chi)$ and compensating for pressure coefficient normalization with respect to the freestream reduced by a $\cos\chi$ factor, we get the sweep effects. For $M_\infty = 4$, $\Delta\theta = 5°$, and $\chi = 50°$ the first two terms in Eq. (26) (after making the sweepback corrections) yield a value of $(C_p)_{\text{second order, 2-D}} = 0.05733851$. For the same case, the finite differenced second-order calculations give $(C_p)_{\text{second order, 2-D}} = 0.0573339$.

Figure 25 shows a typical wing-body arrangement. Here, a right circular cone whose axis is rotated with respect to the wing to avoid a 90° intersection at wing-body junction, is placed on top of the delta wing. Figure 26 shows another arrangement of wing-body combination with a cosine body with no slope discontinuities at the wing-body junction. Calculations performed on these wing-body combinations using the velocity potential approach in Cartesian system are shown in figures 27 and 28 in terms of constant C_p contour lines. For the cone body, the delta wing was at zero degree angle of attack. Thus, in figure 27, the C_p in the 2-D region on the wing is zero. For wing-body arrangements once the grid points were placed along the leading edge the wing-body junction may or may not have points lying on it. In the Cartesian velocity potential formulation if the grid points were not aligned along the leading edge and wing-body junction the solution tends to be very oscillatory. The spikes that are seen in figures 27 and 28 originate at points neighboring the wing-body junction and propagate inwards along Mach lines. As expected the cosine body produces oscillations of smaller magnitude because of a smooth wing-body junction.

Finite Difference Second Order Theory – Systems Approach

Several conical delta wings and wing-body combination cases were run using the first and second order system of equations approach. Most of the cases used a typical η,ξ grid of (11 × 18) and required approximately 400 iterations to converge. All the cases were run on the Berkeley CDC 7600 machine.* A typical first and second order calculation using the systems approach required 10 seconds CPU time.

*This procedure although not strictly speaking necessary was chosen to reduce costs during the contractual effort.

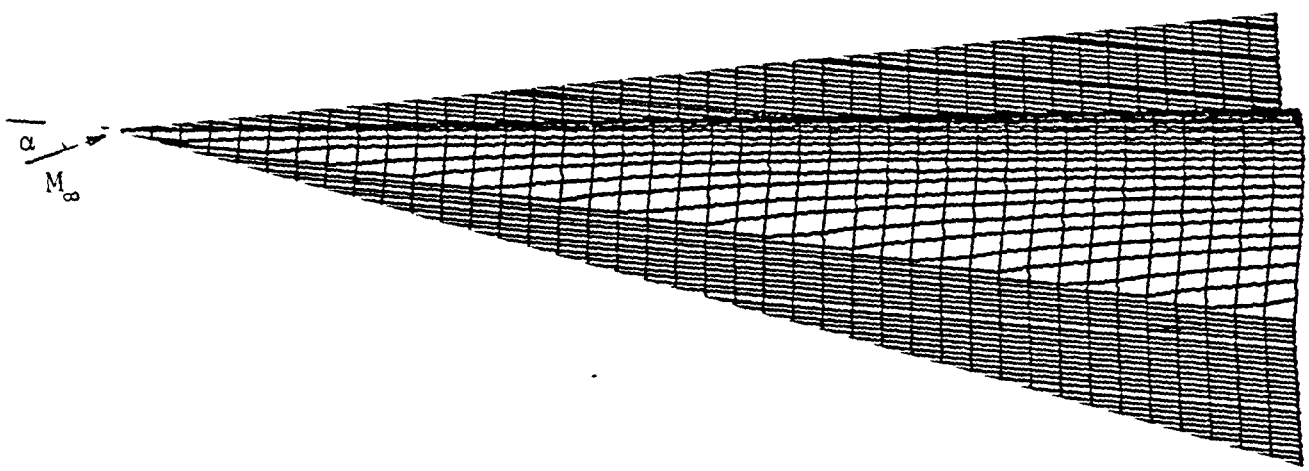

Figure 25. Rotated Circular Cone on a Delta Wing

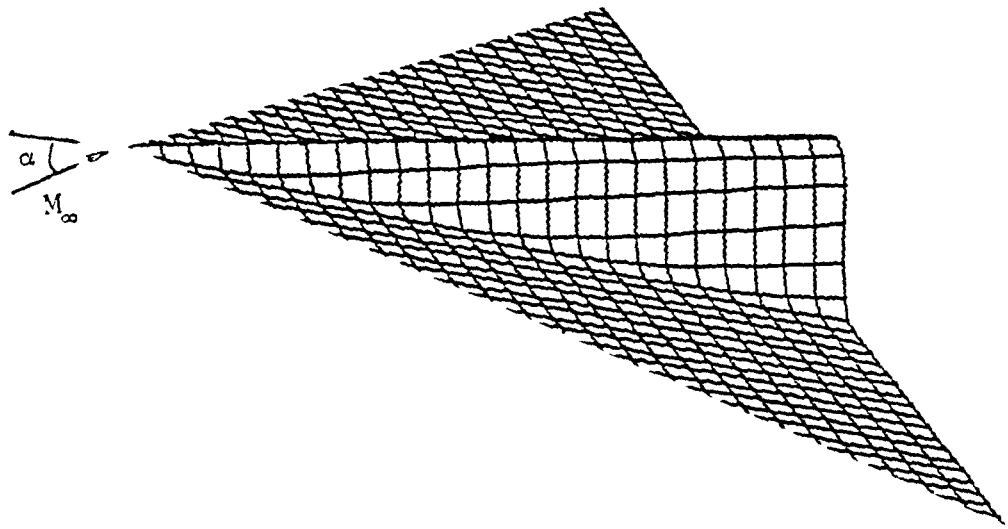

Figure 26. Conical Wing-Cosine Body

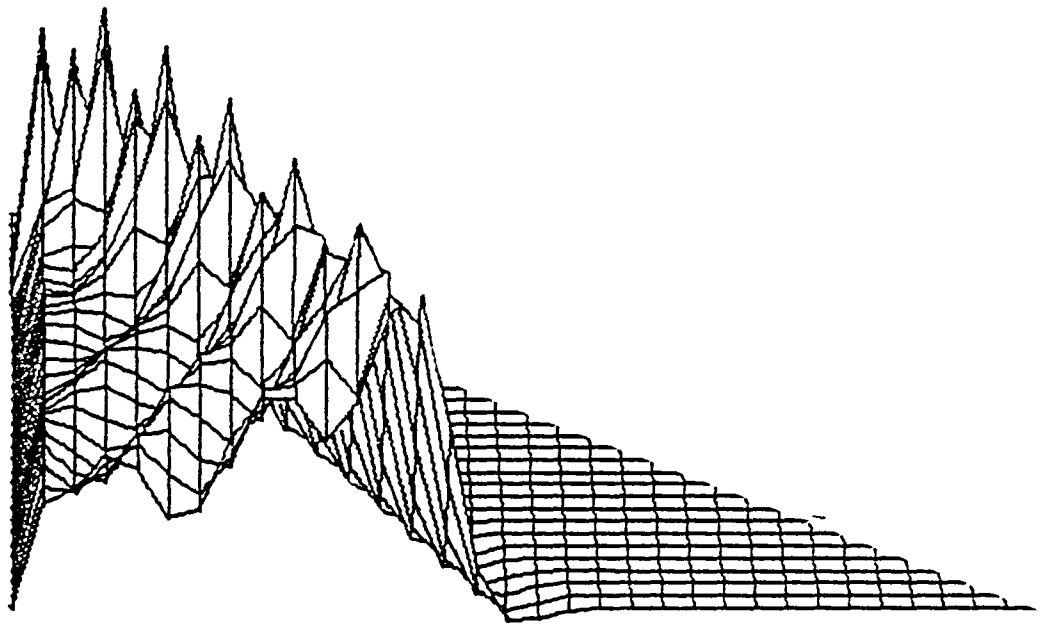

Figure 27. Constant C_p Lines for Wing-Rotated Circular Cone Body. $M_\infty = 5.08$, $\chi = 65°$, $\alpha = 0°$, Cone Semi-angle = 12.4°, the Axis of the Cone is Rotated with Respect to Wing by 6.2°.

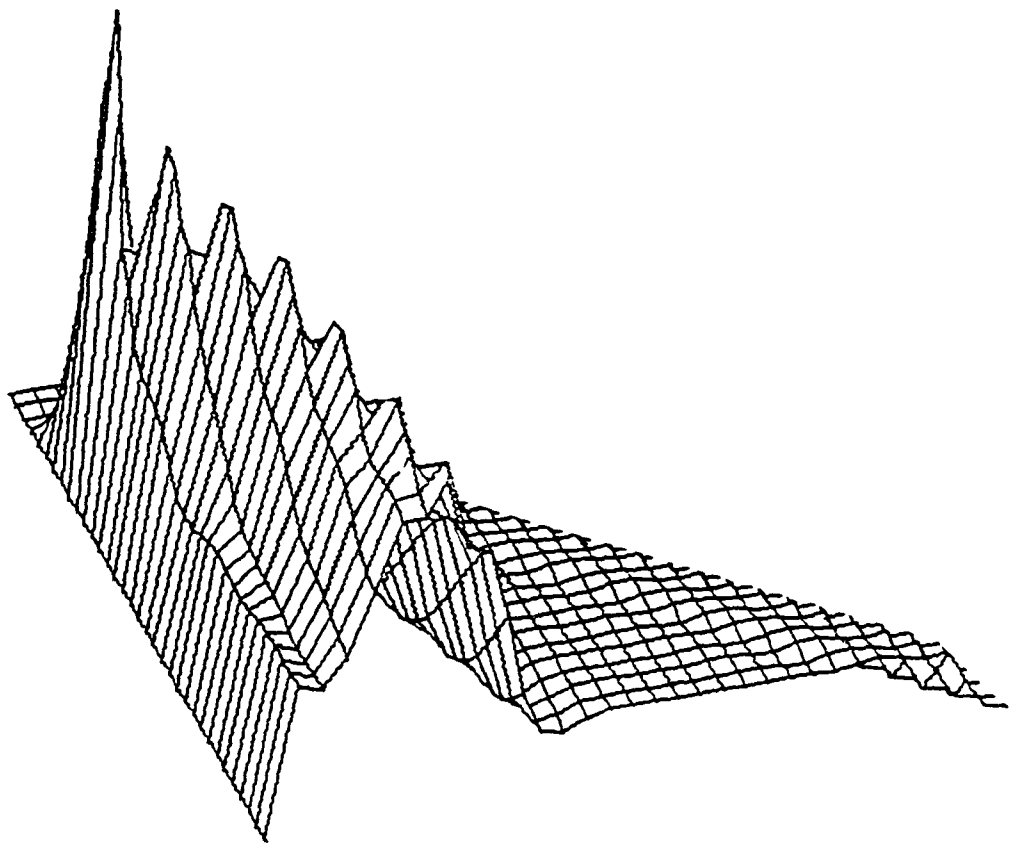

Figure 28. Constant C_p Lines on Wing-Cosine Body. $M_\infty = 4$, $\chi = 50°$, $\alpha = 5°$.

Figure 29 shows the first order solution and the improvements made using the second order solution for a delta wing case of $M_\infty = 4$, $\chi = 50°$ and angle of attack = 5°. The system of equation approach yields a much smoother solution than the velocity potential formulation, especially for the second order calculation. Better flow field resolution in the case of the system of equation approach could be due to the conical transformation.

Figure 30 shows another case of a delta wing for $M_\infty = 6$, $\chi = 70°$, $\alpha = 8°$. The first and second order solutions are compared with the Gentry/Woodward solution presented in Ref. 12, experimental data, and the more exact method of lines calculation. The second order finite difference solution and the Gentry/Woodward solution compare reasonably. It is very clear from this plot that a significant improvement in the results can be achieved using second order approach. However some disagreement with experiments still remain due to the inadequacy of the linear and Gentry theories in predicting the nonlinear shift in conical sonic line location.

Figure 31 shows a typical wing-body calculation for $M_\infty = 6$, $\chi = 70°$, and $\alpha = 8°$. A conical cosine body having the following shape (see figure 26)

$$y = \delta x \left(1 + \cos \pi \frac{\xi}{\xi_b}\right) + \alpha x \qquad 0 \leq \xi \leq \xi_b$$

$$= \alpha x \qquad \xi_b < \xi \leq \xi_{le}$$

is used, where ξ_b is the location of body-wing intersection and ξ_{le} is the leading edge position. The pressure of the body does not change the two-dimensional results as long as the body is contained within the Mach cone. The boundary condition for the body is also applied at y=0, just like for the wing.

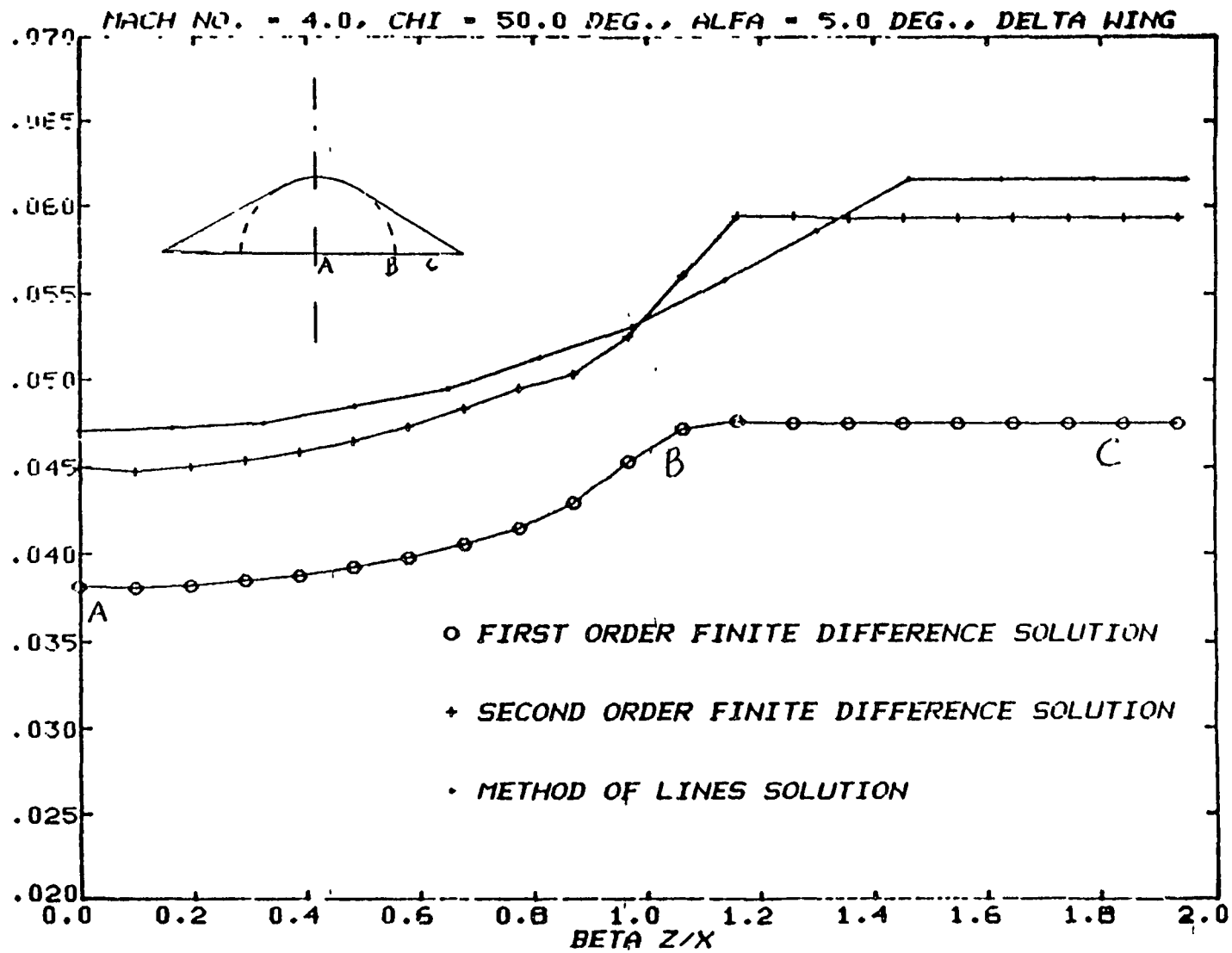

Figure 29. Compression Side — Delta Wing
$M_\infty = 4$, $\chi = 50°$, $\alpha = 5°$

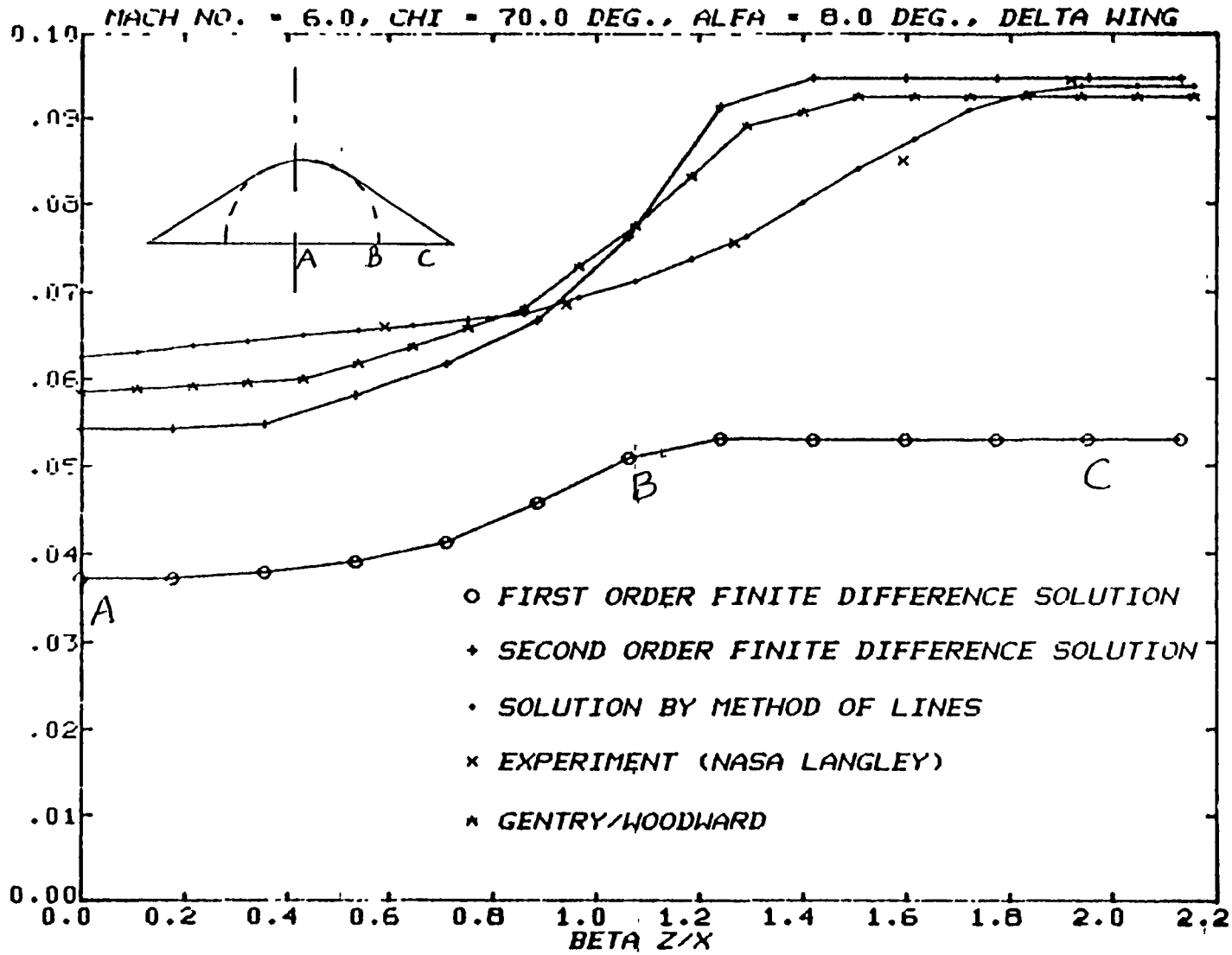

Figure 30. Compression Side — Delta Wing
$M_\infty = 6$, $\chi = 70°$ $\alpha = 8°$

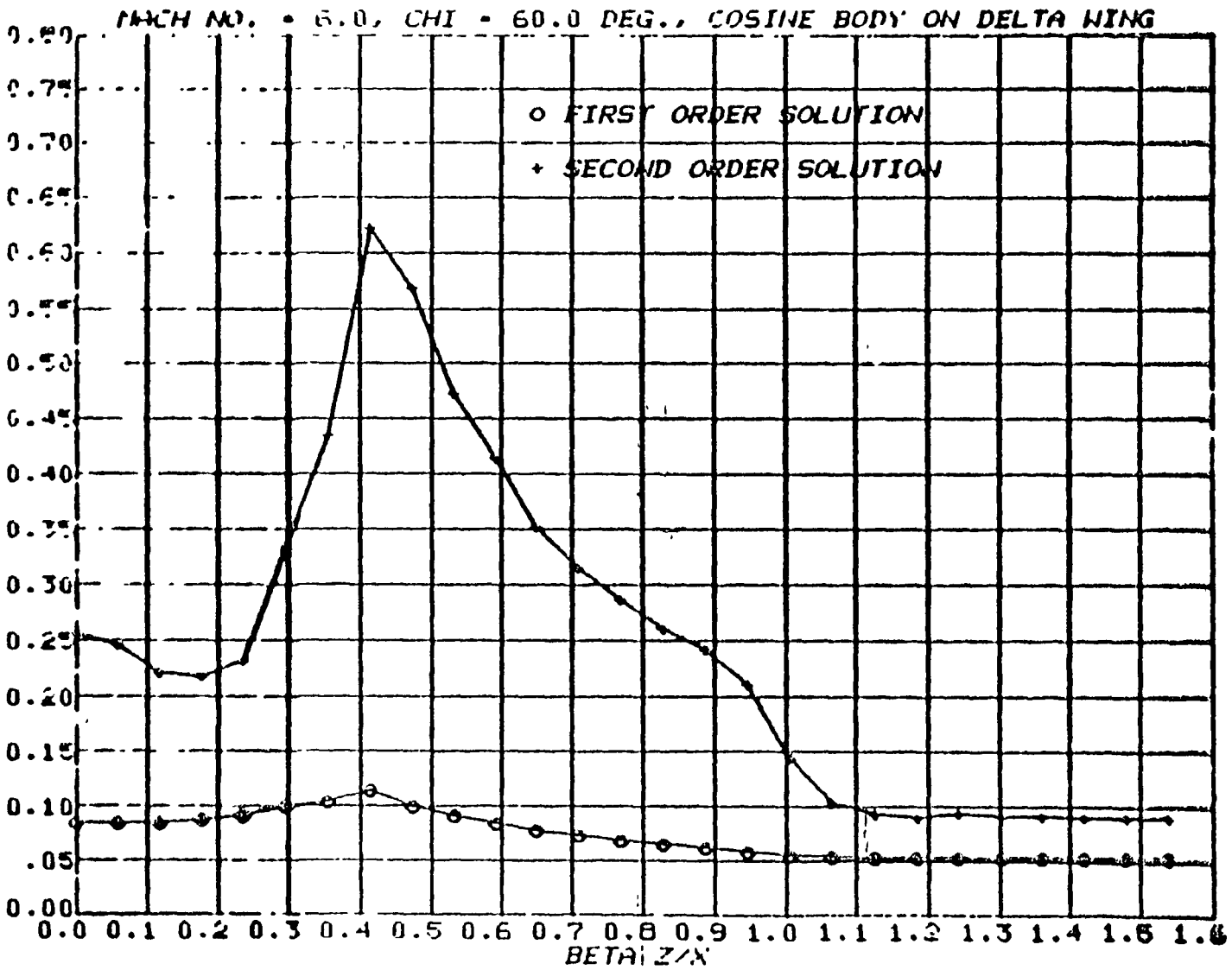

Figure 31. Compression Side — Conical Wing-Body Geometry
$M_\infty = 6$, $\chi = 70°$, $\alpha = 8°$

Comparing figures 30 and 31, it can be seen that the influence of the body completely changes the second order solution in the three dimensional region. Instead of a sonic line in the case of delta wing a compression wave (can be a shock also) is formed terminating the two dimensional region. The flow then undergoes a gradual compression thereby peaking the C_p value. The peak in C_p occurs around the intersection of the wing-cosine body. On the body the flow (cross flow) undergoes a rapid expansion and the C_p value falls down to the centerline value.

Figure 32 shows the results for symmetric subsonic leading edge delta wing cases. For the linearized equations there is a square root singularity at the subsonic leading edge causing C_p to go to infinity. The numerical procedure cannot handle this singular behavior properly and hence forms spikes in the solution near the subsonic leading edge. Results are shown for $M_\infty = \sqrt{2}$, semi wedge angle of 3° and for leading edge sweep angles 69° 56' and 51° 21'. The first and second order results are also compared with analytical results from Ref. 13. The discrepancy between the analytical results and the numerical results require further investigation.

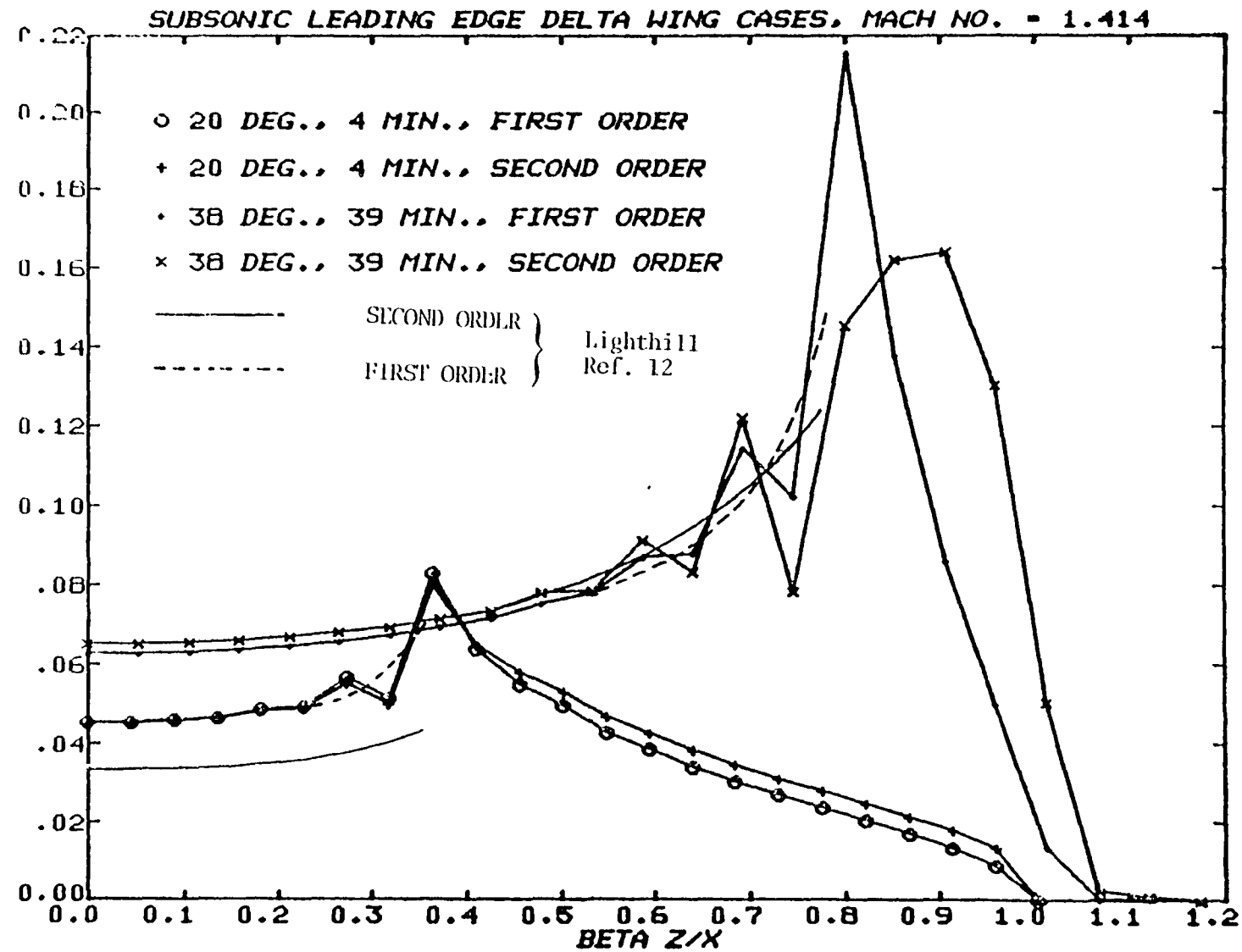

Figure 32. Symmetric Subsonic Leading Edge Delta Wing, $M_\infty = \sqrt{2}$

6.2 Results – Evaluations of Hypersonic Small Disturbance Theory Model

In this section, we apply the formulation devised in Section 5.1 to treat flows over elliptic cones at incidence. This study is intended to illuminate accuracy questions in regard to the initial concept and indicate directions of refinement prior to application to more general configurations.

Referring to figure 33, we consider the elliptic cone in the hypersonic stream at freestream Mach number M_∞ and incidence α. In Eq. (7b) in Section 5.1, by use of a body axis to wind axis transformation, we find that for the shape in figure 33, the body B and shock S have the special representations

$$B = r - xf(\theta) = 0 \tag{1a}$$

$$S = r - xg(\theta) = 0 \tag{1b}$$

where $r = \bar{r}/\delta$, $y = \bar{y}/\delta = r \sin\theta$, $z = \bar{z}/\delta = r\cos\theta$, $r^2 = y^2 + z^2$, and $\theta = \tan^{-1} y/z$. For an elliptical cross section of eccentricity ε and major axis vertex angle δ, we have, with $A \equiv \alpha/\delta$

$$f = r/x = \frac{-A\sin\theta + \sqrt{A^2\sin^2\theta + \varepsilon^2(\sin^2\theta + \varepsilon^2\cos^2\theta)}}{\sin^2\theta + \varepsilon^2\cos^2\theta} \tag{2a}$$

$$= \frac{\varepsilon\sqrt{\sin^2\theta + \varepsilon^2\cos^2\theta} - A\sin\theta}{\sin^2\theta + \varepsilon^2\cos^2\theta} + O(A^2) \text{ as } A \to 0$$

$$f'(\theta) = -(f\cos\theta)\frac{f(1-\varepsilon^2)\sin\theta + A}{\sin^2\theta + \varepsilon^2\cos^2\theta + A\sin\theta} \ . \tag{2b}$$

The pressures on the shock are given by Eq. (3d) where the right hand side is calculated using Eqs. (2). Defining this right hand side as a quantity $S(\theta)$, we obtain in the notation of Eqs. (7) and solving (8)

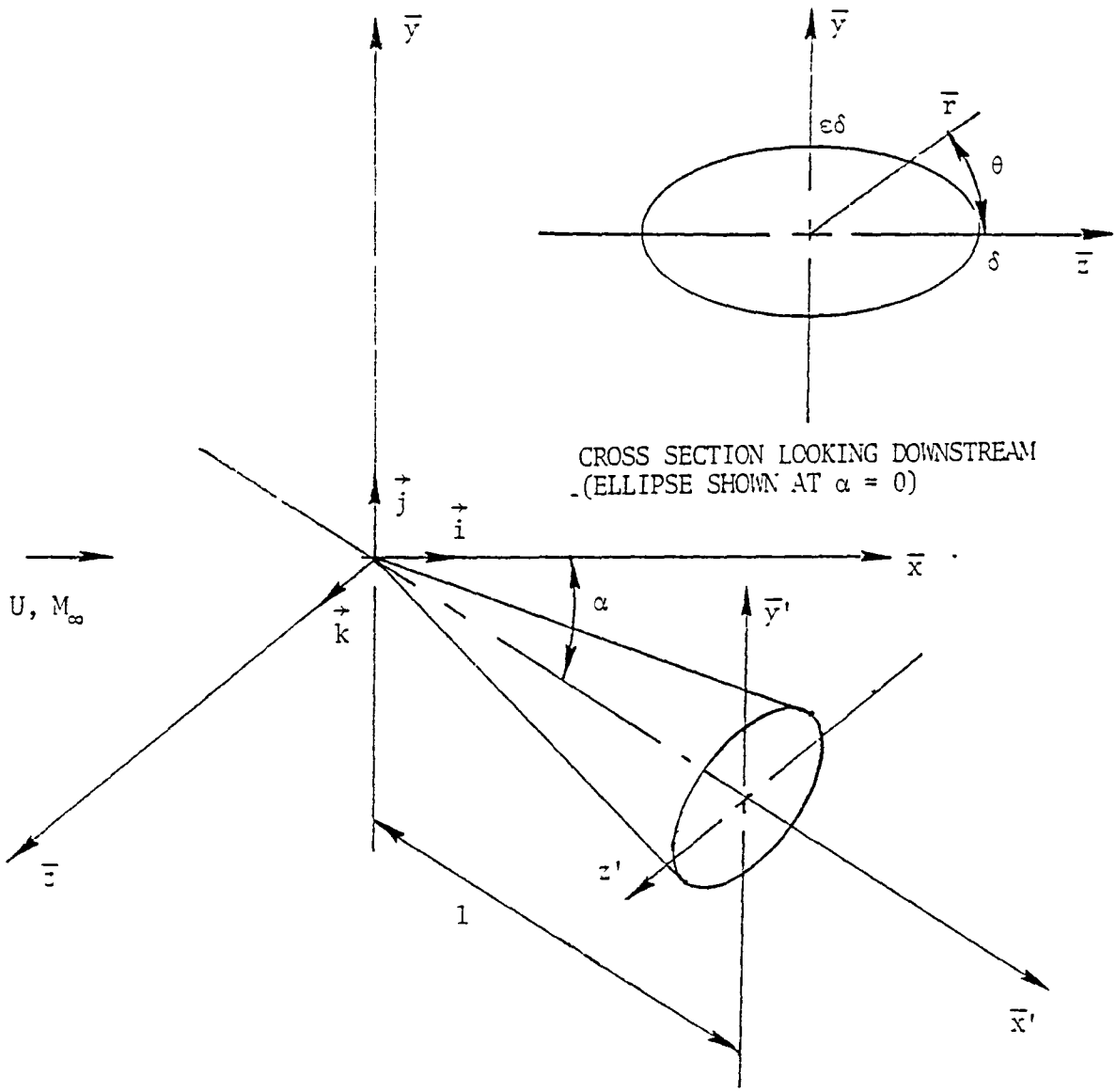

Figure 33. Elliptic Cone Geometry and Notation

$$S = \frac{FF_x}{\sqrt{F^2 + F_\theta^2}} = \frac{f^2}{\sqrt{f^2 + f'^2}} \tag{3}$$

$$T = \frac{\gamma+1}{4} S + \sqrt{\left(\frac{\gamma+1}{4} S\right)^2 + H} \, . \tag{4}$$

For this conical shape, the nonlinear first order partial differential equation in two space variables x and θ becomes the following ordinary differential equation for the reduced shock shape g:

$$g'(\theta) = g \sqrt{(g/T(\theta))^2 - 1} \, . \tag{5}$$

Note that Eqs. (3)-(5) apply to an arbitrary cross section conical body. If a surface integration is used to determine the lift coefficient, then the appropriate expression for a conical body is

$$C_L = \iint_S C_{p_B} \vec{n} \cdot \vec{j} \, dS = \int_{-\frac{\pi}{2}}^{\frac{\pi}{2}} C_{p_B}(\theta) \frac{f[f \sin\theta - f' \cos\theta]}{\sqrt{f^2 + f'^2}} \, d\theta \, . \tag{6}$$

In figure 34, results using the present hypersonic small disturbance "wedge" model are compared to other theories for the α=0 right circular cone (ε=0) case. In contrast to the $M_\infty = \infty$ results previously presented in figure 12, the discrepancies increase from 20% at H=0 corresponding to the strong shock $M_\infty = \infty$ case to about 49% at $H = \beta\delta = 1$ for γ=1.4. The discrepancies could be reduced by employing a lower value of γ associated with a thin shock layer approximation or the previously used somewhat inconsistent approximation employed in Ref. 8 of negligible freestream pressure compared to static pressure on the body. Further evaluation of this case indicates that the present theory makes too gross an approximation of the wave angle T by assuming that the magnitude of transverse component of velocity $|\vec{V}_T| = |\vec{q} - U\vec{i}|$ is conserved across the shock layer. For a wedge in which the

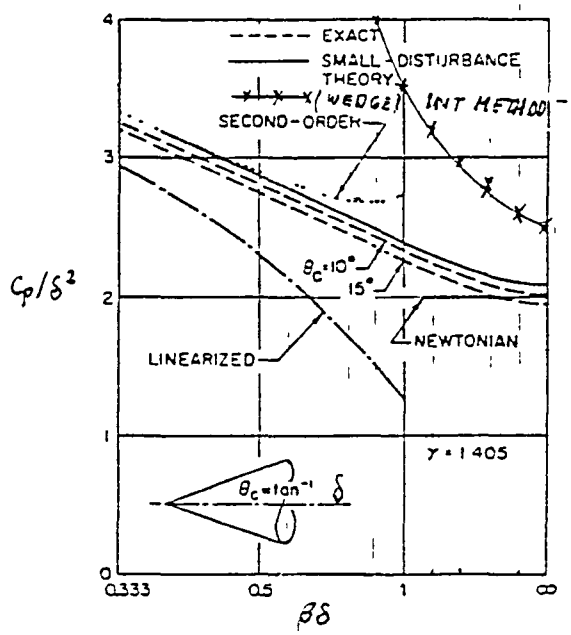

Figure 34. Comparison of Integral Method for Normalized Coefficient Pressure Over Right Circular Cone at Zero Angle of Attack, $\beta = \sqrt{M_\infty^2 - 1}$

flow behind the shock is constant state this assertion is obvious. Accordingly, it would be expected that for relatively planar winglike bodies with supersonic leading edges this approximation may not produce the serious errors associated with the cone. For the latter, however, important flow relief effects occur due to the high three dimensionality. Also implicit in the comparison of figure 34 is the assumption that shock and body pressures are the same. This assertion is apparently not as serious as that concerning the wave angle, T. The error in the latter is only 20% but its appearance as a square aggravates the prediction sensitivity.

Prior to discussing directions for refinement, we turn now to the case $\alpha, \varepsilon \neq 0$, i.e., an elliptic cone at incidence. With the notation given in figure 33, pressures were calculated with our model for an $\varepsilon = 1/2$ cone tested by Chapkis at $M_\infty = 5.8$ and reported in Ref. 14. Results for the pressures on the most lee ($\theta = \pi/2$) and windward rays ($\theta = -\pi/2$) are shown in figure 35 for various angles of attack α. For the windward side in which the thin constant property shock conditions are most closely met, the agreement is reasonable. Degradations occur on the lee side associated with thickening of the layer and resulting nonuniformities in the region. In figure 36, the experimental meridional variation of pressures is compared for the same cone at $\alpha = 0$ and 2° with the predictions from our model. Serious discrepancies occur near the major axis. Newtonian flow results for $\alpha = 0$ are also shown and also indicate serious discrepancies, but near the minor axis. The appropriate Newtonian expression for zero incidence is

$$\frac{C_p}{2\delta^2} = \frac{|\nabla B \cdot \vec{i}|^2}{|\nabla_T B|^2} = \varepsilon^2 \left[\sin^2\theta + \varepsilon^2 \cos^2\theta\right] / \left\{\left[\sin^2\theta + \varepsilon^2 \cos^2\theta\right] + (1 - \varepsilon^2) \sin^2 \cos^2\theta\right\} . \qquad (7)$$

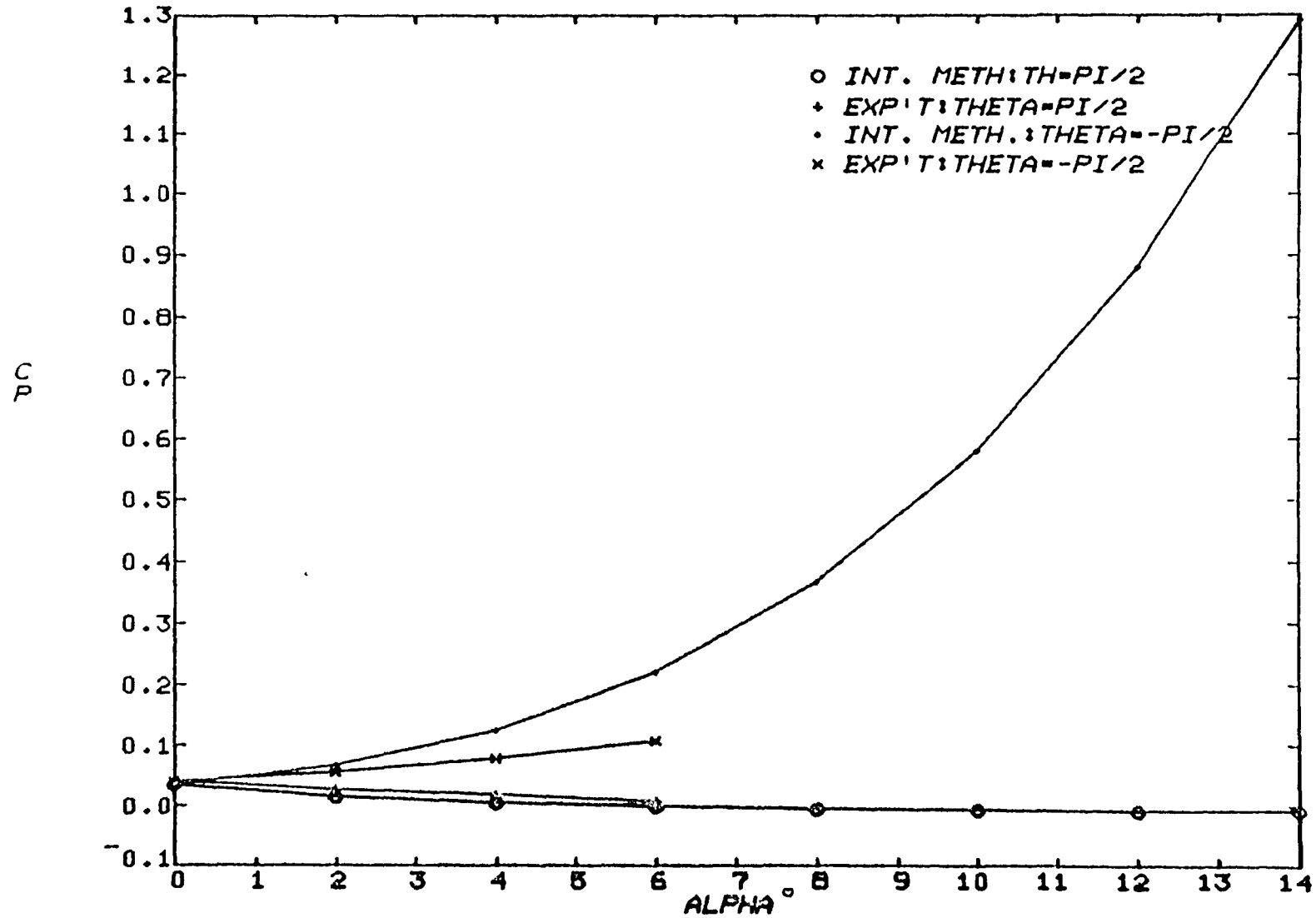

Figure 35. C_p on Elliptic Cone Most Lee and Windward Rays

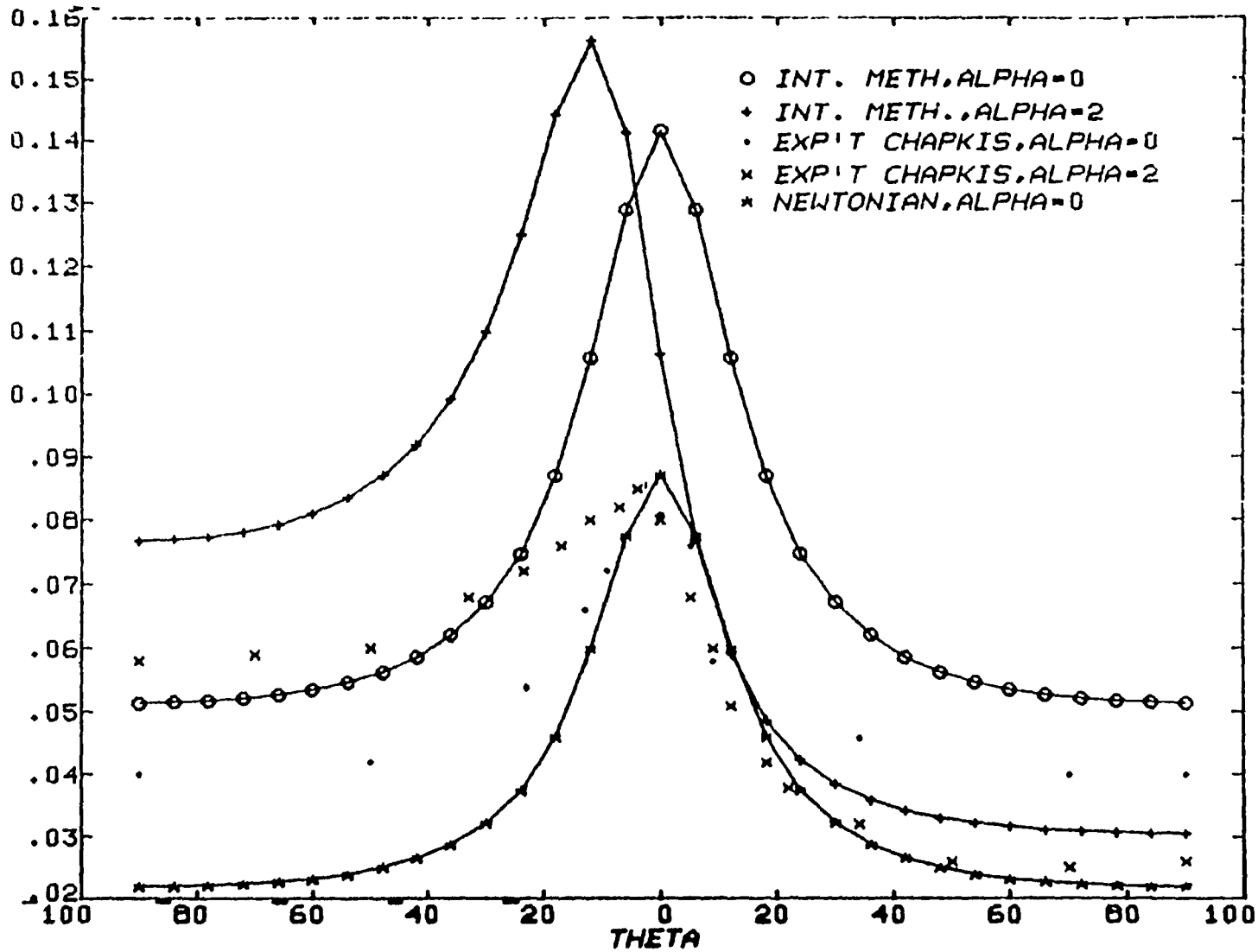

Figure 36. Comparison of Approximate Shock C_p with Experimental Body C_p – Elliptic Cone

For the prediction of C_L by a surface pressure integration, one might expect a beneficial error reduction due to the tilting of the pressure vector in the region where it contributes the least to the lift and the error is the greatest. Unfortunately, for an ellipse, this tilting is also localized to the major axis and no substantial accuracy improvement occurs, as shown in the meridional loading curve of figure 37. Using Eq. (6), we obtain a C_L of 0.05056 in contrast to a value of 0.0278 using Chapkis' measured pressures.

As indicated previously, a crucial feature of the model is its capability to accurately predict the shock wave shape. In the foregoing phase involving the determination of C_L, the application of (5b) in Section 5.1 to the determination of C_L was considered on the grounds that compensating errors could be involved in the evaluation of the σv product and the estimation of ΔA. The determination of ΔA involves the solution of (5) for g. Cauchy-Euler marching was attempted, but it became evident that the singular behavior near $\theta = -\frac{\pi}{2}$ will have to be better understood before this scheme is successful.

More accurate prediction of the shock shape for this and generalized geometries will require suitable refinements in the model in which presumably, more localized integral forms of the equations than (5) in Section 5.1 are used. The existing model utilizes only the surface boundary conditions but does not incorporate the differential equations, particularly that of continuity This aspect is particularly important in distinguishing the highly three-dimensional conical flow considered previously within the framework in the quasi-two-dimensional assumption of $\left|V_T\right|_S = \left|V_T\right|_B$. In future studies, finite volume procedures involving these conservation laws will be more fully developed.

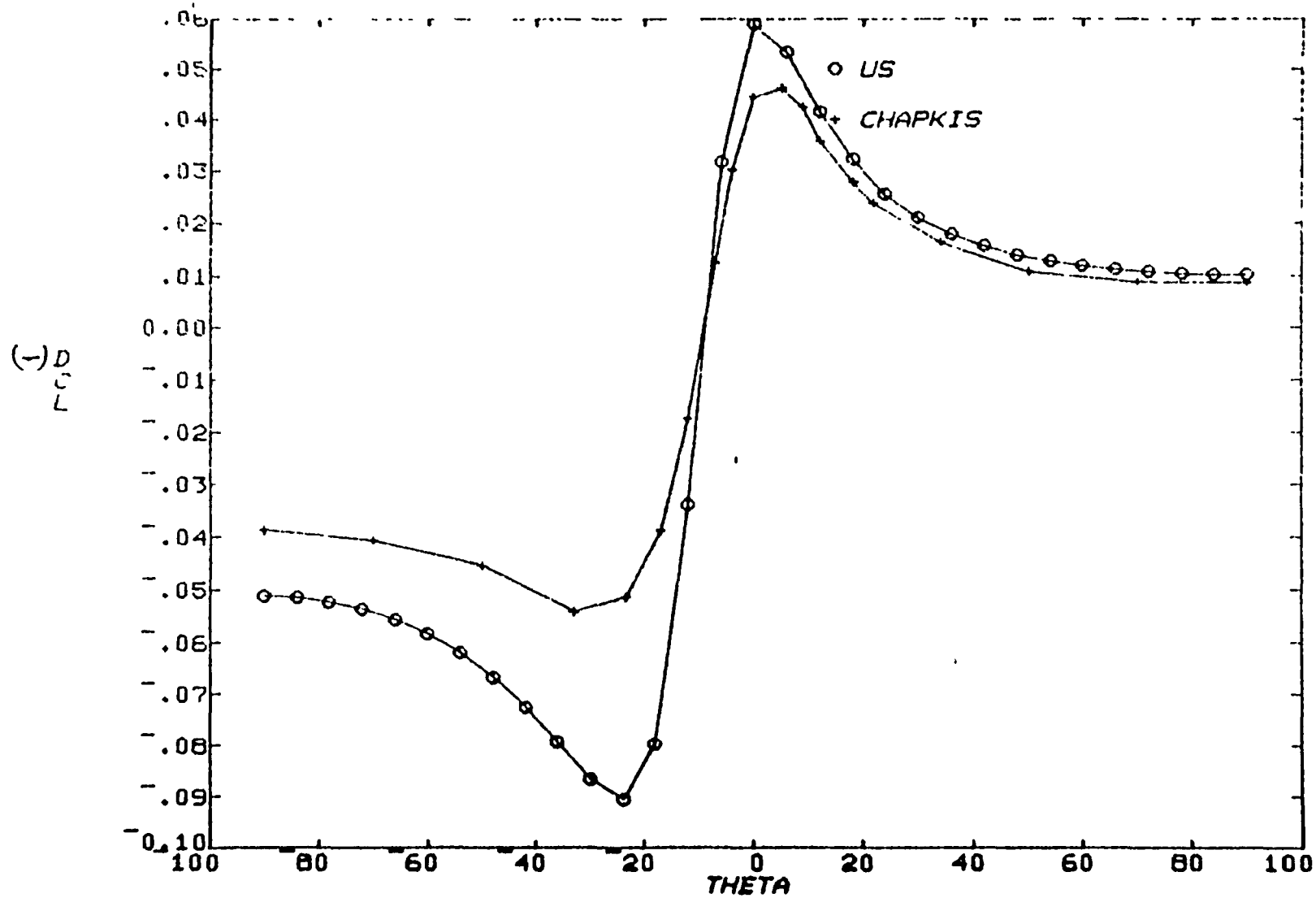

Figure 37. Comparison of Elementary Lifts Integral Method versus Chapkis Experiment, $\alpha = 2$

7. CONCLUSIONS

Based on the theoretical development and comparison with higher order results/experimental measurements, the following findings and conclusions are made.

1. Second order potential theory provides a systematic means of extending linear theory to values of the similarity parameter $M\delta$ of order one.
2. Improved prediction of supersonic/hypersonic aerodynamic characteristic and surface pressures for simple three dimensional shapes has been demonstrated for numerical second order analysis.
3. Additional effort is required to extend the non-linear potential analysis to more general wing-body arrangements and refine the treatment of subsonic edges.
4. Exploratory effort utilizing hypersonic small disturbance theory integral techniques indicates that the approach requires additional development prior to obtaining a rapid gross aerodynamic prediction method.
5. The systems approach has a strong potential for any future code development to handle general three dimensional configurations in much the same manner as existing Euler codes but with sufficient computer time and cost savings to permit use as a preliminary design tool.

8. REFERENCES

1. Van Dyke, M.D., "A Study of Second-Order Supersonic Flow Theory," NACA TN 2200, January 1951.
2. Gunness, R.C., Jr., Knight, C.J., and Sylva, E.D., "Flow Field Analysis of Aircraft Configurations Using a Numerical Solution to the Three-Dimensional Unified Supersonic/Hypersonic Small-Disturbance Equations," NASA CR 1926, February 1972.
3. Malmuth, N., "A New Area Rule for Hypersonic Wing Bodies," AIAA Journal, Vol. 9, December 1971, pp. 2460-2461.
4. Malmuth, N., "Pressure Fields Over Hypersonic Wing Bodies at Moderate Incidence," Journal of Fluid Mechanics, Vol. 59, Pt. 4, August 1973, pp. 673-691.
5. Malmuth, N., "Generalized Area Rules and Integral Theorems for Hypersonic Wing Bodies," AIAA Journal, Vol. 16, No. 9, September 1978, pp. 1019-1022.
6. Courant, R., and Hilbert, D., Methods of Mathematical Physics, Vol. II, Interscience, p. 97 (1962).
7. Chernyi, G.G., Introduction to Hypersonic Flow, translated and edited by R.F. Probstein, Academic Press, New York, 1961.
8. Technical Proposal for Formulation of Aero Prediction Technique for Hypersonic Configuration Design, NA-77-56IL, Rockwell International Los Angeles Division, 6 June 1977.
9. Babenko, K.I., et al., Three-Dimensional Flow of Ideal Gases Around Smooth Bodies, Transl. from Russian by Israel Program for Scientific Transl. (1968).

10. Fowell, L.R., "Exact and Approximate Solutions for the Supersonic Delta Wing," Journal of the Aeronautical Sciences, Vol. 23, No. 8, August 1966, pp. 709-720.

11. South, J.C., and Klunker, E.B., "Methods for Calculating Nonlinear Conical Flows," NASA SP-228, pp. 131-158, 1969.

12. Brooke, D., and Vondrasek, D.V., "Feasibility of Combining Linear Theory and Impact Theory Methods for the Analysis and Design of High speed Configurations," NASA Contractor Report 3069, December 1978.

13. Lighthill, M.J., "Higher Approximations in Aerodynamic Theory," Princeton Aeronautical Paperbacks.

13. Chapkis, R.L., "Hypersonic Flow Over an Elliptic Cone Theory and Experiment," Journal of Aerospace Sciences, Vol. 29, No. 11, November 1961, pp. 844-853.

End of Document